Optical Surface Microtraps based on Evanescent Waves

Dissertation

zur Erlangung des Doktorgrades an der
naturwissenschaftlichen Fakultät
der Leopold-Franzens-Universität Innsbruck

vorgelegt von

Markus Hammes

aus Kabul

durchgeführt am Institut für Experimentalphysik
unter der Leitung von
Univ.-Prof. Dr. Rudolf Grimm

November 2002

Abstract

This thesis reports on the realization of two novel optical trapping schemes that allow for the confinement of dense atomic ensembles close to a material surface. The microtraps use the strong optical dipole force arising from large intensity gradients of evanescent wave light fields and of a strongly focussed beam. The resulting trapping conditions are favorable to implement efficient evaporative cooling or to create a system of reduced dimensionality.

The first microtrap, the focussed beam surface trap, tightly confines an atomic cesium ensemble using a repulsive evanescent wave light field, a strongly focussed far-detuned beam and gravity. The focussed beam is oriented vertically with respect to the dielectric surface and its attractive dipole force provides the horizontal confinement of the trap. The combination of repulsive evanescent wave and gravity confines the atomic ensemble vertically. This conservative microtrap potential is loaded with atoms from a large and dense reservoir of atoms near the dielectric surface via elastic collisions. The combination of the large reservoir and the small dimple potential leads to a local increase in density and phase-space density by up to a factor of 300 and gives rise to elastic scattering rates of about 2 kHz. Subsequent efficient evaporative cooling is applied to further increase the phase-space density of the unpolarized ensemble of initially several million cesium atoms. At $T = 400\,\mathrm{nK}$ a phase-space density of 1.6×10^{-2} is observed showing this approach's potential to reach the Bose-Einstein condensation point.

In a second microtrap scheme, the double evanescent wave surface trap, two overlapping evanescent waves, one repulsive and short-ranged and the other attractive and long-ranged, are used to create a three-dimensional microtrap potential close ($\approx 1\,\mu\mathrm{m}$) to the dielectric surface. Up to 1.5×10^5 atoms can be transferred from the focussed beam surface trap and are then evaporatively cooled to around 100 nK by ramping down the attractive dipole potential. Under these conditions the vertical motion of the atoms in the strongly confining, highly anisotropic potential is inherently quantum mechanical. The vertical ground-state population at this point is 63 % and the phase-space density has increased to about 0.1. Consequently the crossover to two-dimensionality has been reached.

Zusammenfassung

Im Rahmen dieser Arbeit wurden zwei neuartige optische Oberflächenmikrofallen entwickelt und die damit verbundenen physikalischen Fragestellungen untersucht. Bei diesen Fallentypen werden die starken optischen Dipolkräfte evaneszenter Lichtfelder und eines stark fokussierten Laserstrahls benutzt, um neutrale Atome in einem kleinen Volumen nah einer materiellen Oberfläche einzuschließen. Die resultierenden Einschlussbedingungen ermöglichen effizientes evaporatives Kühlen oder die Erzeugung eines zweidimensionalen Atomgases.

Die erste Mikrofalle, die "focussed beam surface trap", erzeugt einen starken Einschluss der Atome durch die Kombination einer repulsiven evaneszenten Lichtwelle, eines stark fokussierten Laserstrahls und der Gravitation. Der fokussierte Strahl ist senkrecht bezüglich der horizontalen dielektrischen Oberfläche orientiert und erzeugt durch seine anziehende Dipolkraft das horizontale Potenzial der Falle. Das Zusammenwirken der Erdanziehung und der abstoßenden evaneszenten Welle sorgt für den vertikalen Einschluss der Atome. Das konservative Mikropotenzial wird aus einem dichten Reservoir kalter Atome nah der Oberfläche über elastische Stöße geladen. Die Kombination aus großem Reservoir und kleinem Dimplepotenzial führt zu einer maximalen lokalen Überhöhung von Dichte und Phasenraumdichte um den Faktor 300 und erzeugt elastische Stoßraten von 2 kHz. Mit anschließender evaporativer Kühlung wird die Phasenraumdichte des unpolarisierten Ensembles weiter erhöht. Bei einer Temperatur von 400 nK beträgt die Phasenraumdichte schließlich 1.6×10^{-2}. Die hohe Effizienz der Evaporation deutet das Potenzial dieser Methode zum Erreichen der Bose-Einstein Kondensation an.

In einem zweiten Mikrofallenschema, der "double evanescent wave trap", werden zwei evaneszente Lichtwellen, eine repulsiv und kurzreichweitig die andere attraktiv und langreichweitig, überlagert um ein dreidimensional einschließendes Mikropotenzial nah der Oberfläche ($\approx 1\,\mu$m) zu erzeugen. Bis zu 1.5×10^5 Atome können aus der focussed beam surface trap transferiert und anschließend durch Absenken des Dipolpotenzials evaporativ auf etwa 100 nK gekühlt werden. Bei diesen Bedingungen ist externe Bewegung der Atome im vertikal stark einschließenden Potential der Falle inhärent quantenmechanisch. Die Bevölkerung des Grundzustands der vertikalen Bewegung beträgt 63 % während die Phasenraumdichte bei etwa 0.1 liegt. Der Übergangsbereich in das zweidimensionale Regime ist damit erreicht.

Contents

Chapter 1

Introduction

At first sight "cooling atoms" does not seem in any way useful to bring about new physics or enhance understanding of it. The reason is probably that the intuitive picture of cooling usually includes the reduction of a system's energy and thus the slowing down or suppression of processes that might be potentially interesting. However, considering how many physicists work today with ultracold atoms and recalling that the Nobel prizes of the years 1997 and 2001 were awarded for research done in this field, it is obvious that this picture is wrong.

The reason that cooling on the contrary can be a useful means to bring out new physics, lies in the fact that removing the thermal energy of an atom allows for its preparation in a well-defined and deliberately chosen state and in the fact that cold atoms can be held and manipulated in traps [Met99]. At very low temperatures the thermal de-Broglie wavelength which represents the spatial spread of an atom due to quantum mechanics, becomes large enough to create a situation in which atoms "feel" each other without interacting through classical forces. Quantum-statistical effects like Bose-Einstein condensation (BEC) or Fermi degeneracy drastically modify the behavior of an atomic ensemble and lead to a new and interesting field of physics [Ket99a].

In a sense atoms are an ideal system to study physics: They are small enough to live in the realm of quantum mechanics, their constituents interact with each other in a way that allows insights into quantum electrodynamics and other theories. They can be used as basic units to form more complex structures from molecules to mesoscopic systems to macroscopic bodies while gradually changing their behavior from intrinsically quantum mechanical to classical. They willingly interact with electromagnetic fields which makes manipulation and the extraction of information easy. And finally they come in a variety of elements, so that for a wide range of demands concerning transition energy, statistics, magnetic properties, collision properties, mass, complexity etc. most often at least one element exists that satisfies the requirements.

The practical issue of cooling neutral atoms is tackled by the invention of various kinds of atom traps. Most importantly the magneto-optical trap (MOT) has lead to

an explosive growth of this field but since then a wide spectrum of traps for neutral atoms has become available [Met99]. They are tools for all sorts of experiments and consequently have evolved to a wide range of different trapping schemes and geometries. Aside from the MOT there are magnetic trapping schemes, dipole trap schemes and all sorts of hybrid traps.

In recent years a new direction in the development of traps has been established: Microtraps constitute versatile tools with useful properties that can be exploited in various physical contexts. They are an attempt to combine the well established atomic quantum system with the technologically advanced field of nanofabrication in order to be able to comply with the increasingly complex tasks of modern experiments and to develop practical applications. The possibility of loading them with coherent matter as well as the option to create such traps with either magnetic fields or light fields has already inspired many new physical questions ranging from interferometry over atom-surface interactions to quantum computing [Fol02]. While after several years the evolution of magnetic microtraps has recently culminated in the realization of BEC in these devices [Ott01, Hän01b], optical microtraps are still at the beginning of a development which can be expected to be equally vigorous.

The work reported on here constitutes a major experimental step in a development of versatile optical microtraps. Two new schemes, the focussed beam trap and the double evanescent wave trap (DEW) were experimentally demonstrated and characterized. The combination of an efficient loading mechanism with the tight confinement of the focussed beam trap allows for the creation of large and very dense atomic ensembles. The resulting conditions facilitate efficient evaporative cooling and make this trap scheme a promising approach to provide coherent degenerate matter waves in an optical microtrap environment. The DEW-trap confines the atomic ensemble in a tight and highly anisotropic potential, making it a suitable tool to reach the transition to a two-dimensional gas. Efficient evaporative cooling from this potential is used to "freeze out" the vertical motion. Combining both microtrap schemes to provide Bose-Einstein condensates in this two-dimensional environment will allow for the investigation of many interesting physical questions related to reduced dimensionality in the future.

Starting with a brief introduction of microtraps in general, Chapter 2 will discuss what properties microtraps offer and for what they are used. Chapter 3 then fills in the details that are needed to understand the particular trap schemes and the physical questions that are addressed. Various technical aspects of the experiment will be presented in Chapter 4 before the Chapters 5 and 6 discuss the measurements related to the characterization of the traps as well as to the progress that has been made with the physical goals. A summary and an outlook will finally be given in Chapter 7.

Chapter 2

Overview: Microtraps for Neutral Atoms

This short chapter intends to provide a brief overview of the properties, implementations and physical questions that are addressed with present microtrap experiments in order to set the stage for the discussion of the evanescent wave surface microtraps of this experiment. An more extensive discussion of microtraps in general can be found in [Fol02].

2.1 Properties of Microtraps

Although microtraps can result from magnetic as well as optical potentials, some general properties are found in most or all schemes. These properties are usually what makes their use appealing. We are interested in those microtraps that feature an atomic ensemble in close proximity to a material surface. The tightly confining potentials are created a short distance from material structures such as wires in free space, wires on substrates or dielectric surfaces.

Tight Confinement

Their most basic property, a small size, comes together with large field gradients of the magnetic or optical fields involved. This leads to large forces which hold atoms in tiny volumes or accurately manipulate their external motion. In magnetic microtraps the steep-gradient fields usually stem from nanofabricated current carrying structures or from thin wires and can reach values of up to 10^7 Gauss/cm [Fol02]. Optical microtraps, on the other hand, usually generate steep intensity gradients by evanescent waves on dielectric surfaces [Dow96].

The tight confinement that microtraps provide can be exploited in various ways. They facilitate the achievement of large atomic densities and therefore speed up processes

that are mediated by collisions. Furthermore they can "freeze out" external degrees of freedom of an atom gas by splitting energy levels to more than the thermal energy of the gas. And finally they are an important ingredient to make use of the so-called "dimple trick" which is the subject of discussion in Section 3.4.3.

Manipulation of External Motion

The strong forces at hand can also be used as means to accurately manipulate the external motion of an atom trapped in a microtrap. Structures such as conveyor belts for neutral atoms [Hän01c] or waveguides [Den99] have already been demonstrated and future plans envision neutral atoms trapped in interconnected waveguides on atom chips as one possible implementation of a quantum computer with many qubits. Even the controlled collision of atoms and the subsequent formation of a molecule is within the reach of microtrap schemes.

Proximity of Material Surface

As many microtrap schemes feature the proximity of a material surface at much higher temperature, the interaction of ultracold atoms with this surface has been a subject of intensive investigations (eg. [For02, Fol02]). Besides unwanted effects such as losses, heating or decoherence, the situation might provide means to connect the atomic system to its environment in a controlled way. In the context of quantum computing this might constitute a possible interface between the quantum system and the classical world.

Another consequence of the small size of microtraps that frequently caused problems and has limited their usefulness in some cases, is the difficulty to load atoms into these traps efficiently. Section 3.4.2 addresses this subject in more detail and presents a quite general loading mechanism that improves the situation for many schemes.

2.2 Implementations

Miniaturization of atom traps has lead to a wide range of different geometries and trap schemes. The ability to exert strong forces on the atoms and to manipulate the details of their motion makes the implementation of complicated designs possible. Still, within the variety of different microtraps we can distinguish two basic categories: magnetic microtraps and optical microtraps.

Magnetic Microtraps

The first magnetic microtraps were created by thin current carrying wires, whose magnetic field was superimposed with an external magnetic field to provide elongated potential minima [Den99]. Since then the technology has evolved to the present state-of-

the-art "atom chip" devices [Fol00] that feature a whole set of different trap geometries for different kinds of experiments on their surface. The availability of well established nanofabrication techniques to produce them has proven to be an important advantage of these devices. Their versatility frequently makes them appear in proposals related to quantum computers or integrated interference devices.

Another advantage of these microscopic magnetic traps is the need for much less electric power and the correspondingly eased problem of heat dissipation. Currents of few Ampères are usually sufficient to create trapping potentials of reasonable depth. The large trap frequencies achieved in magnetic microtraps along with the availability of radiofrequency evaporation has proven to be an excellent combination for the creation of Bose-Einstein condensates [Ott01, Hän01b]. The fact that now also coherent matter becomes available in magnetic microtraps offers a wide spectrum of new interesting experiments.

Due to the close proximity of conducting room temperature material many magnetic microtraps suffer from a detrimental interaction between the cold atoms and the surface. Usually this leads to reduced lifetime or heating of the atoms [For02].

Optical Microtraps

Due to the fact that the creation of an optical microtrap potential is technically more challenging than realizing a magnetic microtrap, the development of optical microtraps is still in its early stages. In this case the profound technical background of modern electronics cannot be used to devise sophisticated optical microtrap schemes. This has impeded the experimental advancement so far. However, the rising number of interesting proposals and theoretical contributions indicates a growing interest in optical microtraps and eventually will lead to a similar technical progress as experienced with the magnetic microtraps.

A class of optical microtraps, which is similar in geometry to the magnetic microtraps are the optical surface microtraps based on evanescent waves. Up to now relatively simple designs have been experimentally exploited [Gau98, Ham02a] and new proposals on integrated optical waveguides [Jr.02] have been made. Compared to magnetic microtraps, the coupling between the dielectric surface and the atoms is much weaker in optical microtraps so that even at very small distances between the atoms and the surface of about one optical wavelength heating and losses due to surface interactions are small. Another very interesting prospect for an optical microtrap are microspheres [Mab94]. Although no atom trap has been demonstrated with these devices up to now, there is extensive research on this field which makes future atom trap devices based on microspheres probable.

2.3 Physical Questions

The wide range of physical topics addressed with microtraps comes with the availability of a variety of different geometries and their useful properties. Without being complete we will name a few applications that have emerged in the past years.

Interferometry and Surface Effects

A subject that has been the main focus of magnetic wire traps and atom chips is interferometry with cold atoms or Bose-Einstein condensates. Efforts have been made to realize the basic constituents such as Y-junctions and with the availability of coherent matter in magnetic microtraps one can expect this field to produce new physical insight very soon. Especially interesting for this type of experiment are questions related to atom-surface interactions. A nice example of the possibilities and the sensitivity of microtrap schemes has been provided by researchers in Tübingen [For02] where the fragmentation of a BEC indicated very weak magnetic fields close to the substrate surface. Particularly important are the implications of surface effects for the coherence properties of cold atoms in microtrap interferometers or quantum computers based on atom chips.

Quantum Computing

Quantum information processing has recently become a hot topic of the microtrap community as microtraps might combine the advantages of slowly decohering neutral atoms with the technologically advanced field of microstructuring. This way researchers working with atom chips hope to eventually create quantum computers which are scalable and allow for the precise manipulation well established in many quantum optics systems. A detailed discussion along with suggestions for a realization can be found in reference [Fol02].

Systems with Reduced Dimensionality

The study of low-dimensional systems has been of interest ever since such systems could be realized in solid state devices and showed markedly different behavior than the usual three-dimensional systems. The fact that quantum statistical effects are strongly influenced by the dimensionality of a system has sparked various efforts to realize this situation with ultracold atoms. Microtraps, whose tight confinements are particularly suited to create environments of reduced dimensionality have been at the focus of these directions. Some initial work has been done with standing wave traps [Bou02] where atoms in the periodical microtrap potentials show altered scattering behavior, and in strongly anisotropic dipole traps that allow studies of the coherence properties in one- or two-dimensional systems [Det01, Gör01]. The double-evanescent wave surface microtrap presented in Section 3.4.5 constitutes a new way to create a two-dimensional atom gas

in a single potential well close to the material surface. It allows for efficient evaporative cooling and in the future will provide Bose-Einstein condensates in this peculiar environment. The physical implications of reduced dimensionality in the context of cesium are discussed in more detail in Section 3.6.3.

The versatility and the fast technological advancement of microtraps will certainly lead to the adding of new applications to this list in the future.

Chapter 3

Physical Background

Laser cooling experiments include a broad spectrum of physical disciplines. As atoms or sometimes molecules are the main object of interest, atomic physics can be considered its foundation. But the field has grown to include several other directions as well. Since lasers are the tool for virtually everything in this context, quantum optics is an integral part of the needed repertoire. Fundamental quantum mechanics and quantum statistics openly manifest themselves in collisional properties or quantum degeneracy and even many-body physics has emerged in this scope since laser cooling experiments can provide model systems which are theoretically and experimentally equally accessible. The following chapter intends to give an overview of how these different disciplines intersect in the context of this particular experiment, and fills in some details necessary to understand the experimental methods and results.

Atomic physics will be addressed in Section 3.1 as it introduces relevant properties of the cesium atom – our object of interest. Section 3.2 will then focus on the quantum optics part and explains the basic principles of the dipole force. Since in particular evanescent waves determine the character of our dipole traps, Section 3.3 is dedicated to their properties and implementations. How atoms and laser fields interact to create ultracold atomic ensembles near a room-temperature surface is the subject of Section 3.4. As not only interactions between atoms and photons but also between atoms themselves determine the dynamics of the system, Section 3.5 is dedicated to the issue of ultracold collisions. Finally Section 3.6 will briefly explain the BEC-state itself and what physics is expected for a two-dimensional ensemble.

3.1 Properties of the Cesium Atom

Up to today laser cooling is applicable only to the alkali atoms and a handful of other elements, such as some metastable noble gases and alkaline earth metal atoms. This is due to the fact that laser cooling heavily relies on energetically convenient closed

electronic transitions in order to achieve the large excitation rates needed to exert sufficiently strong forces on an atom. Although magnetic traps or some dipole trap schemes such as CO_2-laser traps in principle are able to hold also other elements, complete trap schemes are rarely realized. This is because the magneto-optical trap (MOT) as a crucial intermediate trapping and cooling step is not available.

The gravito-optical surface trap (GOST) experiment is dedicated to cooling, trapping and investigating cesium-133. It is the heaviest of all stable alkali atoms and as in lithium, sodium, potassium and rubidium the outer $6S_{1/2}$-electron determines electronic transitions and collisional dynamics. However, due to its large mass, fine-structure and hyperfine-structure are much more pronounced. Figure 3.1 shows the relevant part of the cesium level scheme.

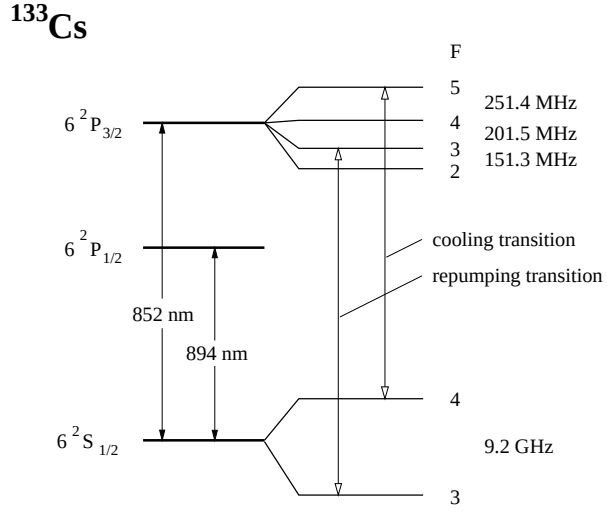

Figure 3.1: *Overview of the Cs D-transitions*

The 133 nucleons couple to a nuclear spin of $I = 7/2$ and in combination with the 55 electrons make cesium-133 a boson. The $6^2S_{1/2}$ ground-state is split into two hyperfine levels ($F = 3, 4$) which are energetically separated by the well known 9.18 GHz determining the modern time standard. The excited $6^2P_{3/2}$ state features four closely spaced hyperfine states ($F' = 2, \ldots, 5$) and its lifetime of 30.6 ns leads to a natural line width of the $6^2S_{1/2} \rightarrow 6^2P_{3/2}$ transition of $\Gamma_{3/2}/2\pi = 5.22$ MHz. The $6^2P_{1/2}$ state with its two hyperfine states ($F' = 3, 4$) has a lifetime of 35.1 ns which leads to a natural line width of the $6^2S_{1/2} \rightarrow 6^2P_{1/2}$ transition of $\Gamma_{3/2}/2\pi = 4.56$ MHz. Indicated are the closed cooling transition $F = 4 \rightarrow F' = 5$ at 852.12 nm and the repumping transition $F = 3 \rightarrow F' = 3$. For most considerations in this context the D_1 line at 894.3 nm can completely be ignored.

3.2 Optical Dipole Potential

The interaction of light with atoms can be categorized in two different regimes that can both be understood by simple intuitive pictures.

The *radiation pressure force* arises from repetitive cycles of absorption and subsequent emission of photons by an atom. During many such cycles a net average momentum is transferred onto the atom and consequently leads to a force that is exploited in a MOT or a Zeeman slower. This force can create accelerations of up to $10^6\,\mathrm{m/s^2}$ (for cesium) but has the disadvantage of heavily disturbing the atomic state. It is in general stronger the closer the laser frequency ω is to the atomic transition frequency ω_0. The difference $\omega_0 - \omega$ is called detuning δ and will play an important role in the following considerations. The radiation pressure force will not be the object of discussion from hereon as it plays a minor role for the experiment and the literature extensively covers this topic ([Met99]).

At sufficiently large laser detuning the radiation pressure force tends to become weak and the *optical dipole force* takes over as the dominant interaction mechanism. To get an intuitive picture of the dipole force it is sufficient to consider the classical model of an atom with a harmonically bound electron (Lorentz model). All important effects manifest themselves in this model and in the case of alkali atoms even quantitative statements can be made up to a good accuracy [Ask62, Kaz73, Coo79, Gor80].

When a polarizable atom is introduced into an electrical field, the field will induce an electric dipole moment in the atom by pulling on its electron. The same happens in case of a laser field except for the fact that this leads to an oscillating dipole moment instead of a static one. The potential energy of the atomic dipole inside the field can be written as

$$U_{dip} = -\frac{1}{2}\langle \vec{p} \cdot \vec{E} \rangle, \tag{3.1}$$

where $\vec{p}$ is the induced dipole moment and $\vec{E}$ the electric field. The factor $1/2$ takes into account that the dipole moment is induced and thus energy for its creation has to be provided. In case of a resonant excitation of the dipole oscillation with the harmonic frequency ω_0 (which is equal to the atomic transition frequency in the Lorentz model) the dipole oscillation is shifted by a phase of $\pi/2$ with respect to the driving field and thus the time average $\langle \vec{p} \cdot \vec{E} \rangle$ vanishes. In case of a driving field frequency below (red detuning) or above (blue detuning) the atomic frequency, U_{dip} takes a negative (red detuning) or positive (blue detuning) value. An intensity gradient of the laser field now translates into a dipole force on the atom and in particular will lead to an attractive force if it is red-detuned and to repulsive force for blue detuning. Since the dipole force is derived from a potential it is a conservative force and hence the need for a MOT or other dissipative mechanisms to load a dipole trap. In addition to this dispersive part of the dipole force there is an absorptive component that leads to photon scattering and thus introduces a non-conservative part to the force. These incoherent processes will either lead to

heating through transfer of photon momentum or else to cooling through dissipative mechanisms as for instance the evanescent wave Sisyphus cooling described in Section 3.3. The absorptive part can easily be included in the Lorentz model by introducing damping. A complete classical treatment that calculates the atomic polarizability $\alpha(\omega)$ using the equation of motion of a damped harmonic oscillator finally yields expressions for the dipole potential U_{dip} and the photon scattering rate Γ_{sc} for the case of a two-level atom at large detuning (i.e. low saturation) [Gri00]:

$$U_{dip}(\vec{r}) = \frac{3\pi c^2}{2\omega_0^3} \cdot \left(\frac{\Gamma}{\omega_0 - \omega} + \frac{\Gamma}{\omega_0 + \omega} \right) \cdot I(\vec{r}), \tag{3.2}$$

$$\Gamma_{sc}(\vec{r}) = \frac{3\pi c^2}{2\hbar\omega_0^3} \cdot \left(\frac{\omega}{\omega_0} \right)^3 \cdot \left(\frac{\Gamma}{\omega_0 - \omega} + \frac{\Gamma}{\omega_0 + \omega} \right)^2 \cdot I(\vec{r}). \tag{3.3}$$

ω_0 denotes the atomic transition frequency, Γ the damping rate, ω the actual laser frequency and $I(\vec{r})$ the position dependent laser intensity. In most practical cases where the absolute value of the detuning $\delta \equiv \omega - \omega_0$ is much smaller than ω_0 the contribution from the so-called counter rotating term $\Gamma/(\omega_0 + \omega)$ can be neglected and the equations take the simplified form:

$$U_{dip}(\vec{r}) = \frac{3\pi c^2}{2\omega_0^3} \cdot \left(\frac{\Gamma}{\delta} \right) \cdot I(\vec{r}), \tag{3.4}$$

$$\Gamma_{sc}(\vec{r}) = \frac{3\pi c^2}{2\hbar\omega_0^3} \cdot \left(\frac{\Gamma}{\delta} \right)^2 \cdot I(\vec{r}). \tag{3.5}$$

The valid relation $\hbar\Gamma_{sc} = \Gamma/\delta \cdot U_{dip}$ reveals the intimate connection between dispersive and absorptive part of the dipole force.

To get from this simplified classical model to a correct quantum mechanical expression one merely has to replace the classical result of the damping rate Γ with the quantum mechanical transition rate

$$\Gamma = \frac{\omega_0^3}{3\pi\epsilon_0\hbar c^3} \cdot |\langle e|\hat{p}|g\rangle|^2. \tag{3.6}$$

$\langle e|$ and $\langle g|$ are the excited state and the ground state of the two level system. They are coupled by the dipole operator $\hat{p}$. An important feature of the dipole force is its scaling with intensity and detuning. Notably U_{dip} scales as I/δ whereas Γ_{sc} goes as I/δ^2. Dipole traps exploit this fact by operating at large detunings and large intensities as this shifts the balance between heating and potential depth in favor of potential. Therefore at very large detunings dipole traps are to a good approximation conservative traps.

All considerations up to now were limited to the case of a two-level system. And in spite of its usefulness for certain approximations, in some special cases of multi-level atoms and laser detunings a more general model which gives credit to the atomic

substructure is needed. As a realistic atom with many electronic transitions, fine structure, hyperfine structure and magnetic sublevels constitutes a prohibitively complicated system, one cannot avoid making certain simplifications and approximations to obtain useful results.

A useful concept to arrive at expressions for light potentials for multilevel atoms is to calculate the perturbative shift of the ground-state in the presence of a light field (AC-Stark shift). Since the detuning is assumed to be large and thus saturation is negligible, the spatially dependent shift of the atomic ground-state can be regarded as a potential the atom is moving in [Dal85]. Quantum mechanics provides an expression for this shift which is of second order in the driving field and therefore goes linear with intensity:

$$\Delta E_g = \sum_{g \neq i} \frac{|\langle i|e\hat{r} \cdot \vec{E}|g\rangle|^2}{\epsilon_g - \epsilon_i}. \tag{3.7}$$

ϵ_g and ϵ_i are the energies of ground- and excited state, $\vec{E}$ is the classical electrical field and $\hat{r}$ is the quantum mechanical position operator. In order to find the actual shift for the ground-state $|g\rangle$ one has to determine all relevant matrix elements $\langle i|e\hat{r}\cdot\vec{E}|g\rangle$ and sum up their contributions. This can still be a formidable task. Life becomes considerably easier as one limits the discussion to alkali atoms and distinguishes between certain cases of different detunings. Omitting any details and referring to the literature [Gri00] we summarize two cases of relevance for this particular dipole trap.

In case of a linearly polarized light field with a detuning large compared to the hyperfine splitting of the excited state but small compared to the fine structure splitting between D_1 and D_2 line, the dipole potential is given by the expression:

$$U_{dip}(\vec{r}) = \frac{\pi c^2}{2} \cdot \left(\frac{\Gamma_2}{\omega_2^3} \frac{2}{\delta_2} + \frac{\Gamma_1}{\omega_1^3} \frac{1}{\delta_1} \right) \cdot I(\vec{r}). \tag{3.8}$$

δ_1 (δ_2), Γ_1 (Γ_2) and $\omega_1/2\pi$ ($\omega_2/2\pi$) are detuning, natural line width and frequency of the D_1 (D_2) transition. Due to the ω^3 dependence of Γ (see Equation 3.6) we find that

$$\frac{\Gamma_1}{\omega_1^3} \approx \frac{\Gamma_2}{\omega_2^3}, \tag{3.9}$$

and thus can simplify Equation 3.8 to yield the following expression:

$$U_{dip}(\vec{r}) = \frac{\pi c^2 \Gamma_2}{2\omega_2^3} \cdot \left(\frac{2}{\delta_2} + \frac{1}{\delta_1} \right) \cdot I(\vec{r}). \tag{3.10}$$

If additionally the laser frequency is much closer to the D_2 line than to the D_1 line, this can further be simplified to yield the final expression applicable for both blue-detuned evanescent waves and the hollow beam introduced in Section 3.4.1:

$$U_{dip}(\vec{r}) = \frac{\pi c^2 \Gamma_2}{\omega_2^3 \delta_2} \cdot I(\vec{r}). \tag{3.11}$$

Note that this is just the result of a two-level atom times 2/3. This factor can be viewed as a weight factor that takes into account the line strength of the D_2 line compared to the D_1 line.

At even larger detunings a different approximation has to be used. When the laser light satisfies the condition that the detunings with respect to both D lines greatly exceed the fine structure splitting of $\Delta\lambda_{FS} = 42\,\mathrm{nm}$ both transitions have to be taken into account. However, one can model the system as a two-level atom with an effective transition defined by the weighted average of both D lines:

$$\omega_{eff} = \frac{2}{3}\omega_2 + \frac{1}{3}\omega_1, \tag{3.12}$$

and a weighted line width defined by

$$\Gamma_{eff} = \frac{2}{3}\Gamma_2 + \frac{1}{3}\Gamma_1 = 2\pi \cdot 4.98\,\mathrm{MHz}. \tag{3.13}$$

Contrary to the considerations for small detunings, one can usually not neglect the counter rotating term in this case. For a laser at 1064 nm ($D_1 : \Delta\lambda = 170\,\mathrm{nm}$, $D_2 : \Delta\lambda = 212\,\mathrm{nm}$) which is used to create the attractive microtrap potentials the contribution of this term is 16%. Finally U_{dip} turns out to be:

$$U_{dip}(\vec{r}) = -\frac{3\pi c^2}{2\omega_{eff}^3} \cdot \left(\frac{\Gamma_{eff}}{\omega_{eff} - \omega} + \frac{\Gamma_{eff}}{\omega_{eff} + \omega} \right) \cdot I(\vec{r}). \tag{3.14}$$

The formulas given above are valid for linearly polarized light only. Circular polarization leads to correction terms that shift the different Zeeman sublevels similar to the magnetic Zeeman shift. Still, the average level shift is equal to the value for the shift caused by linearly polarized light.

Except for the evanescent waves, each light field involved in any of the dipole traps is linearly polarized. But because the evanescent wave beams have their electric field vector oscillate along the plane of incidence (TM-polarization) there are small modifications to the expression for U_{dip}. We still use the result for the linear case as it is a sufficiently good approximation and experiments have not indicated any significant m_f-state dependence.

3.3 Evanescent Waves

Evanescent waves are a characteristic feature of all three dipole trap designs introduced in the next section. We create an evanescent wave by total internal reflection of a laser beam at the vacuum-dielectric interface of a fused-silica prism (see inset of figure 3.3). It offers two important features that make it a very useful tool. Firstly the intensity gradient of an evanescent wave is extremely large. As the light field drops exponentially

in a distance of the order of the optical wavelength the resulting dipole force is very large and allows for the realization of nearly ideal hard wall potentials or other wavelength-sized potential wells (see Section 3.4.5).

Secondly one finds that in the case of a multi-level atom the reflection from an evanescent wave can be inelastic and lead to cooling. Confining atoms in the gravito-optical potential created by an evanescent wave and earth' gravitational field can under certain circumstances include a so-called Sisyphus cooling process and provide a useful trapping scheme to create cold and dense atomic samples near a material surface. Section 3.4.1 will provide details on the realization of this idea.

When a light field is refracted at the interface between a dielectric medium and vacuum, the angle of refraction is determined by Snell's law:

$$n \cdot \sin \Theta_i = \sin \Theta_t. \tag{3.15}$$

Θ_i and Θ_t denote the angle of incidence and the angle of refraction while n is the index of refraction of dielectric medium (in our case $n = 1.45$). At a particular angle of incidence Θ_{crit} the left hand side of the equation becomes 1 and all incident light is totally internally reflected back into the dielectric medium. As obviously the electric field of the light wave cannot drop to zero instantaneously across the surface we have to take a closer look at what is happening at this boundary as $\Theta_i \geq \Theta_{crit}$. In this case Equation 3.15 can still be obeyed when we allow Θ_t to take complex values. One finds (see e.g. reference [Bor91]) that for angles $\Theta_i \geq \Theta_{crit}$ a light wave propagates inside the vacuum along the dielectric-vacuum interface with its field amplitude exponentially declining with distance from the interface. The mathematical expression for the electric field component of this evanescent wave takes the following form [Bou94]:

$$\vec{E}_t(\vec{r}, t) = \varepsilon_t \cdot \vec{\epsilon}_t \cdot e^{-z/\Lambda} \cdot e^{i(k_t x - \omega_L t)}. \tag{3.16}$$

ε_t denotes the electric field amplitude and $\vec{\epsilon}_t$ the polarization vector. Λ is the $1/e$-decay length of the evanescent wave and can be computed using the relation

$$\Lambda = \frac{\lambda}{2\pi\sqrt{n^2 \sin^2 \Theta_i - 1}}. \tag{3.17}$$

λ represents the wavelength of the incident light. The exponential factor $\exp(ik_t x - i\omega_L t)$ is the phase of a plane wave propagating along x, the coordinate defined by the intersection of the surface plane with the plane of incidence. $\omega_L/2\pi$ is the frequency of the light and k_t the evanescent wave's wave number determined by $k_t = 2\pi n/\lambda \cdot \sin \Theta_i$.

In order to find expressions for the electric field amplitude ε_t and the polarization vector $\vec{\epsilon}_t$ that characterize the evanescent wave, one has to match incident and evanescent wave at the boundary. Since we are particularly interested in the intensity I_t of the evanescent wave the following results have been written accordingly. The results are limited to the two relevant cases of polarization $\vec{\epsilon}_i$ perpendicular (TE) and parallel (TM) to the plane of incidence.

TE-polarization

In this case the polarization of the evanescent wave matches that of the incident light

$$\vec{\epsilon}_t = \vec{\epsilon}_i, \tag{3.18}$$

and the expression for I_t takes the following simple form:

$$I_t = \frac{4n\cos^2\Theta_i}{n^2-1} \cdot I_0. \tag{3.19}$$

I_0 is the intensity of the light before it enters the prism. Equation 3.19 assumes that the laser enters the prism perpendicular through an anti-reflection coated face. Note that since the first factor in Equation 3.19 can be larger than one, the intensity of the evanescent wave and thus also the dipole potential can exceed that of the incident beam.

TM-polarization

The calculations in this case turn out to be more complex and yield the following expressions [Bou94]:

$$\vec{\epsilon}_t = \frac{1}{\sqrt{2n^2\sin^2\Theta_i - 1}}(n\sin\Theta_i\vec{e}_z - i\sqrt{n^2\sin^2\Theta_i - 1}\vec{e}_y), \tag{3.20}$$

$$I_t = \frac{4n\cos^2\Theta_i}{n^2-1} \cdot \frac{2n^2\sin^2\Theta_i - 1}{(n^2+1)\sin^2\Theta_i - 1} \cdot I_0. \tag{3.21}$$

The polarization of the evanescent wave is elliptic now with a phase-shifted component perpendicular to the surface of the prism. According to Section 3.2 this leads to ground-state potentials that depend on the value of the magnetic quantum number m_F. The evanescent wave's intensity however, is still larger than in the case of TE-polarization and therefore it is favorable to use this configuration in the experiment in order to maximize the dipole potential. Figure 3.2 shows the $1/e^2$-decay length Λ of intensity as a function of the deviation $\Delta\Theta$ from the critical angle $\Theta_{crit} = 43.6°$ (upper graph) and the intensity ratio I_t/I_0 for TM- (solid line) and TE-polarization (dotted line) as a function of $\Delta\Theta$. The vertical dashed line indicates a $\Delta\Theta$ of 1° as used with the near-resonant evanescent wave. In this case we find Λ to be $0.71\,\mu$m and a ratio I_t/I_0 of 5.40.

The complete vertical potential an atom experiences, is a combination of gravity, the dipole potential of the evanescent wave and at extremely short distances from the prism surface ($\sim 0.1\,\mu$m) the attractive Van-der-Waals interaction between the atom and the dielectric surface. Their effects will be discussed in the following two subsections.

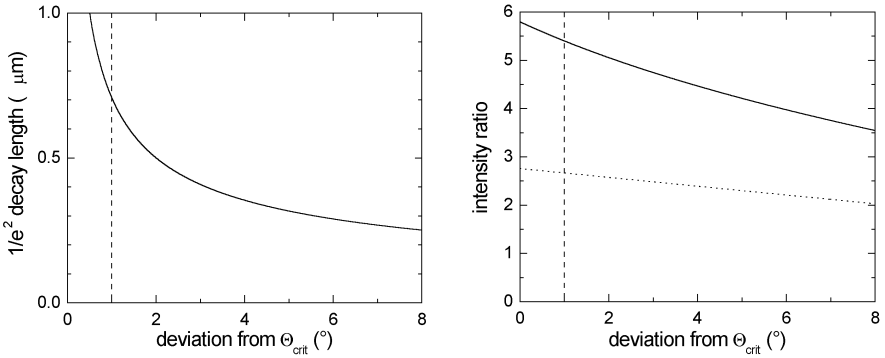

Figure 3.2: *Decay length Λ and enhancement factor I_t/I_0 versus deviation from critical angle.*

Van-der-Waals interaction

The attractive Van-der-Waals force arises from the electromagnetic interaction of an atomic dipole with its mirror image on the dielectric surface. The multilevel structure of the atom, retardation effects and QED corrections make this seemingly simple system interesting but also rather complicated to treat exactly [Har91, Wyl84]. For our purposes it is sufficient to use certain approximations: Firstly we will model the cesium atom as a two-level atom with an effective transition wavelength $\lambda_{eff} = 866\,\mathrm{nm}$. This corresponds to an approach where we disregard any atomic structure except for the D-transition and furthermore replace both individual contributions by their weighted average (see Section 3.2). In addition to that, we will separately treat both distance regimes ($z \ll \lambda_{eff}/(2\pi)$ and $z \gg \lambda_{eff}/(2\pi)$) and use an approximate expression to match them in their transition region. Finally most expressions derived in the literature refer to the case where the surface is perfectly conducting. One can reasonably well describe the dielectric case by simply multiplying the conducting surface results with the expression $(n^2-1)/(n^2+1)$. n denotes the index of refraction of the dielectric. This implicitly assumes, that no resonances of the dielectric coincide with any atomic resonances.

In the case of the atom being very close to the dielectric surface we find a relatively simple expression describing the Van-der-Waals potential. This regime is called Lennard-Jones regime and for the two-level approximation of the cesium atom can be accurately described by the following expression [Cou96]:

$$U_{VdW}(z) = -\frac{n^2-1}{n^2+1}\frac{3}{16}\hbar\Gamma_{eff}\left(\frac{1}{k_{eff}z}\right)^3 = 5.44\cdot 10^{-49}\,\mathrm{kgm^5/s^2}\cdot z^{-3}. \tag{3.22}$$

$\Gamma_{eff}/2\pi = 4.98\,\mathrm{MHz}$ and k_{eff} denote the line width and the wave number of the effective transition.

If the distance z between atom and surface is much larger than $\lambda_{eff}/2\pi$ the surface attraction is proportional to z^{-4} and the regime is called Casimir-Polder regime [Cas48]. In this case relativistic corrections and QED effects significantly modify the classical result and usually don't allow for simple analytical expressions [Wyl84]. Numerical values for U_{VdW} are tabulated in reference [Mar97]. Using this data to find a complete expression for the two-level atom close to a dielectric surface which accurately describes the Lennard-Jones regime and reasonably well approximates the Casimir-Polder regime yields

$$U_{VdW}(z) = -\alpha_{VdW} z^{-3}(1 + 2\pi z/\lambda_{eff})^{-1}, \tag{3.23}$$

with the coefficient $\alpha_{VdW} = 5.44 \times 10^{-49}\,\mathrm{kg\ m^5 s^{-2}}$.

Since atoms usually don't penetrate very far into the repulsive evanescent wave light field, their trajectories are hardly influenced by the Van-der-Waals attraction. Its only significant effect is a reduction of the height of the total potential barrier.

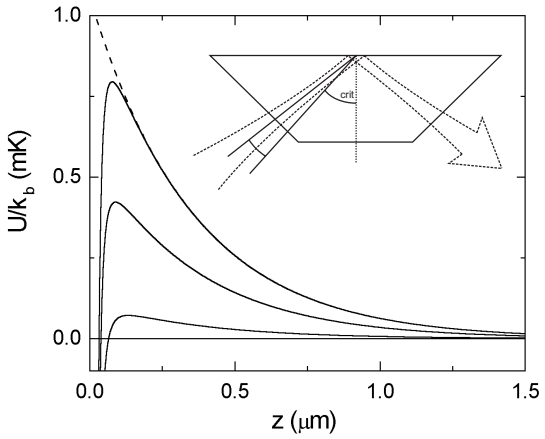

Figure 3.3: *Potential curves for the dipole repulsion alone (dashed line) and the combined potential of dipole repulsion and Van-der-Waals attraction for the three laser powers 45 mW, 25 mW and 5 mW. The other experimental parameters were* $\Delta\Theta = 1°$, $\delta_{EW}/2\pi = 3$ *GHz and* $w = 700\,\mu m$.

Figure 3.3 shows a plot of the combined potential of Van-der-Waals attraction and dipole repulsion for different laser intensities. At the parameters $\Delta\Theta = 1°$, $I_0 = 45\,\mathrm{mW}$, $\delta_{EW}/2\pi = 3\,\mathrm{GHz}$ and a waist of $w = 700\,\mu\mathrm{m}$ the potential barrier of $U/k_B = 795\,\mu\mathrm{K}$ is 75 % of the value without Van-der-Waals attraction. At lower intensity (or larger detuning) the surface attraction becomes increasingly important until at $I_0 \approx 0.1\,\mathrm{mW}$ the potential barrier vanishes completely.

Gravitation

Adding gravitation to this combined evanescent wave potential results in a potential that vertically traps the atoms. It is given by the expression:

$$U(z) = mgz + \hat{U}_{dip} e^{-2z/\Lambda} + U_{VdW}(z). \tag{3.24}$$

m and g denote the mass of the cesium atom the gravitational acceleration respectively. $\hat{U}_{dip}(z)$ is the maximum value of the dipole potential and $U_{VdW}(z)$ the expression given by 3.23.

Releasing atoms into this potential well will result in a bouncing motion. For cesium atoms the thermal energy of $k_B T = 1\,\mu\mathrm{K}$ corresponds to a bounce height in the gravitational potential of $z_0 = k_B T/mg = 6.4\,\mu\mathrm{m}$ whereas the range of the dipole potential is only about $1\,\mu\mathrm{m}$. This justifies the approximation of this potential by a wedge-shaped potential in certain cases. In general this approximation is better the higher the ensemble temperature is. The eigenenergy of the n-th mode in this idealized potential is given by [Wal92]

$$E_n = \hbar\omega_v \left(n - \frac{1}{4}\right)^{2/3}, \tag{3.25}$$

with $\omega_v = (9\pi^2 m g^2/8\hbar)^{1/3}$ being the characteristic frequency of the system. For cesium atoms one finds $\omega_v/2\pi = 2080\,\mathrm{Hz}$ which corresponds to an energy of $\hbar\omega_v/k_B \approx 95\,\mathrm{nK}$. For low temperatures the approximation of a hard wall potential is less accurate (see Section 5.2). A numerical calculation of the trap frequency then yields a value of $\omega_v/2\pi \approx 1.1\,\mathrm{kHz}$ and thus a corresponding temperature of only $\hbar\omega_v/k_B \approx 50\,\mathrm{nK}$.

Assuming a classical trajectory for the atom, one can derive the rate for spontaneous photon scattering during one reflection by integrating the intensity dependent scattering rate over the trajectory of the atom in the repulsive light field. The probability p_{sp} for such an incoherent reflection process is in general (at negligible saturation) small and given by [Söd95]:

$$p_{sp} = \frac{m\Lambda\Gamma}{\hbar\delta} v_\perp. \tag{3.26}$$

$v_\perp$ denotes the velocity component perpendicular to the dielectric surface. In order to derive the average photon scattering rate $\bar{\Gamma}_{sc}$ this result has to be multiplied by the bounce rate Γ_b.

$$\bar{\Gamma}_{sc} = p_{sp} \cdot \Gamma_b = \frac{m\Lambda\Gamma}{\hbar\delta} v_\perp \cdot \frac{g}{2v_\perp} = \frac{mg\Lambda\Gamma}{2\hbar\delta}. \tag{3.27}$$

Notably this result is independent of the vertical velocity of the atom which is a special feature of the exponential evanescent wave potential. The reduced scattering probability of an atom with a small vertical velocity is exactly compensated by its increased bounce rate. A simple calculation shows that this result is even valid for the extreme case of zero temperature where atoms stay motionless in the potential minimum.

3.4 Optical Surface Microtraps

This section introduces the concept of optical surface microtraps whose interesting properties are the main focus of this thesis. It starts with a explanation of the gravito-optical surface trap and discusses how its large trap volume and the efficient optical cooling mechanism provide a dense and cold reservoir ensemble for the consecutive microtrap stages. The interesting issue of loading these conservative microtraps is presented in Section 3.4.2 before Section 3.4.3 explains how the reservoir and the loading process can be combined to exploit the so-called dimple trick. Two implementations of optical surface microtraps realized in this experiment are introduced in sections 3.4.4 and 3.4.5 before Section 3.4.6 summarizes the relevant properties of the different trap schemes.

3.4.1 The Reservoir: Gravito-optical Surface Trap

At this point we summarize all relevant properties of the GOST. The trap has been extensively studied and discussed in a previous thesis [Man99]. It is used as a tool to provide a dense and cold reservoir of cesium atoms close to the dielectric surface. The subsequent microtrap stages draw atoms from this ensemble during the loading process and later replenish losses from it.

The GOST is a trap whose confinement results from a combination of dipole potentials and gravity. Its shape is that of a cylindrical container and its walls consist of repulsive light fields. Atoms are loaded into this trap by steering an atomic cloud prepared in a MOT to a position inside the trapping volume and releasing them. Gravity then pulls the atoms into the GOST where a Sisyphus cooling process based on inelastic collisions from the bottom light field starts to dissipate away most of their energy. This scheme allows for the preparation of more than 20 million cesium atoms at a temperature of less than ten microkelvin, leading to atomic densities of about $10^{12}\,\mathrm{cm}^{-3}$. This section will explain in some detail the potentials, then discuss the Sisyphus cooling mechanism and finally summarize important ensemble properties in this trap.

Confinement

Vertical confinement in the GOST is provided by the gravito-optical potential discussed in the previous section. The evanescent wave is blue-detuned by initially 3 GHz with respect to the $F = 3 \rightarrow F'$ transition, has a power of 45 mW and a $1/e^2$-intensity radius of 0.7 mm. Being incident at $\Theta_i = 44.6°$ (1° deviation from Θ_{crit}) and TM-polarized, this amounts to a total potential in the center of the evanescent wave spot of $U/k_B = 780\,\mu\mathrm{K}$ including Van-der-Waals interaction. The potential barrier is sufficient to repel atoms that are released from a height of almost 5 mm.

Without any horizontal confinement atoms would escape from the trap within milliseconds due to their lateral velocity and diffuse reflections from the evanescent wave

atom mirror. Horizontal confinement is realized by a repulsive light field with a ring shaped cross section at the prism surface (hollow beam). An axicon optic (see Section 4) creates this 820 μm wide (diameter) perimeter of about 20 μm thick light walls that are placed concentrically on the evanescent wave spot and complete the 3D-confinement of the GOST. The hollow beam contains about 400 mW of $1.6 - 3$ nm detuned light, is linearly polarized and creates a potential barrier of up to $U/k_B = 93\,\mu$K. This potential is not very large compared to the approximately 80 μK that atoms gain during a fall from a height of 0.5 mm. Thus the need arises for fast dissipation of this gravitational energy before it is coupled from the initially vertical motion into the horizontal plane and leads to trap loss through the hollow beam walls. The detuning of the hollow beam is much larger than the 3 GHz of the evanescent wave because its comparably small intensity gradient allows atoms to penetrate deep into the light walls where they would be subject to strong photon scattering and thus heating if the detuning was small. The photon scattering rate at the center of the hollow beam wall is around 100 photons per second but since an atom stays most of the time in the dark inner region of the trap where virtually no photon scattering occurs the average value is much below that. Figure 3.4 shows the geometry of the vertical and horizontal potential of the GOST.

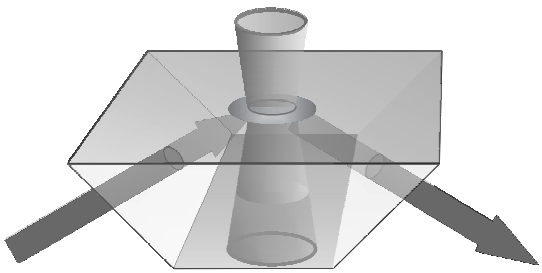

Figure 3.4: *Scheme of the GOST*

Vertically the combination of the hard repulsive wall of the evanescent wave and the long-ranged gravity create a wedge-shaped potential while the hollow beam confines the atoms in a cylindrical box potential. It is evident that the huge trapping volume of the GOST which is of the order of cubic millimeters along with its advantageous property of holding atoms undisturbed by light in dark inner regions of the trap, favors trapping of large and dense atomic ensembles. A challenge that remains, is how to load atoms into the trap and getting rid of transfer energy that originates from releasing atoms at a distance from the trap minimum.

Cooling

A central feature of the GOST is the aforementioned Sisyphus cooling mechanism. Its cooling is based on inelastic reflections of the atoms from the evanescent wave which transfers vertical kinetic energy into internal degrees of freedom and then radiates this excess energy away using a repumping process. Figure 3.5 explains the details of the cooling cycle.

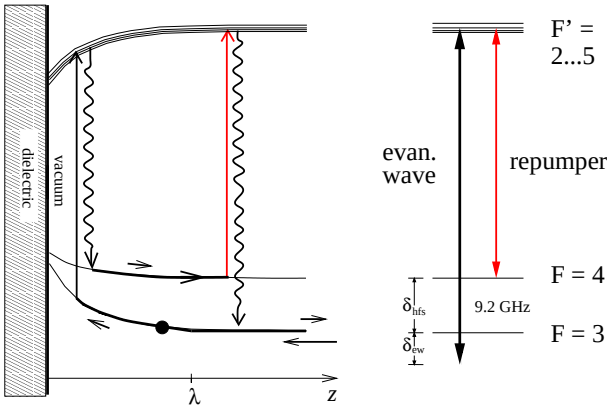

Figure 3.5: *Sisyphus cooling process in the GOST*

Shown is a simplified level scheme of the two ground-states ($F = 3, 4$) and the excited state manifold with their corresponding light shifts in the field of the evanescent wave. The evanescent wave detuning with its 3 GHz is small enough to resolve the hyperfine splitting of the ground-state while being large in comparison to the splitting of the $6\,P_{3/2}$ state. This justifies the simplification of a three level atom. As atoms are predominantly kept in their absolute ground-state manifold ($F = 3$) an atom will likely enter the evanescent wave in this state during a reflection process. Due to the repulsive force of the light field it has to climb a potential hill and in most cases is reflected coherently by the dipole potential. This process is entirely elastic, occurs at a rate of about 1 kHz and neither leads to cooling nor to heating of the atom. But with a small probability the atom will be excited into the $6\,P_{3/2}$ state by an evanescent wave photon during its passage through the intense region of the light field. It will stay in this state for about 30 ns without significantly moving and will then deexcite into either the $|F = 3\rangle$ state or the $|F = 4\rangle$ state. Returning into the $|F = 3\rangle$ state constitutes a heating process as a photon recoil energy is deposited on the atom. The interesting case is the deexcitation into the upper $|F = 4\rangle$ state. In this case the atom leaves the evanescent wave light field on a less strongly curved potential because the detuning of the evanescent wave laser is larger by 9.18 GHz with respect to the $F = 4 \rightarrow F'$ transition. This optical pumping process therefore transferred vertical kinetic energy into internal energy of the atom and damped its mechanical motion. The average loss

of vertical kinetic energy during such a cooling reflection is found to be [Söd95]:

$$\frac{\Delta E_\perp}{E_\perp} = -\frac{2}{3} \cdot \frac{\delta_{Hfs}}{\delta_{Hfs} + \delta_E W} \approx 0.5. \tag{3.28}$$

$\Delta E_\perp / E_\perp$ is the relative loss of vertical kinetic energy, δ_{Hfs} the hyperfine structure splitting and δ_{EW} the detuning of the evanescent wave. To prevent the release of internally stored energy back into the atomic motion and to prepare the atom for another such cooling process the cycle is closed by a repumping laser. This very weak laser resonant on the $F = 4 \rightarrow F' = 4$ transition pumps the atom back into the $|F = 3\rangle$ ground-state and thereby makes it transfer the internal energy into photon energy. It is important that the repumping process does not occur while the atom is still inside the light field because this would impede the cooling process. The probability for such a premature repumping is however small since the repumping laser is weak and the light of the evanescent wave shifts the atom out of resonance. It is now straightforward to arrive at expressions for the cooling rate β and the limit temperature T_{min}. Once the atoms are released into the GOST with their excess gravitational energy the cooling process starts to dissipate away this energy and continues until an equilibrium between cooling through this Sisyphus process and heating by the inherent photon scattering is reached. To get an expression for the temperature limit one sets cooling and heating rate equal and solves for the temperature T_{min}. The cooling rate is the product of the probability of an incoherent reflection the relative energy dissipated and the reflection rate of the atoms. This leads to the expression [Söd95]:

$$\beta = p_{cool} \cdot \frac{\Delta E_\perp}{E_\perp} \cdot \nu_{refl} = \frac{q}{3} \cdot \frac{\delta_{Hfs}}{\delta_{EW}} \cdot \frac{mg\Lambda}{\hbar(\delta_{EW} + \delta_{Hfs})} \cdot \Gamma. \tag{3.29}$$

p_{cool} denotes the probability of an incoherent reflection, ν_{refl} the reflection rate and q is the probability of a scattering process ending in the upper hyperfine state (0.25). m is the cesium mass, Λ the decay length of the evanescent wave and Γ the natural line width of the transition. At a detuning of 3 GHz and an evanescent wave decay length of 0.71 μm β results to be 1.62 s^{-1}.

To get an expression for the heating rate we first have to find the heating arising from a single scattering event. Reference [Min87] states that at large detunings the increase of thermal energy due to one scattered photon equals the recoil energy of the photon

$$E_{rec} = \frac{\hbar^2 k^2}{2m} = \frac{k_B T_{rec}}{2}. \tag{3.30}$$

The desired expression for the heating rate can now easily be derived by counting the number of scattered photons per cooling reflection multiplying this number with the increase in temperature and finally multiplying it with the rate at which such a process

occurs. The final result for the temperature limit then becomes:

$$T_{min} = \left(\frac{1}{q} + \frac{1}{q_r}\right) \cdot \left(1 + \frac{\delta_{EW}}{\delta_{Hfs}}\right) \cdot T_{rec}. \tag{3.31}$$

q_r denotes the branching ratio of a transition from the $|F' = 4\rangle$ state into the absolute ground-state $|F = 3\rangle$. With $q_r = 0.34$ and $\delta_{EW}/2\pi = 3\,\mathrm{GHz}$ we find a theoretical temperature limit of about $2\,\mu\mathrm{K}$.

In addition to the Sisyphus cooling process the ensemble temperature is influenced by a few other contributions. Firstly the fact that repumping photons are predominantly absorbed while an atom is bouncing upwards leads to a geometric cooling in the same way that the absorption of photons from the evanescent wave leads to a heating due to the directional nature of this light field. Secondly heating through photons from the hollow beam slightly increases the limiting temperature and finally a photon reabsorption process in dense atomic samples gives rise to an atom number dependent increase of the equilibrium temperature [Ham99].

Note that the Sisyphus cooling process only works on the vertical motion of the atom. Overall cooling is then mediated through coupling of horizontal and vertical motion by elastic collisions and diffuse reflections from the evanescent wave. In case of a further detuned hollow beam ($\Delta\lambda$ up to 3 nm) the reduced potential can allow for plain evaporation from the trap and cooling will be due to a combination of Sisyphus and plain evaporative cooling. For large atomic samples of more than 10^7 atoms we find experimentally that the temperatures are in the range of $5 - 10\,\mu\mathrm{K}$ depending on the detuning and intensity of the hollow beam.

Ensemble Properties

Assuming thermal equilibrium of the atomic ensemble one can derive expressions for the needed thermodynamical quantities. The number density is of particular interest as it for instance determines via the elastic scattering rate the pace at which evaporative cooling can take place. The position dependent density is given by a basic expression from statistical physics:

$$n(\vec{r}) = \hat{n} \cdot \exp\left(\frac{U(\vec{r})}{k_B T}\right). \tag{3.32}$$

$U(\vec{r})$ is the local potential and $\hat{n}$ a normalization constant. $\hat{n}$ is chosen such that the density is normalized to satisfy $N = \int n(\vec{r}) dV$. In the following we will assume the ideal potential shapes of a box potential horizontally and a hard wall potential in case of the evanescent wave. For the temperatures that one deals with in the GOST this approximation is sufficient. However as temperatures fall below $1\,\mu\mathrm{K}$ certain refinements of the model become necessary as we will see in Section 5.2. Due to the box-like potential

laterally, the density is constant in this direction and one arrives at an expression for n that only depends on the height z:

$$n(\vec{r}) = n_0 \cdot \exp\left(\frac{mgz}{k_B T}\right). \tag{3.33}$$

Now we can make use of the normalization to find that the peak density can be written as

$$n_0 = \frac{Nmg}{\pi k_B T r_{HB}^2}. \tag{3.34}$$

r_{HB} represents the radius of the hollow beam. The two quantities determining the density are therefore the atom number N and the ensemble temperature T.

Aside from the peak density n_0 one is interested in the average density $\langle n \rangle$ as it is an important quantity for the analysis of losses due to ultracold collisions (see Section 3.5). It is defined by

$$\langle n \rangle = \frac{\int n(\vec{r})^2 dV}{\int n(\vec{r}) dV}, \tag{3.35}$$

and turns out to be exactly $n_0/2$ for the GOST potential.

The equipartition theorem states that each atom carries on the average $3/2\, k_B T$ in kinetic energy and the virial theorem relates this to the energy stored in the potential. The average potential energy $\bar{U}_{pot}$ in a combined potential of 2D-box and 1D-wedge amounts to exactly 2/3 of the average kinetic energy and hence the average total energy is $5/2\, k_B T$. This is for instance used to calculate the temperature increase of a trapped ensemble due to the scattering of one photon per atom. The 200 nK of recoil energy are distributed over the degrees of freedom and lead to an increase of $\Delta T = 2/5 \cdot 200\,\text{nK} = 80\,\text{nK}$.

The peak phase-space density of a completely unpolarized gas in the GOST can be calculated by

$$D = \frac{1}{7} \cdot n_0 \cdot \lambda_{dB}^3, \tag{3.36}$$

with $\lambda_{dB} = h/\sqrt{2\pi m k_B T}$ being the thermal de-Broglie wavelength. The factor of 1/7 takes into account that the ground-state is seven-fold degenerate. We finally get

$$D = \frac{1}{7} \cdot \frac{g\hbar^3 (2\pi)^{3/2}}{\pi r_{HB}^2 \sqrt{m}} \cdot \frac{N}{(k_B T)^{5/2}}. \tag{3.37}$$

As density and thus also peak phase-space density depend on the details of the potential these expressions take different forms in case of the microtraps.

3.4.2 Loading of Microtraps

Now that we have a cold and dense atom reservoir at hand, the next step is to transfer as many atoms as possible into the microtraps. All trap schemes discussed here, feature

very far-detuned light fields in order to prevent heating and losses. In this sense their potentials are conservative. An important consequence is, that an atom entering a microtrap from outside will right away leave the light field at some other point with unchanged kinetic energy. Although the microtrap potential has changed the atom's motion, it did not trap the atom due to the lack of a dissipative mechanism. However, there are still two mechanisms that can lead to a reduction of an atom's kinetic energy and thus to trapping even in a conservative trap.

At the instant, the microtrap laser is switched on, the atom is exposed to a time-dependent potential. During this process energy can be transferred from outside into the system or vice versa. In this particular case it depends on the position and motional state of an atom whether it looses enough energy to remain trapped in the light field or, on the contrary, gain energy in this altered potential.

The following considerations demonstrate how the transfer efficiency of this loading scheme is derived for the focussed beam trap described in the next section. This trap is implemented by focussing a red-detuned laser beam to the center of the GOST trap volume (see figure 3.7) and thus modifying the horizontal potential according to figure 3.8. The attractive well is an example of a so-called "dimple" which gives rise to the astonishing properties of the microtraps discussed below.

Only atoms that are inside the light field at the moment it is switched on and whose kinetic energy is below the potential energy at this point will remain trapped in the dimple. It is obvious that both the spatial overlap between reservoir ensemble and microtrap volume as well as the reservoir temperature are crucial parameters that determine the efficiency of this loading scheme. Adjusting these parameters in order to optimize the atom transfer is called "phase-space matching".

In order to derive a transfer efficiency one has to integrate the phase-space distribution function $\rho(\vec{p},\vec{r})$ in the shape it takes before the dimple is switched on over the relevant region in phase-space. We can restrict ourselves to a two-dimensional calculation since neither the potential shape of the microtrap nor the horizontal density profile vary significantly with the vertical coordinate z. $\rho(p,r)$ then takes the form

$$\rho(p,r) = \frac{1}{\Omega} \cdot \exp\left(-\frac{p^2}{2mk_BT}\right), \tag{3.38}$$

for $r < r_{HB}$ and $\rho(p,r) = 0$ elsewhere. Ω is the partition function defined by $\Omega = \int d^2p \int d^2r \exp(-p^2/2mk_BT)$. The phase-space coordinates used are the modulus of momentum p and the radial distance from the trap center r. This distribution function is now integrated over the region of phase-space that leads to an atom being trapped. The criteria for this to occur are:

$$r < r_{HB}, \tag{3.39}$$

$$\frac{p^2}{2m} < \hat{U} \cdot \exp\left(-\frac{2r^2}{w^2}\right). \tag{3.40}$$

The second equation expresses the requirement that the total energy of a trapped atom must be below zero. m denotes the cesium mass, $\hat{U}$ the maximum of the dimple potential and w is the $1/e^2$-intensity radius of the beam. After simplifying and evaluating the p-integral we arrive at the expression

$$\epsilon = \frac{2\pi}{\pi r_{HB}^2} \int_0^\infty dr \left(r - r \cdot \exp\left(-\frac{\hat{U}}{k_B T} \cdot \exp\left(-\frac{2r^2}{w^2} \right) \right) \right), \tag{3.41}$$

for the transfer efficiency ϵ. This integral can now be evaluated numerically. For the experimental parameters of our trap, $\hat{U}/k_B = 48\,\mu\text{K}$, $T = 4\,\mu\text{K}$ and $w = 32\,\mu\text{m}$ this yields a transfer efficiency of 0.9 %. The poor transfer efficiency is mainly due to the bad spatial overlap between reservoir and microtrap.

In order to improve this number one could think of increasing the size of the microtrap (provided that its depth can be kept constant) and thus to overcome the limitation imposed by the spatial overlap. However there is a drawback of this approach. The large gain in density and peak phase-space density that the dimple provides (see next section) is conditional on the fact that the dimple (i.e. the modification of the potential) is small compared to the size of the reservoir. As one increases the microtrap size and manages to transfer a larger fraction of atoms into it, the less gain in density and peak phase-space density results from it. The two different dimple trap configurations studied in this experiment somewhat represent the opposite extremes of this statement.

Fortunately the GOST provides another mechanism that can further increase the transfer efficiency without suffering from this problem. Because of the large and dense ensemble trapped in the GOST, elastic collisions between two initially untrapped atoms frequently occur within the light of the red beam. As such a collision redistributes the kinetic energy of the collision partners there is a certain probability that one of the colliding atoms finds itself trapped inside the dimple while the other carries away its missing energy. Obviously also the opposite process where an initially trapped atom is kicked out of the dimple by the collision with a fast atom exists. The exact dynamic of this loading process is rather complicated and will be further discussed in Chapter 5. However it is possible to derive a steady state result for the transfer efficiency assuming a completely thermalized gas.

In a thermalized ensemble the phase-space distribution function is modified according to the newly introduced potential:

$$\rho(p, r) = \frac{1}{\Omega'} \cdot \exp\left(-\frac{p^2}{2mk_B T} \right) \cdot \exp\left(\frac{\hat{U}}{k_B T} \cdot \exp\left(-\frac{2r^2}{w^2} \right) \right). \tag{3.42}$$

The partition function Ω' is now calculated from the accordingly modified phase-space integral. The transfer efficiency ϵ results from the identical steps as in the previous calculation and like before, the final integral has to be evaluated numerically. The same experimental parameters of $\hat{U}/k_B = 48\,\mu\text{K}$, $T = 4\,\mu\text{K}$ and $w = 32\,\mu\text{m}$ now yield a much

larger transfer efficiency of 4.2 %. At a reservoir size of 3.5×10^6 atoms the collision loading provides 1.5×10^5 atoms held in the dimple trap.

Up to now we have discussed the loading of a microtrap that has abruptly been added to the reservoir. From what has been said above, this leads to a transfer of energy from outside the system onto a certain fraction of the atoms. Depending on the strength of the microtrap potential and on the fraction of atoms involved, this consecutively heats the ensemble. In order to prevent this, the microtrap potential has to be ramped up adiabatically. In fact, two relevant time scales can be distinguished in this context.

The time scale of single particle motion, i.e. the smallest oscillation period of an atom in the idealized harmonic potential, determines an upper limit for how fast the microtrap potential can be applied without significantly transferring energy onto the atoms. At trap frequencies of usually few hundred Hertz this is not a requirement that is hard to meet.

Strictly speaking adiabatic is equivalent to *reversible* which in turn means, that the entropy of the system remains unchanged during this process. In that sense the introduction of the microtrap has to take place slow enough for the ensemble to be in thermal equilibrium at all times. This thermodynamic definition which applies to the whole ensemble rather than to single particles therefore imposes a much stricter requirement on the timing of the loading process: The introduction of the microtrap has to take place on a time scale which is slow compared to the thermalization time of the reservoir ensemble and therefore is on the order of seconds.

Reference [Wen00] contains a theoretical treatment of this dimple loading and provides numerical results on the differences between abrupt and adiabatic loading. It shows that these differences a astonishingly small. Particularly in case of the strong and wide dimple trap we have taken care to satisfy the above stated requirements for adiabatic transfer.

3.4.3 The Dimple Trick

It is well known that adiabatically varying the strength of a potential without changing its shape does not lead to a change in phase-space density of a trapped atom gas. A compression will in general be compensated by an increase in temperature and vice versa. In case of an adiabatic modification of the *shape* of a potential, however, this restriction does not hold any longer and locally the density and phase-space density might be significantly different. This so-called "dimple trick" was first suggested and experimentally confirmed by P. Pinkse *et al.* [Pin97]. The authors report the increase of the peak phase-space density of an ensemble of magnetically trapped hydrogen by 2 during an adiabatic transition of the trapping potential between two distinct shapes. In contrast to evaporative cooling (Section 3.6.1) this approach constitutes a way to reversibly change the local phase-space density. D. Stamper-Kurn *et al.* have made use of this fact and investigated the reversible formation of a Bose-Einstein condensate by

adiabatically increasing the peak phase-space density of a sodium gas by more than 50 [SK98].

The dimple trick relies on two constituents: A large reservoir of interacting (elastically colliding) atoms and a local modification of the trap potential. As the potential is adiabatically transformed into a combined reservoir-dimple system, the reservoir ensemble will adjust the local density by thermalization in such a way that the density $n(\vec{r})$ satisfies the relation $n(\vec{r}) \propto \exp(U/k_B T)$. A local modification of the potential as shown in figure 3.6 will therefore strongly increase the density within the dimple. An increase of the phase-space density now results from the fact that while density as a local quantity increased, the global quantity temperature stayed nearly constant. This is due to the reservoir that absorbs excess energy introduced during this process. In principle this scheme allows for arbitrary increases of the peak phase-space density as has been shown in reference [SK98]. It is important that the dimple potential is not deep enough to accommodate all reservoir atoms, as this will remove the reservoir and prevent an enhancement of the peak phase-space density. A theoretical discussion of this useful effect can be found in references [Pin97] and [Wen00].

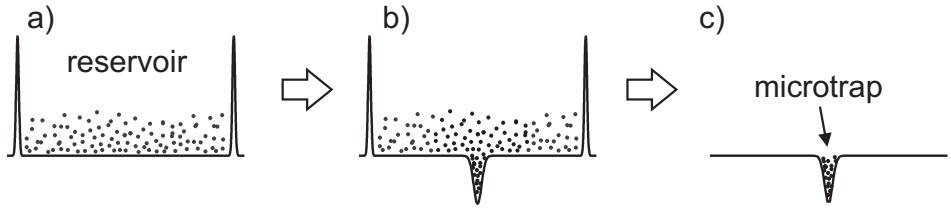

Figure 3.6: *The three stages of microtrap preparation: Preparation of the reservoir (a). Thermalization loading of the microtrap (b). Removal of the reservoir (c).*

In order to make use of the dimple trick, the microtrap experiments discussed below used the preparation stages depicted in figure 3.6. After the GOST has prepared a dense and cold reservoir ensemble, the dimple potential is added either adiabatically or abruptly depending on the particular case. Thermalization then loads the dimple potential and causes peak density and peak phase-space density to drastically increase. Finally the reservoir is removed by switching off the hollow beam and about 200 ms later, when all reservoir atoms have laterally escaped, consecutive evaporation steps from the microtrap can be initiated.

3.4.4 The Focussed Beam Surface Trap

A straightforward implementation of a microtrap is the focussed beam surface trap or "dimple trap". Figure 3.7 shows how it is realized by placing a tight focus of a far red-detuned laser beam inside the center of the GOST trapping volume. The laser

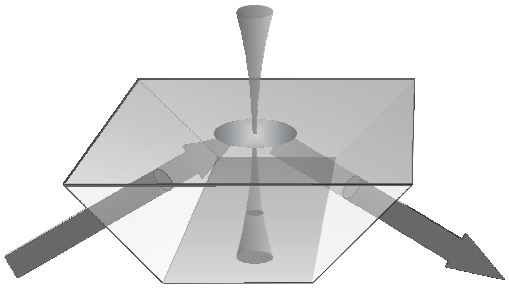

Figure 3.7: *Scheme of the focussed beam surface trap (dimple trap).*

propagates through the prism from below in order to prevent reflection from the prism surface which would lead to interference structures at the place of the atoms. In a first set of experiments this was a 330 mW Nd:YAG beam focussed to 32 μm. The resulting potential is $U/k_B = 48\,\mu$K deep and modifies the total horizontal potential according to figure 3.8.

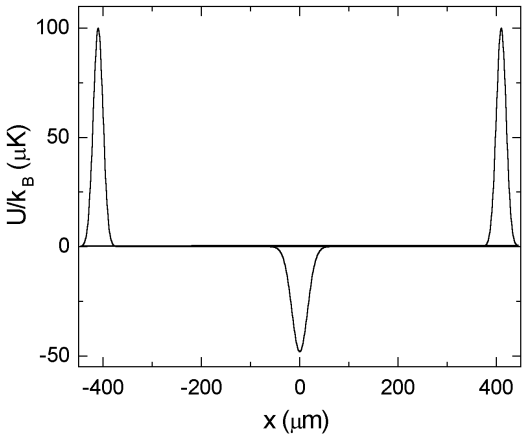

Figure 3.8: *Horizontal potential of the combination of hollow beam and dimple trap.*

Note that in addition to the horizontal attraction a vertical force caused by the intensity gradient along the propagations line of the beam exists if the beam focus does not coincide with the dielectric surface. We can estimate the magnitude of this force by looking at the harmonic approximation of the z-component of the potential:

$$U(z) \approx U_0 \cdot \frac{z^2}{z_R^2}. \tag{3.43}$$

This approximation is reasonable, if the focus is less than the Rayleigh length $z_R = \pi w_0^2/\lambda \approx 3\,\mathrm{mm}$ away from the prism. U_0 is the minimum value of the potential and w_0 denotes the $1/e^2$ radius of the beam at the focus. We can compare the effect of gravity to this dipole force by calculating the potential energy corresponding to a displacement of $10\,\mu$m for both cases. The corresponding gravitational potential energy is $1.56\,\mu$K whereas the dipole potential in this case is only $\Delta U/k_B = 5.3 \times 10^{-4}\,\mu$K. Evidently this force is negligibly small compared to the evanescent waves's dipole force and even smaller than the gravitational force so it can be disregarded in all following considerations. The dimple potential arises from a far-detuned laser at 1064 nm and is therefore nearly conservative.

The fact that the atomic density inside the dimple trap is very large compared to the reservoir, makes atoms vulnerable to density dependent loss mechanisms. In order to suppress the light induced collision loss discussed in Section 3.5.2 the standard 3 GHz blue-detuned evanescent wave of the GOST is replaced by a very far detuned one in the dimple. Most of the measurements discussed below have been performed with a 1.6 nm blue-detuned evanescent wave whereas the results from the tight dimple configuration have been obtained with a evanescent wave at a detuning of only 128 GHz.

Ensemble Properties

The following considerations will provide some useful formulas describing ensemble properties in the dimple. A very important parameter in this context is the trap frequency ω at which an atom oscillates inside a microtrap. Depending on the configuration, the dimple features trap frequencies of few hundred Hertz. Measurements determining ω are discussed in Section 5.3. Strictly speaking the trap's potential is not harmonic in shape and thus gives rise to a broad spectrum of trap frequencies. Atoms of higher energy in general oscillate with lower frequencies. However, since the ensemble temperature in this case is much lower than the trap depth the potential can be approximated by a harmonic potential up to a good accuracy. All following formulas refer to the harmonic case In this approximation the combined potential of the dimple is harmonic in the horizontal x-y-plane and wedge-shaped along the vertical z-direction. The density of the atomic sample is therefore given by

$$n(\vec{r}) = n_0 \cdot \exp\left(-\frac{r^2}{r_0^2}\right) \cdot \exp\left(-\frac{z}{z_0}\right). \tag{3.44}$$

To arrive at this expression one makes use of the fact that the potential is cylindrically symmetric. $r^2 \equiv x^2 + y^2$ is the radial coordinate in the x-y-plane, $r_0 \equiv \sqrt{2k_BT/(m\omega_r^2)}$ the radius and $z_0 \equiv k_BT/(mg)$ the height at which the density has decreased to $1/e$. ω_r is the radial trap frequency in the dimple trap while m and g denote mass and earth' acceleration respectively. By introducing an effective volume $V_0 \equiv \pi r_0^2 z_0$ one can write the peak number density conveniently in terms of the number of trapped atoms:

$$n_0 = \frac{N}{V_0}. \tag{3.45}$$

The mean density $\langle n \rangle = 1/N \cdot \int n^2(\vec{r})dV$ and mean quadratic density $\langle n^2 \rangle = 1/N \cdot \int n^3(\vec{r})dV$ are related to n_0 by the following simple expressions:

$$\langle n \rangle = \frac{n_0}{4}, \tag{3.46}$$

$$\langle n^2 \rangle = \frac{n_0^2}{9}. \tag{3.47}$$

The determining parameters of these quantities are the atom number N, temperature T, and the trap frequency ω_r. Peak- as well as average density scale as

$$n_0 \propto \frac{N\omega_r^2}{T^2}. \tag{3.48}$$

Note that differently from the case of the GOST, the density now depends quadratically on the inverse temperature which has important consequences for evaporative cooling. Namely this leads to a stronger compression of the sample as temperature is decreased and thus simplifies the task of evaporative cooling at constant or increasing thermalization rate.

The resulting peak phase-space density can be obtained from expression 3.36 which takes the form

$$D = \frac{1}{7} \cdot \sqrt{2\pi m} g \omega_r^2 \hbar^3 \cdot \frac{N}{(k_BT)^{7/2}}. \tag{3.49}$$

It shows that also the peak phase-space density has a more favorable dependence on T than in case of the GOST potential.

3.4.5 The Double Evanescent Wave Trap (DEW)

The double evanescent wave trap (DEW trap) is a second interesting microtrap scheme that addresses a somewhat different physical topic. It has been proposed by Y.B. Ovchinnikov *et al.* already in 1991 [Y.B91]. The microtrap potential is formed by adding a red-detuned evanescent wave with a large decay length to the gravito-optical potential of the GOST (see Figure 3.9). This attractive light field alters both the vertical and the

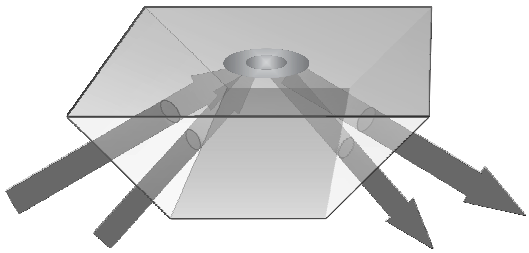

Figure 3.9: *Scheme of the double evanescent wave trap*

horizontal potential in a way that very close ($\approx 1\,\mu$m) to the prism surface an attractive potential well is formed whose vertical extension is only about one optical wavelength while horizontally being a few hundred micrometers wide. This extreme anisotropy can be exploited to realize an atomic system close to two-dimensionality.

Figure 3.10 shows the vertical part of this potential. Horizontally it resembles that of the dimple trap. The total potential of this combination can be written as

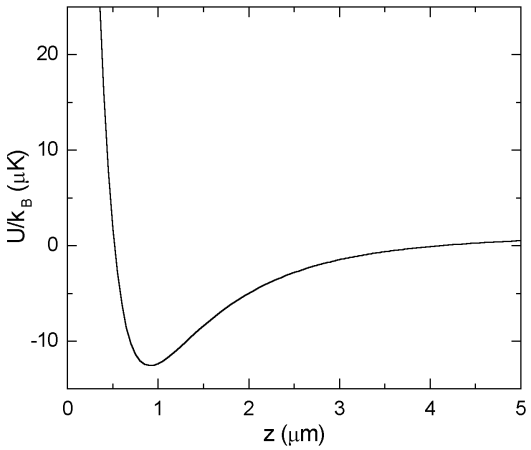

Figure 3.10: *Potential of the DEW-trap close to the prism surface for the experimental parameters specified in the text. The short-ranged Van-der-Waals interaction has been omitted.*

$$U(\vec{r}) = U_b(x,y)\exp\left(-\frac{2z}{\Lambda_b}\right) - U_r(x,y)\exp\left(-\frac{2z}{\Lambda_r}\right) - \alpha_{VdW}\cdot z^{-3}\left(1+\frac{2\pi z}{\lambda_{eff}}\right)^{-1} + mgz, \tag{3.50}$$

where U_b and U_r are the optical potentials of blue- and red-detuned evanescent wave directly at the surface ($z = 0$) given by $U_i(x, y) = \hat{U}_i \exp(-2x^2/w_i^2 - 2y^2/w_i^2 \cos^2 \Theta_i)$, $(i = b, r)$. w_i is the waist of the beam, Θ_i its angle of incidence and Λ_i the $1/e^2$-intensity decay length. The approximate expression for the Van-der-Waals attraction has been introduced in Section 3.3. The experimental parameters used for the measurements of Chapter 6 were as follows: The blue-detuned evanescent wave is created by a 1.15 W laser beam at a detuning of 1.6 nm. It is focussed to a waist of $w_b = 400\,\mu$m and hits the prism surface at an angle Θ_b deviating by 3.2° from the critical angle of $\Theta_{crit} = 43.6°$. The evanescent wave decay length Λ_b is therefore 395 nm and the potential barrier at the center of the light spot is $U_b/k_B = 325\,\mu$K. The attractive part of the DEW potential stems from a 1.2 W beam at a wavelength of 1064 nm focussed to only $w_r = 160\,\mu$m. At an angle of incidence of $\Theta_r = 43.8°$ which corresponds to a small deviation of $\Delta\Theta = 0.2°$ from the critical angle, the resulting evanescent wave features a decay length of $\Lambda_r = 2.0\,\mu$m and gives rise to a total potential at the center of the light spot of $U_r/k_B = 43\,\mu$K. The combined potential of both light fields together with gravity and Van-der-Waals interaction creates a well of $13\,\mu$K depth at a distance of $0.9\,\mu$m from the dielectric surface.

In order to load the trap one has to overcome the same problems as before in the dimple trap since the trapping volume is small and the trap conservative. In principle the same thermalization loading scheme could be applied to load this vertical "dimple" by elastic collisions. However since the lifetime of atoms inside the DEW-trap is only of the order of 1.4 seconds (see Chapter 6) the enhancement effect of this scheme is very small. Best loading results from a good matching of the phase-space distribution in the previous dimple trapping stage with the region of phase-space that leads to trapped atoms in the DEW-trap.

In order to determine the absolute values of peak density and phase-space density, it is necessary to derive expressions for the different trap frequencies in the DEW trap. In general the procedure is as follow. First, one determines the harmonic approximation of the potential at its minimum position x_0:

$$U(x) = \frac{1}{2}\frac{\mathrm{d}^2U}{\mathrm{d}x^2}\bigg|_{x=x_0}(x - x_0)^2 + \ldots, \tag{3.51}$$

and then extracts the trap frequency $\omega/2\pi$ by comparing this result to the general expression of the harmonic oscillator:

$$U(x) = \frac{1}{2}m\omega \cdot (x - x_0)^2. \tag{3.52}$$

In case of the vertical potential of the DEW-trap we start out with the slightly simplified expression

$$U(z) = U_b \exp\left(-\frac{2z}{\Lambda_b}\right) - U_r \exp\left(-\frac{2z}{\Lambda_r}\right), \tag{3.53}$$

which neglects the influence of gravity and Van-der-Waals attraction and assumes that no horizontal motion takes place during the oscillation. For a very weak attractive evanescent wave this approximation breaks down as gravity becomes comparable to the attractive dipole force. Performing the somewhat tedious calculation as sketched above finally yields the approximate expression for the vertical trap frequency ω_z in the DEW-trap:

$$\frac{\omega_z}{2\pi} = \frac{1}{\pi}\sqrt{\frac{1}{m}\left(\frac{U_r}{\Lambda_r}\right)^{\frac{\Lambda_r}{\Lambda_r-\Lambda_b}}\left(\frac{U_b}{\Lambda_b}\right)^{\frac{\Lambda_b}{\Lambda_b-\Lambda_r}}\left(\frac{1}{\Lambda_b}-\frac{1}{\Lambda_r}\right)} \tag{3.54}$$

For the parameters provided above, we calculate a vertical trap frequency of 10.6 kHz. Figure 3.11 shows the dependence of this quantity on the power P_r of the red evanescent wave beam. Notably the trap frequency at $P_r = 0$ is zero in this model. A more realistic approach including gravity and the attractive Van-der-Waals interaction would yield a trap frequency of $\omega/2\pi = 1.1\,\text{kHz}$ at $P_r = 0$ as expected from the considerations in Section 3.3.

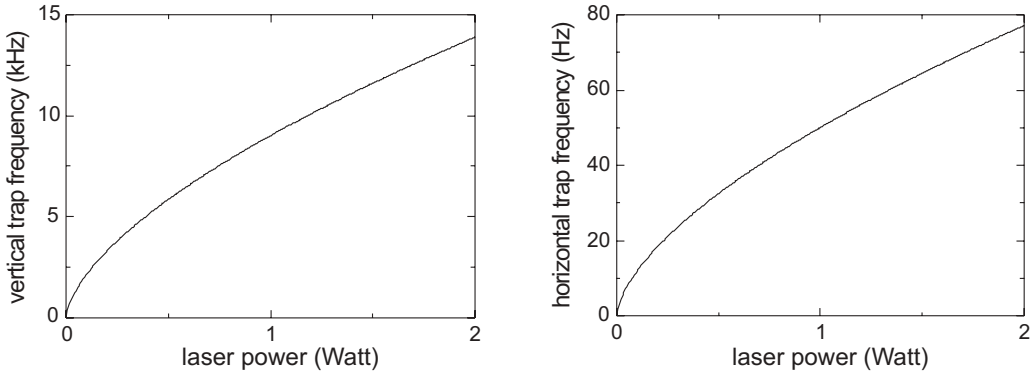

Figure 3.11: *Calculation of the vertical and horizontal trap frequency in the DEW-trap as a function of the red-detuned laser power excluding the influence of gravity and Van-der-Waals. The experimental parameters are given in the text.*

The horizontal trap frequency is obtained from a similar approach as explained above. In this case the gaussian intensity profile of the laser determines the shape of the trap potential. Under the assumption of an atomic ensemble whose temperature is significantly below the trap depth, the harmonic approximation is reasonably good and yields

$$U(r) = 2U_0\left(\frac{r}{w_0}\right)^2. \tag{3.55}$$

U_0 is the potential at the center of the beam and w_0 is its $1/e^2$ radius. Note that U_0 depends on the vertical position of the oscillating atom, as the laser intensity and thus

also U_0 fall off exponentially with the distance from the dielectric surface. Therefore, for each set of experimental parameters the vertical trap minimum has to be calculated, before a trap frequency can be obtained[1]. Starting with the simplified vertical potential given in Equation 3.53 we obtain an expression for value of the potential in the minimum:

$$U_0 = U_b \left(\frac{\Lambda_r U_b}{\Lambda_b U_r}\right)^{-\frac{\Lambda_r}{\Lambda_r - \Lambda_b}} - U_r \left(\frac{\Lambda_r U_b}{\Lambda_b U_r}\right)^{-\frac{\Lambda_b}{\Lambda_r - \Lambda_b}}. \tag{3.56}$$

Inserting this expression into Equation 3.55 and simplifying, yields the following result for the horizontal trap frequency $\omega_h/2\pi$:

$$\frac{\omega_h}{2\pi} = \frac{1}{\pi w_0}\sqrt{-\frac{1}{m}U_b \left(\frac{\Lambda_b U_r}{\Lambda_r U_b}\right)^{\frac{\Lambda_r}{\Lambda_r - \Lambda_b}} \left(1 - \frac{\Lambda_r}{\Lambda_b}\right)}. \tag{3.57}$$

Figure 3.11 shows the trap frequency as a function of the red-detuned laser power with the experimental parameters provided above and a beam waist $w_0 = 160\,\mu$m. Due to fact that the laser beam hits the prism at an angle Θ, the trap frequency in the direction defined by the plane of incidence is lower by a factor of $1/\cos\Theta$.

The tight vertical potential of the DEW-trap offers comparable conditions in terms of peak density and peak phase-space density as the dimple, even though the number of trapped atoms is usually much smaller. In order to find expressions for density and peak phase-space density in the DEW-potential one can use a similar approach as was employed before. In this case, however, the vertical potential is of harmonic form instead of the wedge-shape of the gravito-optical potential. The overall potential is therefore that of a 3D harmonic oscillator and gives rise to a density distribution of the form

$$n(\vec{r}) = n_0 \cdot \exp\left(-\frac{x^2}{x_0^2}\right) \cdot \exp\left(-\frac{y^2}{y_0^2}\right) \cdot \exp\left(-\frac{z^2}{z_0^2}\right), \tag{3.58}$$

introducing the $1/e$-radii $X_0 = \sqrt{2k_B T/m\omega_X^2}$ $(X = x, y, z)$. Normalization again yields the peak density n_0:

$$n_0 = N \cdot \left(\frac{m}{2\pi k_B T}\right)^{3/2} \cdot \omega_x\omega_y\omega_z. \tag{3.59}$$

The mean density and mean squared density are given by $\langle n\rangle = n_0/\sqrt{8}$ and $\langle n^2\rangle = n_0/\sqrt{27}$. The peak phase-space density can be written as

$$D = \frac{1}{7} \cdot N \left(\frac{\hbar\bar{\omega}}{k_B T}\right)^3, \tag{3.60}$$

[1]Strictly speaking, this approach still includes further approximations. Because of the different beam waists of red- and blue-detuned evanescent wave, a horizontal displacement from the center of the light spots invariably results in a shift of the minimum of the vertical potential. The horizontal potential therefore slightly deviates from a true gaussian profile. If, however, the blue-detuned evanescent wave spot is considerably larger than the red-detuned one, this effect is of minor importance and can be neglected.

with the average trap frequency $\bar{\omega} = \sqrt[3]{\omega_x \omega_y \omega_z}$. Section 3.6.3 will further address the two-dimensionality aspect of this trap.

3.4.6 Summary of Trap Properties

Since the specific trapping potential determines the functional relation between the experimentally accessible parameters N, T and ω_0 and the figures of merit, n_0 and D, each trap has its own mathematical expressions for these. Table 3.1 summarizes which idealized potential shapes constitute the full trapping potential and to what expressions for n_0 and D this leads. The last column relates the mean total energy per particle to the ensemble temperature.

Trap	*Potential*	*Peak density*	*Phase-space density*	$\bar{E}$
GOST	2D-box + 1D-wedge	$n_0 \propto N/T$	$D \propto N/T^{5/2}$	$5/2 k_B T$
Dimple	2D-H.O. + 1D-wedge	$n_0 \propto N\omega_0^2/T^2$	$D \propto N\omega_0^2/T^{7/2}$	$7/2 k_B T$
DEW-trap	3D-H.O.	$n_0 \propto N\omega_x\omega_y\omega_z/T^{3/2}$	$D \propto N\omega_x\omega_y\omega_z/T^3$	$3 k_B T$

Table 3.1: *Summary of the relevant properties of the different traps.*

Another relevant property, that is specific for each trapping potential is the scaling of the temperature T with the laser power P during an *adiabatic* change of the *strength* of the potential[2]. When lowering the laser power in order to apply some evaporation ramp, the ensemble temperature is simultaneously reduced by two independent mechanisms. Contrary to the evaporative cooling which reduces temperature and increases phase-space density at the cost of trapped particles, the adiabatic cooling reduces temperature and peak density in such a way that phase-space density stays constant. This condition can be used to find a scaling law between laser power P and temperature T that allows for a clear separation of both mechanisms during evaporative cooling.

We start with a general expression for the peak phase-space density and demand that it remains unchanged by a variation of P.

$$D \propto n_0 \cdot T^{-3/2} = const. \tag{3.61}$$

The specific details of the trapping potential now enter via the dependence of n_0 on the laser power P. The situation becomes very easy when considering the standard

[2]It is important to demand that the *shape* of the potential remains unchanged. If this is not the case, an adiabatic modification of the potential can still cause the local phase-space density to change. Exactly this fact is exploited by the dimple trick.

GOST. In this case, the 2D-box potential and the hard-wall of the evanescent wave render the peak density completely independent of P and therefore we find that there is no adiabatic expansion (or adiabatic compression) in the GOST.

The situation changes as we consider the dimple trap. Here, the density is influenced by a change of the laser power via the trap frequency. Substituting the relation

$$n_0 \propto \frac{\omega^2}{T^2}, \tag{3.62}$$

into Equation 3.61 we find

$$D \propto \frac{\omega^2}{T^{7/2}}. \tag{3.63}$$

Since $\omega^2 \propto P$ (see Chapter 5) we immediately find that during an adiabatic change of the dimple laser power, T varies as

$$T(P) = T(P_0) \cdot \left(\frac{P}{P_0}\right)^{\frac{2}{7}}, \tag{3.64}$$

with P_0 being the initial laser power. During an evaporation ramp which features both mechanisms, exactly a contribution given by Equation 3.64 has to be attributed to the adiabatic change.

In case of the DEW-trap this relation is slightly more complicated due to the fact that no simple expression describes the functional relation between ω_z and P. Using the same arguments as before we find that an adiabatic change of the red-detuned laser influences the ensemble temperature according to the following equation:

$$T(P) = T(P_0) \cdot \sqrt[3]{\frac{\omega_z(P) \cdot P}{\omega_z(P_0) \cdot P_0}}. \tag{3.65}$$

ω_z denotes the vertical trap frequency. For practical use one has to plug in the numerically or experimentally determined values for $\omega_z(P)$ (see Section 6.3).

Obviously in all three traps the dependence of T on P is small and this suggests that significant temperature changes during evaporative cooling are indeed mainly due to the removal of energetic atoms.

3.5 Ultracold Collisions

Ultracold collisions play a very important role for the dynamics of the atomic ensemble. On the one hand they mediate thermalization, facilitate evaporative cooling and load the conservative microtraps while on the other hand inelastic collisions are responsible for losses, heating and limitations in the efficiency of evaporative cooling. These two

aspects of interatomic encounters are particularly pronounced in cesium because the atom exhibits anomalous scattering behavior. The details of this peculiarity are discussed later in the text. The following sections will briefly explain elastic and inelastic collisions and its consequences for this experiment.

The main distinction between collisions of atoms at room temperature and those at a few microkelvin is the relative velocity of the colliding atoms. Ultracold collisions however, are not only the low-energy extension of processes already known from thermal atoms but rather show some new properties that have been extensively investigated in recent years [Wal94, Wei99]. New scattering aspects in ultracold collisions mainly arise from the fact that the collision time, due to the small relative velocity, is long enough for optical excitation times to become comparable to the collision time and secondly because the collision energy is small enough that long range details of the interatomic potentials become important for the scattering process. The dynamics of these low-energy processes are inherently governed by quantum mechanics which fortunately makes life easy in most relevant cases. At low temperatures these collisions with few exceptions occur purely isotropic and can be described by a single parameter called the *scattering length* a.

3.5.1 Elastic Collisions

Elastic collisions or "good collisions" as they are sometimes called are the only significant process that makes an atomic ensemble relax to its equilibrium state after being externally disturbed. They eventually lead to the cooling effect during evaporation and provide low-energetic atoms that can be filled into the conservative microtraps. The most important feature of elastic collisions is that they only redistribute the kinetic energy of both colliding atoms without releasing energy from internal sources or light fields (exothermal) or removing kinetic energy (endothermal) by exciting internal degrees of freedom. Consequently these collisions can only lead to heating or cooling of an atomic ensemble if at the same time atoms are removed. The rate at which thermalization and thus evaporative cooling can occur is determined by the rate of elastic collisions in the sample. One can say that they are the pacemakers of dynamics. In this context especially the elastic scattering cross section σ, the elastic collision rate γ_{el} and the thermalization time T_{th} are relevant parameters and will be discussed in the following.

The collision process between two low-energetic atoms is most suitably treated by a partial wave expansion of the scattering wave function. Due to the small relative momentum of the collision partners only a few partial waves at small angular momentum numbers ($l = 0, 1, 2$) play into the dynamics and usually even a reduction of the problem to s-wave scattering ($l = 0$) is sufficient. In this case all scattering is purely isotropic and most consequences can be summarized by a few parameters, most importantly the s-wave scattering length a. For some situations (scattering of identical fermions, shape resonances, some Feshbach resonances or particularly long-ranged interatomic

potentials) higher orders of partial waves have to be taken into account.

Scattering theory [Sak94] states the simple result that as the relative momentum approaches zero the total cross section of two non-identical atoms colliding in an arbitrary (but short-ranged) potential is given by [3]

$$\sigma = 4\pi a^2, \tag{3.66}$$

where the s-wave scattering length a is defined by

$$a = -\lim_{k\to 0} \frac{\tan \delta_0(k)}{k}, \tag{3.67}$$

and δ_0 is the scattering phase. k is the wave number of the de-Broglie wave related to the relative motion of the atoms. Note that all specific information about the interatomic potential is contained in a and that σ becomes constant at small k. This can intuitively be understood if we recall that at small k or $ka \ll 1$ the de-Broglie wavelength of the scattering wave packet is much larger than the "range" of the potential represented by a and thus cannot resolve any details of it. The scattering length a and its implications on scattering properties will be revisited in later sections.

The Cesium Atom

The potentials that govern the detailed collision in our case are the singlet and the triplet potential which apply to the two cases of relative orientation of the electronic spins of the colliding atoms. In this situation the coupling between the two electron spins replaces the coupling between electron spin and nuclear spin of a single atom. The free atom state $|F, m_F\rangle$ is projected onto the singlet and triplet states which determine the scattering process. The singlet (a_S) and the triplet (a_T) scattering length are the main parameters that summarize the details of the collision process. Experimentally their values have been determined to $a_S = 280 \pm 10\,\mathrm{a_0}$ and $a_T = 2400 \pm 100\,\mathrm{a_0}$ (a_0 being the Bohr radius) using high-resolution Feshbach spectroscopy [Chi00, Leo00]. Obviously both are positive and exceptionally large in cesium. Due to the large values for a_S and a_T the scattering between two ground-state cesium atoms, which is usually a mixture of singlet and triplet scattering, will in general feature a large scattering length regardless of the specific m_F-states of the collision partners. The anomalously strong scattering influences elastic as well as inelastic scattering and is caused by several effects:

Firstly both molecule potentials are of such a form that they support a bound state of the cesium dimer close to the dissociation threshold and this in turn leads to a so-called zero-energy resonance [Arn97] that gives rise to the large values for a_S and a_T. This last

[3] If we consider scattering between atoms in a single m_F-state we have to take into account that we are then dealing with identical bosons which leads to a doubling of the total s-wave scattering cross section and excludes p-wave scattering.

bound state is particularly close to the dissociation energy for the triplet potential. Due to this resonance also the expression for the elastic scattering cross Section 3.66 has to be modified and now becomes [Dal99]:

$$\sigma = \frac{4\pi a^2}{1 + k^2 a^2}. \tag{3.68}$$

The two important limiting cases are

$$ka \ll 1, \quad \sigma(k) \approx 4\pi a^2 \quad \text{low-energy limit} \tag{3.69}$$

$$ka \gg 1, \quad \sigma(k) \approx \frac{4\pi}{k^2} \quad \text{unitarity limit} \tag{3.70}$$

With moderate values for the scattering length a around few ten a_0 in other alkali atoms the low-energy limit is applicable already at a few microkelvin temperature. In cesium, however, the transition between both regimes defined by $k^2a^2 = 1$ takes place only at around $T \approx 1\,\mu\text{K}$ due to the extremely large scattering length. The result is a more complicated quantitative analysis since all expressions that contain σ now also implicitly depend on temperature. The thermalization serves as an example to illustrate this point. In the low-energy limit of constant elastic scattering cross section, Monte Carlo simulations [Arn97] have shown that about three collisions per atom are sufficient to rethermalize an ensemble originally not in equilibrium. In cesium however, collisions at small relative velocities have a larger elastic scattering cross section but hardly contribute to thermalization since only little kinetic energy is transferred by them. Consequently a cesium ensemble needs on the average about ten elastic collisions per atom to rethermalize. In order to calculate the time T_{th} needed for such a thermalization we first derive an expression for the elastic collision rate γ_{el} from the expression [Jea82]

$$\gamma_{el} = \bar{n} \cdot \sigma(\bar{v}_{rel}) \cdot \bar{v}_{rel}. \tag{3.71}$$

$\bar{n}$ is the average atomic density, σ the elastic scattering cross section and $\bar{v}_{rel}$ the average relative velocity between two atoms. Inserting expression 3.68 and the relation $\bar{v}_{rel} = \sqrt{16k_BT/\pi m}$ for a Maxwell-Boltzmann distribution we arrive at an expression for γ_{el} which depends on the mean density and temperature:

$$\gamma_{el} = \bar{n} \cdot \sqrt{\frac{16k_BT}{\pi m}} \cdot \frac{(2\pi a\hbar)^2}{\pi\hbar^2 + 16ma^2k_BT}. \tag{3.72}$$

T_{th} can then be derived from the approximate relation [Arn97]:

$$T_{th} \approx 10 \cdot \gamma_{el}^{-1}. \tag{3.73}$$

A second unusual property of cesium is the large influence of its so-called indirect spin-spin coupling [Mie96]. This coupling mechanism between the spins of the two

valence electrons of the colliding ground-state atoms is mediated by a coupling between electron spin and excited electronic states of the dimer with angular momentum via the spin-orbit interaction. The coupling breaks the spherical symmetry of the collision process as it couples the total electron spin to the axis of the molecule. In lighter alkali atoms this mechanism is strongly suppressed and can in general be neglected. In cesium however, this coupling is strong [Leo00] and leads to two important consequences: Firstly it explains the strong dipolar relaxation loss observed in magnetic traps [Söd98] and secondly it gives rise to a relatively strong coupling between s-wave scattering states and rotating molecular states of the molecular dimer and thus to a rich spectrum of more than 30 Feshbach resonances found for the various states of cesium [Ker01].

Feshbach Resonances

Feshbach resonances are scattering resonances that arise from the fact that an unbound scattering state and a bound state of a different molecular potential have similar energy and are coupled by some mechanism [Fes62, Tie92]. If in addition to that, both states have different magnetic moments, one can energetically shift them against each other using an external magnetic field and therefore drastically change the scattering properties of this state. Figure 3.12 which is taken from reference [Ker01] shows the scattering length a of the polarized $|F = 3, m_F = 3\rangle$ state of cesium versus the applied magnetic field. Scattering of this state is a mixture of singlet and triplet processes. Several narrow Feshbach resonances can be seen. A strong increase of a starting from $-2000\,a_0$ at zero field leading to vanishing scattering at 17 Gauss and to large and positive scattering length above this value is due to a broad Feshbach resonance at around -10 Gauss (or equivalently at 10 Gauss for the $|F = 3, m_F = -3\rangle$ state). This feature is useful to tune the scattering properties of a polarized cesium ensemble or the mean field interaction of a Bose-Einstein condensate. Using a resonance to increase the absolute value of a leads to a strong increase of σ until the unitarity limit is reached ($ka \gg 1$) and the elastic scattering cross section takes the approximate a-independent form

$$\sigma(k) \approx \frac{4\pi}{k^2}. \tag{3.74}$$

Feshbach resonances are a useful and easy to implement tool to enhance evaporation but have not yet been used in this experiment. Any measurements have been performed on unpolarized samples up to now.

3.5.2 Inelastic Collisions

When talking about inelastic collisions in the context of laser cooling the cesium atom can serve as a very illustrative example. Only due to its inelastic collision processes which are generally up to three orders of magnitude more severe as compared to Rubidium-87 have attempts to create a cesium BEC failed until recently. Again the zero-energy

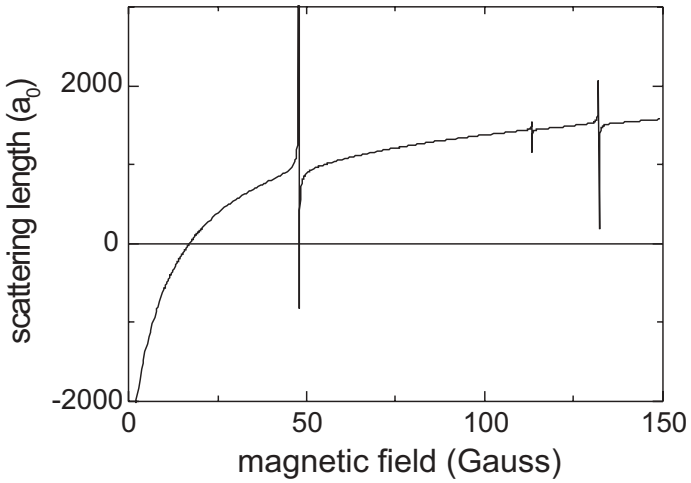

Figure 3.12: *Several Feshbach resonances of the $F = 3, m_F = 3$ state of cesium [Ker01]. The large feature at low fields arises from a broad Feshbach resonance at -10 Gauss.*

resonance together with the strong spin-spin coupling mechanism described above are responsible for these problems. It prevents the creation of a BEC in magnetic traps [Söd98] and has similarly foiled efforts in many dipole traps so far [Han01a].

Inelastic collision processes can be categorized according to the number of cold atoms involved in such a process. Independent of ensemble density, atoms can always be removed from a trap by collision with thermal background gas atoms. The transfer of kinetic energy is generally much larger than the trap depth and therefore this kind of collision inevitably leads to trap loss. Background gas collisions can effectively be suppressed by establishing vacuum conditions of the order of 10^{-11}mbar. The resulting lifetime limit is of the order of minutes and usually longer than any other relevant timescale.

Most important for this particular experiment are two-body processes in which two cold atoms collide and by some coupling mechanism transfer energy from an external (e.g. a light field) or an internal energy reservoir into the relative motion. This usually leads to the removal of both atoms from the trap or at least heats the ensemble. A wide spectrum of mechanisms is available for such a process and we will restrict the discussion to the ones relevant for this trap.

m_F-State Changing Collisions

Binary collisions that change the magnetic substate of the $|F = 3\rangle$ ground-state can, depending on their energy splitting and on the trap depth lead to loss of atoms from the

trap. In the current experiments unpolarized samples with a non-vanishing population in all seven m_F-substates ($m_F = -3, \ldots, 3$) are used and are thus subject to exothermal collisions as soon as the degeneracy of these states is lifted by the Zeeman shift. At the present experimental parameters these effects should however be of importance only at very low potentials and also heating should not occur as this mechanism would equally lead to exothermal and endothermal collisions. In future experiments the atoms will be polarized to the $|F = 3, m_F = 3\rangle$ state so that angular momentum and energy conservation prevent these collisions. The energy splitting between neighboring m_F-states is $\Delta E/k_B = 16.8\,\mu$K per Gauss and thus will sufficiently separate the m_F-states at the B-field values above a few Gauss.

Collisions at Blue Detuning

Another important inelastic process that has already been extensively investigated [Ham99] in this trap, are collisions that occur in the presence of a blue-detuned light field. This type of inelastic collision couples energy from the vast reservoir of the evanescent light field into the atomic motion using the following mechanism. Apart from the attractive Van-der-Waals interaction between two neutral atoms in the ground-state there are long-ranged excited state molecular potentials that show a C_3/R^3 dependence and are due to the resonant dipole-dipole interaction. The fact that they involve at least one electronically excited atom makes the coupling to a light field inevitable. This can either be a red-detuned light field which comes into resonance with an attractive molecular potential or a blue-detuned light field that excites the colliding pair into a repulsive molecular state. Figure 3.13 illustrates how these light-assisted collisions take place in case of an alkali D line.

While light-assisted collisions in red-detuned lasers have important implications for instance in a MOT, the collision mechanism of interest in the GOST and the microtraps involves the blue-detuned light of the repulsive evanescent wave. As two atoms collide they can be resonantly excited into the repulsive $S_{1/2} + P_{3/2}$ molecular potential by an evanescent wave photon around the classical Condon point R_c where the resonance condition is met. The strong repulsion between the atoms in this potential curve subsequently transforms part of the energy corresponding to the detuning of the evanescent wave into kinetic energy and generally ejects both atoms from the trap. The detuning of $\delta_{EW}/2\pi = 3\,$GHz corresponds to a thermal energy of 144 mK which is much larger than the trap depth.

To derive the dependence of the rate coefficient β of this process on the detuning and the intensity of the laser field involved, we make use of a simple semiclassical model. First we assume that the rate coefficient β is proportional to the probability p_{R_c} for an atom to approach its collision partner up to a distance R_c and to the probability p_{exc} for the excitation by the light field:

$$\beta \propto p_{R_c} \cdot p_{exc}. \tag{3.75}$$

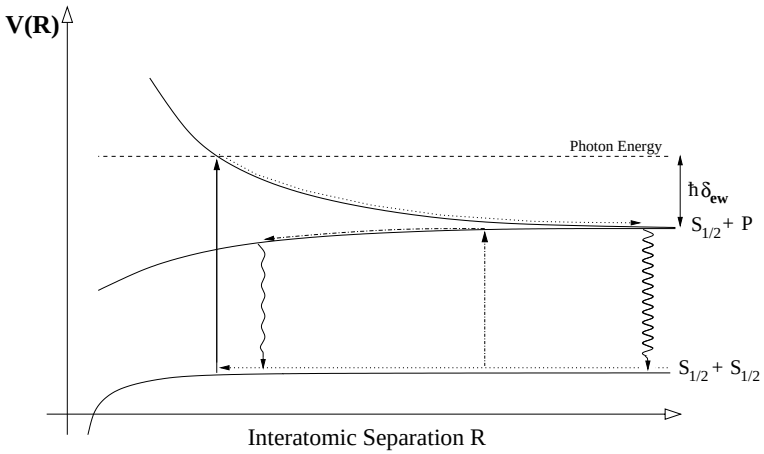

Figure 3.13: *The two relevant electronic transitions involved in light-assisted inelastic collisions. The repulsive molecular potential is excited by blue-detuned light, whereas the attractive potential can be excited by red-detuned light fields.*

One finds that $p_{R_c} \propto \delta_{EW}^{-1/3}$ (from the shape of the potential) and uses a semiclassical Landau-Zener model [Bal94] to obtain $p_{exc} \propto I \cdot \delta^{-4/3}$. I represents the intensity of the evanescent wave. The overall dependence of β on intensity and detuning of the evanescent wave thus turns out to be

$$\beta \propto \frac{I}{\delta_{EW}^2}. \tag{3.76}$$

This result has been confirmed by measurements reported on in reference [Ham99]. Rate coefficients for the near-resonant evanescent wave are of the order of $10^{-12}\,\mathrm{cm}^3/\mathrm{s}$ and can be significantly reduced by using the far-detuned evanescent wave instead. The light of the red-detuned microtrap laser is so far from resonance, that it virtually does not cause any light-assisted collisions.

Three-body Collisions

Another sort of inelastic collision process that now involves three ultracold atoms in one incidence is appropriately labelled three-body collision. In such an event two of the colliding atoms form a dimer while the third partner carries away binding energy and momentum. Usually this leads to a removal of three atoms from the trap although in rare incidences where the binding energy is below the trap depth it can also result in heating. Due to the difficulty of experimentally distinguishing three-body losses from binary loss processes there exist few data on rate coefficients and their role has constantly been the object of speculations. The event rate generally depends on whether identical particles or mixed states collide and it also has a strong dependence on the temperature of the

sample. Theoretical considerations imply that the rate coefficient for three-body loss L_3 scales as the scattering length a to the fourth power and has a strong dependence on temperature. A recent experiment by T. Weber et al. [Web02] has experimentally confirmed this model in the case of cesium by exploiting the tunable scattering length and measuring the three-body loss in a CO_2-laser trap.

All three categories of collisions in general contribute to the loss from a trap. A differential equation describing the atom loss takes the form [Wal94]:

$$\frac{\dot{N}}{N} = -\alpha - \beta\langle n\rangle - L_3\langle n^2\rangle. \tag{3.77}$$

α is the coefficient representing background gas collisions, β summarizes the effects of all binary loss processes and L_3 is the loss coefficient due to three-body collisions. Depending on the actual scaling of $\langle n\rangle$ and $\langle n^2\rangle$ with N, one can either analytically or numerically solve this equation and use the solution as a model whose fit parameters α, β, L_3 are adjusted to give agreement with the experimental decay curve. Due to the strong dependence of L_3 on temperature and the degree of polarization, and because of the difficulty to experimentally separate binary and three-body processes, the value for L_3 obtained from a fit is usually sufficient only to provide an upper bound for the rate of these processes.

3.6 Towards Two-Dimensionality and Quantum Degeneracy

This final section of the chapter will give an overview of the experimental goals and prospects and explain how the important tool of evaporative cooling is applied to pursue them.

Each of the two microtrapping schemes represents one of the two relatively independent physical topics that are addressed. While the strong anisotropy of the DEW-trap is exploited to investigate two-dimensional behavior and how it affects scattering and issues connected to BEC, the dimple trap is aimed at achieving a BEC in three dimensions and investigate stability and scattering issues that have become accessible in the context of Feshbach tuning.

Since the reduction of dimensionality and the phase transition to BEC inherently rely on extremely low temperatures and high phase-space densities, the program to achieve these goals essentially reduces to further cooling and increasing phase-space density. Optical cooling schemes usually run into problems at phase-space densities close to the condensation threshold because of density related problems such as for instance radiation trapping. When it finally comes to the last cooling step it necessarily has to be taken by evaporative cooling. At this point it should be emphasized that whenever we talk of

cooling it essentially means *phase-space cooling*, i.e. the reduction of temperature with a simultaneous increase of phase-space density.

3.6.1 Evaporative Cooling

Due to its efficiency and suitability in a wide range of temperatures and density regimes evaporative cooling is up to date the only feasible method to reach quantum degeneracy. Evaporation in magnetic traps [Ket96] covers typically around seven orders of magnitude in phase-space density and its usefulness also for hybrid traps [Web02] or pure dipole traps have made evaporative cooling a widespread and universal tool. In the context of atomic gases it has first been proposed in 1986 by H.Hess [Hes86] and was demonstrated on laser cooled samples by Davies et al. [Dav95] and Petrich et al. [Pet95] independently. It marks a major breakthrough in laser cooling experiments as can be seen by the prompt attainment of BEC in the same year [And95]. A comprehensive review article on evaporative cooling can be found in [Ket96].

The underlying principle of evaporative cooling is the selective removal of energetic atoms from an atomic ensemble and subsequent thermalization. While the first step leads to a reduction of the average energy of the ensemble the second step takes care of a translation of this reduced energy into a reduced temperature. If the truncation parameter η defined by the value of the energy (in units of the thermal energy $k_B T$) that leads to a removal of an atom from the trap is large enough, the evaporative cooling leads not only to a reduction in temperature but also to the demanded increase in peak phase-space density. It is obvious that the main drawback of evaporative cooling is the inherent loss of atoms.

Plain and Forced Evaporation

One distinguishes between two cases of evaporative cooling: Plain evaporative cooling occurs when a potential hosts an ensemble whose temperature is large enough that a significant fraction of the atoms has sufficient energy to leave the trap. In this case hot atoms will escape from the trap and cool the remaining sample until a temperature of about $T \approx 1/10 \cdot U/k_B$ is reached and evaporation stops. The potential itself is unchanged during this process. This form of evaporation takes place for instance when atoms are transferred from a deep into a shallow trap or when a continuous heating process exists that boils atoms from the trap until a balance between heating and cooling through loss of hot atoms is established.

In contrast to this plain evaporation, forced evaporation is applied by a continuous reduction of the trapping potential which forces the ensemble to continuously accommodate to the progressively shallower potential. The reduction speed of the potential depth is usually chosen in such a way that the ratio between the selection parameter η defined by the potential brim and the thermal energy of the ensemble $k_B T$ stays constant.

The various implementations of forced evaporative cooling in general only differ in how the energetic atoms are removed from the ensemble. While the standard method in magnetic traps and some hybrid traps is RF-evaporation that uses radiofrequency transitions between different m_F-states to drive energetic atoms into untrapped states, the most common way in dipole traps is lowering some optical potential. An often encountered problem of this scheme is the simultaneous reduction of density and thus elastic collision rate while the potential is being lowered. Only hard wall potentials such as the evanescent wave don't suffer from this disadvantage. Because of this reduction of the collision rate it is much harder to attain conditions for runaway evaporation in dipole traps which is most likely the reason that only two experiments have managed to create BEC in a dipole trap up to this day [Bar01, Web02]. The microtrapping schemes initially have such large elastic collision rates ($\sim 1\,\mathrm{kHz}$) and short thermalization times that even though evaporation progressively slows down, it is still fast enough to ensure good efficiency.

Time Scale of Evaporation

If one considers forced evaporative cooling, an important point is how fast the potentials can be lowered while still maintaining efficient evaporation. This essentially boils down to the question of how fast high energetic atoms that are removed by the energy selection can be replenished by elastic collisions within the ensemble. The faster this replenishment takes place the faster can the potential be lowered without affecting the efficiency of evaporation. Reference [Ket96] states the result for the case of a large truncation parameter η which is kept fixed relative to the thermal energy of the ensemble:

$$\frac{\dot{N}}{N} = \sqrt{2}\gamma_{el}\eta e^{-\eta}. \tag{3.78}$$

N is the number of trapped atoms. This rate of evaporating atoms is therefore a function of the elastic collision rate γ_{el} and the truncation parameter η. The larger the elastic collision rate of the atomic sample, the faster are high energetic atoms produced. The η dependence stems mainly from the Boltzmann distribution that determines how probable the production of a high energetic particle is. Evidently one can reasonably fast cool an ensemble at large truncation parameters if only the elastic collision rate is sufficiently large.

Evaporation Efficiency

The evaporation efficiency is an important parameter that determines what gain in phase-space density can be achieved with a given number of atoms. It is the deciding parameter of whether an attempt to create a BEC is successful or fails. Defined by the

relation

$$\epsilon \equiv \frac{\ln\left(\frac{D'}{D}\right)}{\ln\left(\frac{N}{N'}\right)}, \tag{3.79}$$

it can be understood as the orders of magnitude gain in phase-space density per order of magnitude of lost atoms. D' and D are the values of the phase-space density at the end and the beginning of the evaporation respectively, while N' and N denote the corresponding atom numbers. In the ideal case of an isotropic selection of energetic particles the expected efficiency is found to be $\epsilon = \eta - 3$ with the truncation parameter η. The most efficient forced evaporation experiments in magnetic traps reach ϵ-values of about three which corresponds to a factor 1000 increase in phase-space density for each order of magnitude of lost atoms. So the higher its value the larger is the gain in phase-space density per lost atom.

There are several factors that determine the efficiency of evaporative cooling. A very important one is the ratio of "good" to "bad" collisions. While the elastic collisions that mediate thermalization are labelled "good" collisions, all inelastic collisions that lead to losses constitute the "bad" ones. Evaporative cooling is therefore essentially a race between thermalization and losses. A favorably large ratio of "good" to "bad" collisions leads to a situation where losses on the timescale of thermalization are small or even negligible. In this case the selection parameter η can be chosen to be large in order to obtain a good evaporation efficiency. In case of a poor ratio of "good" to "bad" collisions this parameter has to be relatively small and consequently the evaporation has to be fast in order to achieve any gain in phase-space density at all. This usually leads to a poor evaporation efficiency. Particularly helpful in this context is the attainment of "runaway" evaporation that is defined by a progressively increasing thermalization rate during the evaporation. In this case the evaporation can be performed progressively faster with constant efficiency and unless new severe loss mechanisms set in, the attainment of BEC is straightforward.

Another aspect of importance for the efficiency of the evaporation is how energetic atoms are selected for removal. If the selection mechanism probes the kinetic energy of a particle in only one or two degrees of freedom, atoms moving with a large kinetic energy along another direction will not be removed. The fact that a certain fraction of the energetic atoms is unaffected by the selection mechanism leads to a reduced evaporation efficiency. In general it is desirable that the solid angle from which the selection mechanism can remove atoms is as large as possible.

3.6.2 Bose-Einstein Condensation

Bose-Einstein condensation is the quantum statistical phenomenon that a bosonic ensemble satisfying the requirement

$$D = n \cdot \lambda_{dB}^3 = 2.612, \tag{3.80}$$

for its phase-space density D, macroscopically populates the absolute ground-state of the system. λ_{dB} is the thermal de-Broglie wavelength defined by

$$\lambda_{dB} = \frac{h}{\sqrt{2\pi m k_B T}}. \tag{3.81}$$

Equation 3.80 can be interpreted as a criterion for the parameters density n and temperature T at which an atomic wave packet with the extension λ_{dB}^3 overlaps with adjacent atomic wave packets. The BEC phase transition has first been observed in a dilute atomic vapor of Rubidium-87 atoms [And95] in the year 1995. Since then a variety of excellent review articles (e.g. [Ket99b]) have been published that describe the astonishing properties of this coherent state. Bose-Einstein condensates from a number of different elements have been created, mostly by the standard technique of using radiofrequency evaporation in a magnetic trap.

The peculiar properties of the cesium atom (see Section 3.5) make it an interesting candidate for the production of a BEC but due to these very same properties standard methods of RF-evaporation are bound to fail [Söd98]. After cesium has also resisted many attempts to create a BEC in optical dipole traps, which are not subject to the detrimental dipolar relaxation, very recently a Bose-Einstein condensate of cesium has been achieved by T. Weber and coworkers [Web02]. The prospect of being able to tune the scattering properties as well as the mean field interaction of the condensate make it a very fruitful object to study. Particularly in combination with a 2D environment this will lead to interesting new physics. The next section will focus on this subject.

In the GOST experiment only unpolarized samples have been used up to now. This implies that expression 3.80 for the phase-space density has to be multiplied with a degeneracy factor of 1/7 since the atoms presumably populate all seven substates of the $|F = 3\rangle$ ground-state. In the next stage of the experiment we will polarize the atomic ensemble to the $|F = 3, m_F = 3\rangle$ state. This will remove the degeneracy factor of 1/7 and allow for Feshbach tuning of the interaction properties according to what was said in Section 3.5. In particular, choosing the sign of the scattering length determines whether the condensate has an attractive (negative a) or a repulsive (positive a) mean field interaction and therefore determines whether it is stable or not.

3.6.3 Two-Dimensionality

Reducing the dimensionality of an atomic gas does not imply the reduction of interesting physical questions. On the contrary this brings about the existence of new effects and altered behavior as compared to the three-dimensional case. Two-dimensionality in this context essentially means *kinematically* two-dimensional or "freezing out" the vertical motion. In that sense a two-dimensional atomic gas is created as soon as the thermal energy $k_B T$ of the gas is much smaller than the lowest excitation energy of one direction of the confinement and thus this degree of freedom becomes energetically unavailable

for the atoms. Although atoms don't move along this direction the extension of their ground-state wave function $l_0 = \sqrt{\hbar/m\omega_0}$ is nonzero. (ω_0 denotes the trap frequency of the strongly confined direction.) One can distinguish between three separate regimes in the context of 2D:

Scattering in 2D, $l_0 \ll a$

For a thermal energy far below the vibrational energy the vertical extension of the wave function is essentially equal to this extension of the ground-state l_0. If additionally the scattering length a is much larger than l_0, the scattering has to be treated purely two-dimensional. In this situation the elastic as well as the inelastic scattering behavior is strongly modified. Reference [Pet01] calculates the altered properties of scattering in such a two-dimensional environment and states that it has to be treated truly two-dimensional in the sense that one spatial dimension is completely disregarded. In this case for instance the dependence of the elastic scattering rate γ_{el} on the scattering length a exhibits a pronounced resonance behavior as opposed to the 3D case in which $\gamma_{el} \propto a^2$. This offers interesting prospects for the case of cesium which allows for tuning of a. Up to now this regime of two-dimensionality has not been accessible for experiments with cold atoms and theories have yet to be confirmed experimentally.

Boundary to 2D, $k_B T \leq \hbar\omega_0$

In the experimentally easier accessible temperature regime of $k_B T \leq \hbar\omega_0$ scattering can still be treated with the standard methods of three-dimensional scattering theory. The strong confinement however, leads to significant deviations from the 3D behavior for instance in the dependence of the elastic scattering cross section on temperature. While in 3D in the unitary limit ($|a| \to \infty$) the elastic scattering cross section is $\sigma = 4\pi/k^2$ and thus strongly increases with decreasing temperature the elastic scattering cross section in the tightly confined situation is practically temperature independent due to a constant contribution of the zero-point oscillation to the relative momentum during the scattering process. One also expects thermalization between the tightly confined and the more or less free degrees of freedom to go exponentially less rapid with decreasing temperature

$$\frac{\Delta\dot{T}}{\Delta T} \propto \exp\left(-\frac{\hbar\omega_0}{T}\right), \tag{3.82}$$

as due to simple symmetry arguments only collisions that change the total number of vibrational quanta by an even multiple of $\hbar\omega_0$ are allowed. This strong restriction leads to a thermal decoupling of the degrees of freedom at $k_B T \approx \hbar\omega_0$. It proves to be hindering for the case in which cooling is not applied simultaneously to all degrees of freedom. Partly, these theoretical predictions have been tested and confirmed by experiments at Stanford and Paris [Vul99, Bou02].

A Degenerate Gas in 2D, $\mu \ll \hbar\omega_0$

The thermal energy of a degenerate gas is usually negligible compared to the mean field energy of the condensate. Therefore the criterion for a transition into the 2D regime is in this case given by the requirement $\mu \ll \hbar\omega_0$, where μ is the interaction energy of a weakly interacting BEC which in 3D corresponds to the chemical potential of the condensate [Gör01]. In the context of a degenerate gas the restriction of the atoms to one or two dimensions leads to a modified coherence behavior. While a characteristic property of a standard 3D BEC (aside from the macroscopic population of a single quantum state) is its global phase coherence, a condensate of reduced dimensionality exhibits spatial phase fluctuations in a degenerate state that has been labelled quasi-condensate (QC) [Kag87]. The coherence length in such a case is not equal to the extension of the condensate in contrast to the 3D case [Blo00]. Only at temperatures well below the transition temperature T_c can a BEC in the three-dimensional sense be established. The reason for this peculiarity is the fact that in a two-dimensional homogeneous system no long-range order can be established [Mer68] and only due to the modification of the density of states by the atom confinement [Bag91] can a true condensate be created at some temperature $T \ll T_c$. First experimental indication for such a quasi condensate has been received in a two-dimensional system of atomic hydrogen adsorbed on a liquid helium surface through the suppression of inelastic losses [Saf98]. Other experiments have loaded 3D BECs into 1D or 2D traps to investigate the coherence properties in situations of reduced dimensionality [Gör01, Det01].

Cesium is a particularly interesting case in the context of reduced dimensionality, as the tunability of its interaction properties via the Feshbach resonance can be exploited to reversibly cross the transition from the 3D to the 2D case according to the criterion $\mu \ll \hbar\omega_0$. The interaction energy μ depends on the scattering length of the atoms and can therefore be adjusted in a wide range as has been demonstrated by reference [Web02].

Another prediction that arises from a theoretical analysis is made in reference [Pet00]. In two dimensions the mean field interaction of a degenerate gas is claimed to depend on the frequency ω_0 of the tight confinement which implies the possibility of tuning the condensate interaction similar to a Feshbach resonance by simply changing trap parameters such as laser power.

In our experiment questions related to two-dimensionality can be addressed by exploiting the strong anisotropy of the DEW-trap. In the horizontal directions with their approximately 50 Hz trap frequency the atoms move essentially free at a few hundred nanokelvin ensemble temperature (50 Hz trap frequency correspond to an energy splitting of about 2.4 nK). On the other hand, the tight vertical confinement of approximately 12 kHz leads to a transition into the 2D regime ($k_B T = \hbar\omega_0$) at more than 500 nK which is well within the range of attainable temperatures in the GOST. Cooling is done through evaporation by lowering the laser intensity which in turn also lowers the trap frequen-

cies. Therefore the actual temperatures for the transition are closer to 100 nK than to 500 nK. Chapter 6 shows experimental results and further discusses them.

Chapter 4

Experimental Setup and Procedures

A modern laser cooling experiment has to comply with a variety of technical demands. It has to decelerate atoms from the extreme thermal velocities, cool them to virtually zero Kelvin, keep them for seconds or even minutes without significantly disturbing their delicate state and finally be able to extract information from the feeble signals emitted by a few as 1000 atoms. In view of these requirements it is not surprising that even though the theoretical background and initial experimental ideas were already present for decades, it was the technical progress in vacuum and especially laser technology that sparked the beginning of the field of laser cooling.

Stable and easily tunable lasers provide the means to exert strong forces for the deceleration of atoms and to accurately address and manipulate atomic substates for cooling and diagnostics. At the same time the combination of ultrahigh vacuum (UHV) environment, magnetic fields and light forces fulfill the imperative requirement of thermally isolating the laser-cooled atoms from room temperature surfaces sometimes as little as $1\,\mu$m apart.

This chapter will provide an overview of what the most important technical ingredients of the GOST project are, explain the measurement procedures and describe the preparation of the cold atom reservoir for the microtraps. Emphasis will be placed on the most recent improvements and newly introduced setups while details of already established parts can be found in the references [Mos99, Man99, Ham99, Ryc00].

Section 4.1 explains the vacuum system that is used to maintain a vacuum of pressures below 10^{-11} mbar while at the same time providing a steady flux of 10^8 cold Cs-atoms per second from the atomic source. Section 4.2 is dedicated to the various lasers used for MOT, Zeeman slower and the three dipole trap stages. It addresses issues like stabilization, optical setup, intensity and frequency control. As virtually all manipulation, cooling and diagnosis relies on lasers, this section constitutes the main part of this chapter. Section 4.3 focusses on how the measurement cycle is structured and what means of diagnosis are used to extract information from the atoms. Finally Section 4.4 will characterize the reservoir of cold atoms provided by the GOST.

4.1 Vacuum System

The main purpose of the vacuum apparatus is to isolate the ultracold atoms from the environment. The predominant challenge arising in this context is maintaining UHV-conditions while at the same time allowing for a constant and high flux of Cs-atoms into the trapping region. This problem is solved by using separate sections of the apparatus for the creation of an effusive atomic beam and for the trapping and cooling experiments. The two parts are connected via a differential pump section that maintains a pressure gradient of up to three orders of magnitude between its ends. A photograph and a schematic overview of the complete apparatus is shown in figure 4.1.

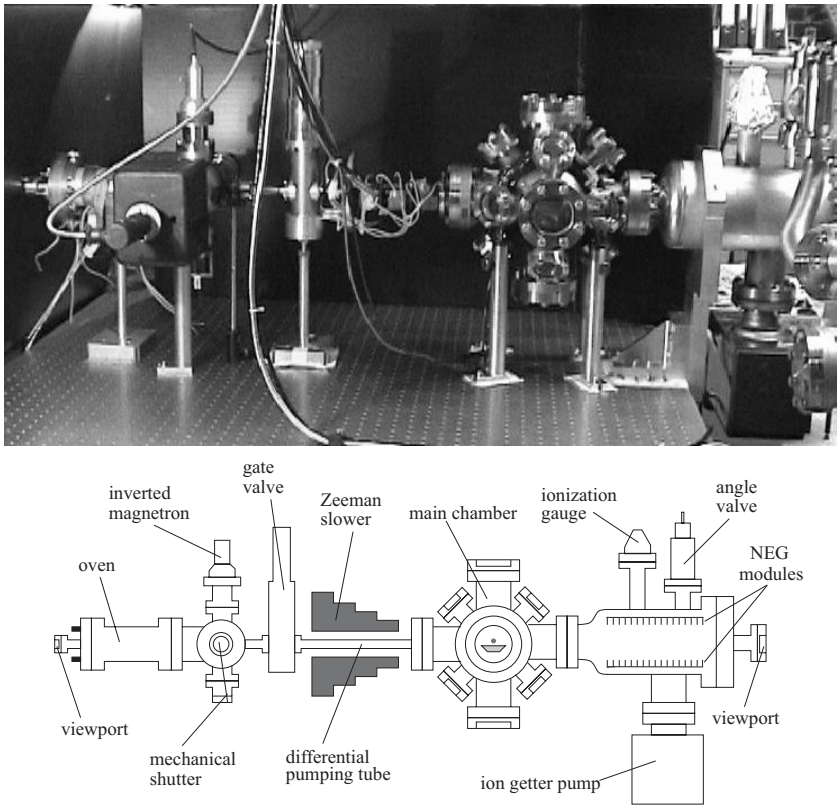

Figure 4.1: *Picture and schematics of the vacuum apparatus.*

It has a length of about 1.5 meters and sits on a vibration damped optical table. The following sections will go into more detail concerning the various components.

4.1.1 Atom Source and Atomic Beam

The cesium atoms are stored and released from ten Cs-dispensers inside a heated oven chamber. The dispensers are hollow metallic sticks of about 4 cm length which contain chemically bound cesium-133 along with some getter material. The release of atoms is initiated and controlled by an electrical current of 2 ampéres through the dispensers which heats them to several hundred degrees and breaks the chemical bond of the cesium compound. This method allows for clean and controlled handling of the very reactive and poisonous cesium. At an oven temperature of 85 ° C cesium has a vapor pressure of 10^{-4} mbar. A 2 mm wide hole then creates the effusive atomic beam that passes through the various parts of the apparatus and supplies the MOT with Cs-atoms. Attached to the oven behind the nozzle is a 6-way-cross which hosts an inverted magnetron vacuum gauge, an ion-getter-pump, a step-motor driven wobble stick serving as an atomic beam shutter and a vacuum valve used to connect a turbo pump for dispenser exchange. After passing this section the atomic beam propagates through a short flexible tube introduced to relief stress between the different parts of the apparatus and to have the possibility of aligning the atomic beam with the differential pump section. A valve used to seal off the experiment section during dispenser exchange connects the flexible tube with the differential pump section. This section consists of a stainless-steel tube of 45 cm length whose inner diameter increases in five steps from 4 mm up to 9 mm. This section has two purposes: Firstly it maintains large pressure gradients of more than three orders of magnitude between its ends and thus allows for experiments to take place in a UHV-environment of 10^{-11} mbar with corresponding storage times of minutes while at the same time vast amounts of atoms are released at comparatively high pressures of 10^{-4} mbar at its opposite end. Secondly it hosts the Zeeman slowing section, where a combination of four magnetic coils placed coaxially around the vacuum tube and a near resonant laser beam counterpropagating the atomic beam decelerate the fast thermal atoms down to a few meters per second. The atom source and atomic beam section create a flux of 10^8 slow atoms per second which directly proceed into the experiment chamber.

4.1.2 Experiment Section

The core piece of the apparatus that hosts all traps is a spherical stainless-steel chamber which has openings on two opposite sides; one being the entry point of the atoms and the other a passage into a large pump section. In addition to these there are 16 anti-reflection coated viewports (for 852 nm) used to shine lasers into the chamber and to detect fluorescence from the atoms using a CCD-camera. 0.5 cm below the center of the chamber lies the surface of a fused-silica prism that serves as the vacuum-dielectric interface on which the evanescent waves are created. The prism has a trapezoidal baseline, a five on four centimeters surface and is situated on a titanium holder which sits

on the bottom viewport of the chamber. Both the bottom surface and the angled sides of the prism are anti-reflection coated for 852 nm and 1064 nm. The top surface is left uncoated in order to prevent any unwanted interference effects of the evanescent waves.

Two magnetic coils of 250 windings each are wound directly on the outer surface of the chamber. They are placed 9 cm apart from each other and connected in anti-Helmholtz configuration to create the quadrupole field for the MOT. The coil axes lie perpendicular to the plane defined by the atomic beam and gravity. Three pairs of additional coils are attached to the chamber in three perpendicular orientations in order to be able to create small nearly homogeneous field components in any direction at the location of the atoms. That way one can compensate earth magnetic field and additionally position the atom cloud of the MOT arbitrarily by shifting the point of zero magnetic field.

A large pump section is connected to the main chamber opposite of the entry point of the atomic beam via a 5 cm wide opening. Its purpose is to efficiently pump the volume of the experiment chamber and to remove the part of atoms that due to their initially large velocity could not be slowed and trapped. A viewport situated on the opposite side of the pump chamber serves as entry point for the Zeeman slowing laser. Additionally the pump chamber hosts a valve to connect a turbo pump and a UHV-gauge. Finally two pumps provide the necessary pumping power needed to meet the vacuum requirements. One of them being a strong ion-getter pump attached to the bottom of the apparatus and the other a pair of Non-Evaporative-Getter modules (NEG-modules) that provide most of the pumping power and conveniently after once being activated don't rely on electrical power.

4.2 Laser Setup

The various lasers used for the different traps play a key role in this experiment. They exert strong forces and allow for a deceleration of the atoms with several thousand times earth acceleration g, they take care of energy dissipation and cool atoms from about 100° C to microkelvin within milliseconds, they provide a variety of different trap designs for all kinds of experimental purposes and finally enable the experimentalist to extract accurate information from the system, in some cases even without disturbing it significantly. The reason that laser light plays this universal role, is that it constitutes a large energy reservoir (compared to the kinetic energy of the atoms) that can be coupled to either internal or external degrees of freedom of the atom in a very controlled way. Depending on detuning and intensity it can give rise to either dissipative or conservative forces and with a sufficiently small linewidth can separately address atomic substates as little as MHz apart. The fact that it can couple the external motion of an atom to internal electronic transitions using the photon recoil or spatially dependent light shifts gives rise to sophisticated and efficient cooling schemes. In order to exploit these

possibilities one has to be able to control intensity and particularly frequency very well. The following sections discuss the implementation of the different lasers associated with the various traps and how the requirements concerning stability and geometry are being met. Some of the less recent parts of the experimental setup have been explained in other sources before ([Mos99, Man99, Ham99, Ryc00]) and have turned out to be standard by now, so that most details can be omitted here.

4.2.1 MOT and Zeeman Slower

This section will briefly discuss the technical ingredients that make up the MOT and the Zeeman slower. Both are by now considered standard tools in many laser cooling experiments and are routinely used as an atom collecting and pre-cooling stage for other trap types such as dipole traps or magnetic traps. Even though explanations will be kept short, this should not suggest that MOT and Zeeman slower play a minor role in the experiment. Only due to the impressive capture velocity of the MOT is it possible to bridge the huge gap between thermal atom velocities and those that can be held in a dipole- or magnetic trap. Besides, only during the MOT-phase is it possible to gather information from the atoms using fluorescence detection.

Light Sources

The light used for all near resonant applications such as the MOT, Zeeman slower, different repumping beams, absorption imaging or the evanescent wave is provided by laser diodes (SDL-5712-H1) operating near 852 nm. These so-called DBR-diodes feature a layer of spatially periodical index of refraction behind the laser-active semiconductor material that selectively reflects light of a narrow frequency band back and thus passively stabilizes the frequency to a few ten MHz. Up to 100 mW of near-infrared light at 852 nm are available from each laser diode. The frequency can be tuned by either adjusting the current through the diode or by changing the diode temperature using an integrated peltier element. While modifying the diode current allows for for fast (kHz-MHz) frequency modulation within a small frequency interval, tuning the diode temperature changes frequency in a several hundred GHz wide range without mode hops at a rate of ~ 70 GHz/s. During the standard mode of operation, the diode temperature is stabilized at a certain value, while the diode current is used to actively lock the laser frequency to an atomic reference.

Frequency Lock

Operating a MOT at a few MHz detuned below the atomic transition makes accurate and reliable frequency stabilization imperative. Since both transfer into the GOST and all diagnostics depend on a stable MOT operation and in particular on stable laser

frequencies, considerable effort has been made to replace the former polarization lock scheme [Mos99] with a new scheme where the laser frequency is locked to a grating stabilized master laser of about 100 kHz linewidth. This scheme has the advantage of both preventing slow drifts of the lock frequency and providing a smaller frequency width as compared to the former setup. The introduction of this scheme proved to be a major improvement in terms of reproducibility of measurement results and will therefore be explained in some detail at this point.

Both the diode laser providing light for the closed cooling transition $F = 4 \rightarrow F' = 5$ of the MOT and the diode laser used as a light source for the Zeeman slowing beam are locked to a stable reference laser (master laser) by comparing the beat signal between master laser and secondary laser with an external frequency reference generated by a voltage controlled oscillator (VCO). Since the frequency of the repumping transition ($F = 3 \rightarrow F' = 3$) proved to be uncritical in terms of stability the corresponding laser diode is still stabilized by the polarization lock scheme.

The master laser consists of a laser diode (SDL-5410) which has its frequency locked to 170 MHz below the $F = 4 \rightarrow F' = 5$ transition. It is stabilized using the diode current for fast frequency adjustments and an external grating (Littrow configuration) for slow ones in a wider range. The frequency reference is provided by a modulation-transfer spectroscopy signal obtained from a 170 MHz blue shifted beam passing through a cesium vapor cell. This RF-scheme provides a Doppler free, robust signal with a good signal to noise ratio. In particular it is subject to much less long term drift as for instance the polarization lock scheme. Details of this spectroscopy scheme can be found in [Raj80, Shi82]. The frequency width of this laser is about 100 kHz with no significant long term drift of its absolute frequency.

In order to lock MOT- and Zeeman laser to this reference a beat signal between the reference laser and one of the secondary lasers is obtained according to figure 4.2. After the collimated and shaped beam has passed through an optical diode, two weak (few mW) parasitical beams are extracted from the main beam at the front and rear surface of a beamsplitter substrate. One of these beams passes through a saturation spectroscopy setup and is detected on a photodiode. This spectroscopy signal serves as an absolute frequency reference. The second beam of about 3 mW power is overlapped with the reference laser beam on a fast photodiode (bandwidth 1 GHz) after its polarization and beam parameters have been adjusted to match those of the reference laser. The fast beat signal between both light fields of about two hundred MHz is translated into an electronic RF-signal by the photodiode and further processed by a chain of RF-electronics as shown in figure 4.3. The scheme, that is used here has been introduced in reference [Sch99]. The aim is now to create an error signal from this beat signal that features a steep slope and an adjustable zero crossing at the desired laser frequency. To accomplish this, the beat signal is first compared to a reference frequency provided by a VCO using an RF-mixer. Since the mixer generates both the sum- and the difference frequency as output signal, a lowpass filter is added to the chain that removes the

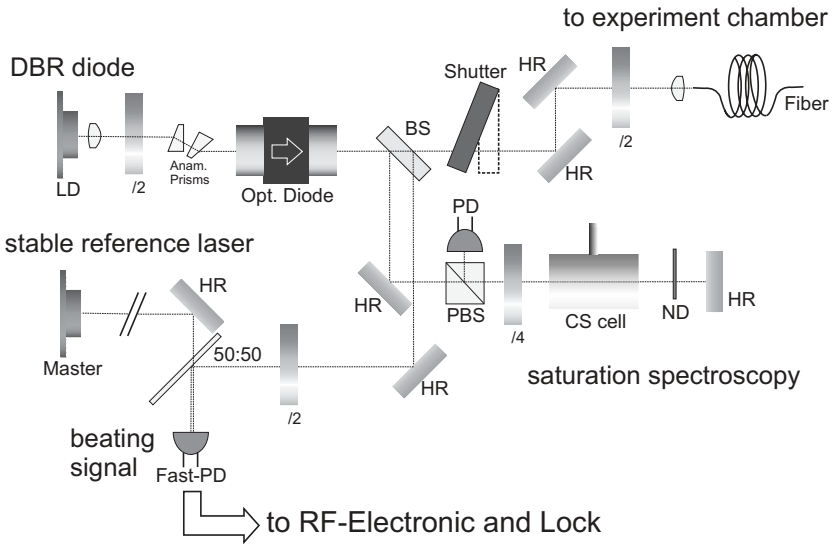

Figure 4.2: *Optical setup for the frequency lock of the MOT- and the Zeeman slowing laser.*

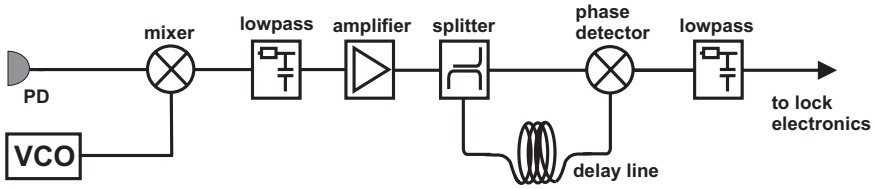

Figure 4.3: *Schematics of the RF electronics used to generate an error signal [Sch99].*

higher sum frequency. The remaining signal is the amplified and split in two parts by a power splitter. While one branch directly proceeds to a phase detector the other branch features a delay line (3 m BNC-cable) that causes a frequency dependent phase shift between the two signal parts. The phase detector now translates this shift into a DC-voltage between -1 and 1 volt thus providing the desired error signal. The slope steepness can be adjusted by changing the length of the delay line while the position of the zero crossing is conveniently tunable through the frequency of the VCO. Figure 4.4 shows the spectroscopy signal and the error signal obtained by a frequency sweep over the relevant range. The VCO voltage and thus the oscillator frequency is adjusted such that the error signal has a zero crossing slightly (8 MHz for the MOT laser and 25 MHz in case of the Zeeman slower laser) to the left (red detuning) of the bottom dip of the spectroscopy signal ($F = 4 \rightarrow F' = 5$ transition). Shifting the detuning during

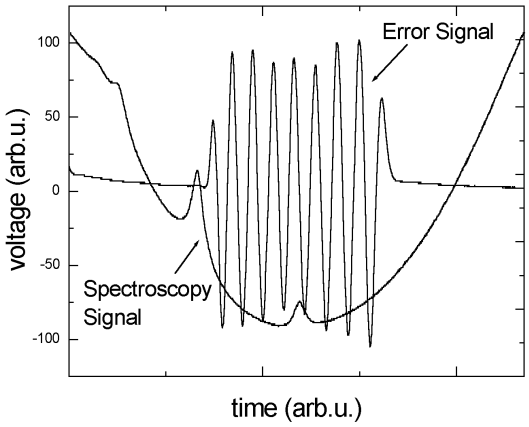

Figure 4.4: *Reference signal from the saturation spectroscopy and error signal as obtained by the beat lock scheme*

transfer into the dipole trap to $-60\,\mathrm{MHz}$ is accomplished by ramping the VCO voltage to the corresponding value. This results in the zero crossing of the error signal and thus the laser frequency being dragged along. In the current setup the accessible frequency ranges from $-122\,\mathrm{MHz}$ up to $+44\,\mathrm{MHz}$ with respect to the $F = 4 \rightarrow F' = 5$ transition and is limited by the VCO frequency range. In order to measure the frequency width of a secondary laser a beat signal between a second stable reference laser and the locked secondary laser was taken. Its width of about 1 MHz indicates a similar frequency width for the secondary laser. (As this is significantly larger than the frequency width of the reference laser the main contribution stems from the secondary laser.) Besides from the improved long term stability this implies a factor of ten improvement of the frequency width.

MOT Geometry

After being frequency stabilized the laser light has to be brought into the vacuum apparatus. The following section briefly discusses the geometrical setup of MOT and Zeeman slower.

In order to prevent stray light from any near-resonant laser during the dipole trapping stage, these lasers have been set up on a separate table apart from the vacuum apparatus and the atoms. During MOT operation this light is coupled into polarization maintaining single-mode fibers and guided onto the main experiment table. Aside from the suppression of potentially harmful near-resonant stray light this has the advantage of geometrically decoupling the optical setup on opposite sides of the fiber leading to enhanced stability. Separate fibers are used for the beams driving the MOT-cooling and

MOT-repumping transitions whereas both Zeeman slower beams are simultaneously coupled into one fiber. After leaving the fiber, both MOT beams are collimated to a waist of 0.7 cm, overlapped at a polarizing beam splitter cube and then split into five separate beams. One is shone horizontally through the center of the experiment chamber while the other four beams symmetrically enter the vacuum in a plane perpendicular to the horizontal MOT beam. The intensity of each beam amounts to 10.4 mW/cm^2 which is 9.4 times the saturation intensity of cesium. In this configuration the intersection of the six beams lies about 0.5 cm above the center of the prism surface and approximately coincides with the point of zero field strength of the MOT quadrupole field. At a current of 4 A running through the quadrupole coils the atoms experience a field gradient of $\approx$ 20 Gauss/cm in the strong (horizontal) axis and half of it in the weak axis.

The combined cooling-repumping beam of the Zeeman slower is formed in such a way that it optimally overlaps with the atomic beam. This is realized by making it converge to a small focus at the place of the oven nozzle after entering the vacuum apparatus with a waist of approximately 1.5 cm. Its power at this point is 30 mW. It is circularly polarized by a quarter waveplate at the entrance viewport. Since it is passing right through the MOT cloud with a detuning of only 25 MHz there is a visible effect of pushing the atoms into the direction of the atomic oven.

4.2.2 The Gravito-optical Surface Trap

Technically the GOST consists of only three laser fields. The evanescent wave providing the vertical confinement and the Sisyphus cooling process as described in Chapter 3, the hollow beam confining the atoms laterally and finally the repumping laser that closes the Sisyphus cooling cycle. The relative simplicity of this trapping scheme manifests itself in terms of reproducibility and forgiveness regarding alignment or frequency adjustment. The following paragraphs discuss technical aspects related to these three lasers and their relevant experimental parameters.

Evanescent Wave

Two different laser sources alternatively provide light for the evanescent wave, depending on whether optical Sisyphus cooling is applied or far-detuned and nearly conservative potentials are required. The light used for the dissipative evanescent wave is derived from a 150 mW output laser diode similar to the ones used for the MOT and the Zeeman slower. Actively locking the frequency is not necessary in this case since the detuning of +3-+6 GHz with respect to the $F = 3 \rightarrow F'$-transition is much larger than the passive stability of the temperature stabilized DRB-diode of roughly few ten MHz. The evanescent wave laser can be detuned at a rate of 70 GHz per second by changing the diode temperature using the integrated peltier element. This option is used to apply an evaporation ramp of up to 200 GHz detuning as discussed in Section 4.4.2. The

optical setup is illustrated in figure 4.5. A set of anamorphic prisms and an optical

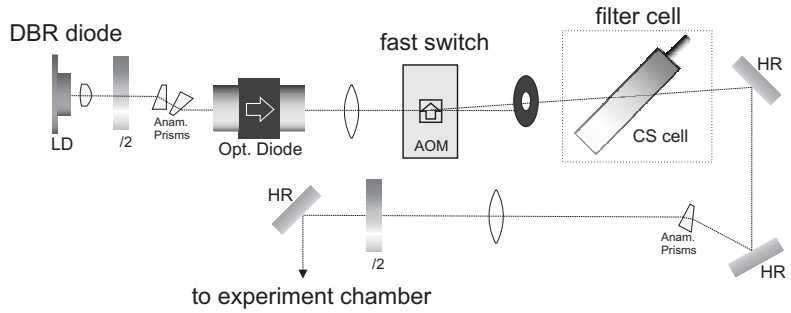

Figure 4.5: *Optical setup for the near resonant evanescent wave*

diode take care of beam shaping and prevent back reflection into the laser diode. A 200 MHz acousto-optical modulator (AOM) allows for fast switching operations (within microseconds) which are needed to accurately measure the ensemble temperature in the GOST (see Section 4.3.5). Before the laser light is finally shaped using an anamorphic prism (creating an elliptical beam cross section to yield a circular evanescent wave spot on the prism surface) and a focussing lens to adjust the beam waist to the desired value, it has to pass through a heated cesium vapor cell that absorbs any remaining fraction of resonant photons [Ham01]. This filter cell becomes necessary because otherwise a detrimental fraction of photons that is emitted into side modes of the diode laser through amplified spontaneous emission will cause strong heating any time the evanescent wave detuning is at a multiple of the 36 GHz corresponding to the mode spacing of the diode laser cavity and a side mode comes into resonance. At a temperature of 50° C the cesium vapor inside the cell is optically thick for resonant light and that way gets rid of unwanted heating. A half-waveplate sets the polarization to TM in order to optimize the evanescent wave intensity according to the considerations in Section 3.3. Finally the evanescent wave spot is placed at the desired spot on the prism surface using a mirror fixed on top of a linear translation stage. Shifting the translation stage and changing the horizontal angle of the mirror allows for moving of the spot without changing the angle of incidence of the evanescent wave beam. The evanescent wave beam has a power of typically 45 mW, is focussed to a spot size of 700 μm (waist) in both directions and for optical cooling features a detuning of $3 - 6$ GHz above the $F = 3 \rightarrow F'$ transition. At an angle of incidence of one degree above the critical angle of $\Theta_{crit} = 43.6\,^\circ$ this amounts to a peak dipole potential at the center of the spot of around $U/k_B = 800\,\mu$K The $1/e$-decay length of intensity turns out to be $\Lambda = 0.71\,\mu$m.

In case a conservative evanescent wave potential is needed, two options are at hand. In experiments concerning the evaporation from the GOST or the tight dimple (see Section 5), the same laser diode as previously used for the optical cooling was temperature

tuned to provide light of up to 200 GHz detuning. At 200 GHz detuning the potential is reduced to about $U/k_B = 12\,\mu$K. Later, in experiments studying the wide dimple configuration and the DEW-trap, light from the titanium:sapphire laser was extracted from the hollow beam setup and prepared by a similar setup as used for the diode laser. In this case no filtering vapor cell is needed. As already listed in Chapter 3 the beam parameters are as follows: The beam has a power of 1.15 W at a detuning of typically 1.6 nm. It is focussed to a waist of $w_b = 400\,\mu$m and hits the prism surface at an angle Θ_b deviating by 3.2° from the critical angle of $\Theta_{crit} = 43.6°$. Its decay length Λ_b is therefore 395 nm and the potential barrier at the center of the light spot $U_b/k_B = 325\,\mu$K.

Hollow Beam

Horizontal confinement is provided by the hollow beam. Although its axicon optics manages to create light walls of a focus quality comparable to a Laguerre-Gaussian beam of the order 100 it naturally cannot achieve field gradients similar to the one created by an evanescent wave. It is therefore necessary to operate the laser at much larger detunings in order to avoid detrimental photon scattering rates and thus the need for much more laser power arises in order to create sufficiently large potential walls. In the current setup a titanium:sapphire laser which is pumped by a 10 W laser at 532 nm (Coherent Verdi-V10) provides up to 1.6 W of light at a wavelength of between 849.1 nm and 851.1 nm corresponding to a blue detuning of between 1 and 3 nm with respect to the Cs D_2 line at 852.1 nm. The output beam passes through an optical diode and a 200 MHz AOM which splits the light into a zeroth, a first and a second order beam that are used as the hollow beam, a far detuned evanescent wave (see Section 3.4.4) and a wavelength monitoring beam respectively. The experiments on evaporative cooling in the GOST reported on in Section 4.4.2 were performed in a different configuration. In order to be able to decrease the hollow beam intensity using the AOM it was necessary to use the first order beam as hollow beam. In these cases no far detuned evanescent wave derived from the titanium:sapphire laser was applied.

The light intended for the creation of the hollow beam is coupled into a polarization maintaining single-mode fiber to clean the transverse mode ($TEM_{0,0}$ being desired) and geometrically decouple the axicon optics from the section in front of the fiber. Figure 4.6 gives a schematic overview of the optics used to create the ring-shaped focus. After leaving the fiber the light is collimated and again focussed to an intermediate image plane by two achromatic lenses (AC). The axicon is introduced slightly behind the focussing achromat and leads to the creation of a ring instead of a point-like focus. The distance between the achromat and the axicon determines the diameter of the ring focus. To remove stray light from the inner perimeter of the hollow beam a coated glass substrate with a dark spot of almost the same size as the ring focus is placed inside the ring in this image plane. This plane is then imaged onto the prism surface in a near 1 : 1 image by two achromatic lenses of 300 mm focal length. The light enters the vacuum chamber

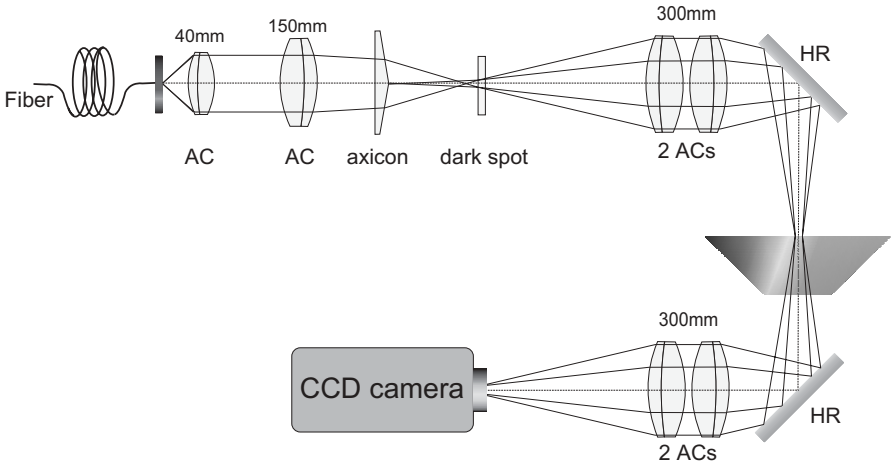

Figure 4.6: *Optical setup used to generate the ring-shaped focus.*

through the top viewport and leaves it through the bottom. For alignment purposes it is then identically imaged onto the CCD-chip of a monitor camera. This camera shows the relative positions of the hollow beam, all three evanescent waves and the red focus on the prism surface. It is a useful and extensively used tool to overlap the different light fields.

The parameters of the hollow beam unless otherwise specified are the following: Its total power of about 400 mW at the surface of the prism is distributed over a ring with a diameter of 820 μm and a $1/e^2$-wall thickness of about 20 μm. At a detuning of 1.6 nm this amounts to a potential depth of $U/k_B = 93\,\mu$K. In measurements where the hollow beam intensity has to be stabilized or dynamically changed, a photodiode is placed in the beam instead of the monitoring camera. Its signal is used as a feedback for the intensity lock electronics.

It turned out that the most critical part of the hollow beam setup is the single-mode fiber as the inserted power is far beyond specified tolerances. This leads to significantly higher insertion loss and a slow degradation of the fiber. Details on the setup and in particular on the alignment can be found in [Ham99].

Repumping Beam

In addition to the two retaining lasers a repumping beam that transfers atoms gotten into the $F = 4$ state back into the $F = 3$ ground state is needed. This very weak (few μW) repumping beam is resonant with the $F = 4 \rightarrow F' = 4$ transition and is continuously applied during the GOST and the dimple phase. As it is 250 MHz below the $F = 4 \rightarrow F' = 5$ transition it can be derived from the beam of the Zeeman slowing laser by extracting a small part and shifting it 225 MHz further to the red using an

AOM. An optical fiber guides the light to the vacuum apparatus where it illuminates the trapping region from above.

4.2.3 The Focussed Beam Surface Trap

The aim of the surface microtraps is to create very dense atomic ensembles close to the surface of the prism. Since inelastic collision processes which are assisted by trap light of any kind get progressively worse as the density of the ensemble increases it is necessary to use far-detuned light fields in order to suppress these processes. In the case of the attractive microtraps in which atoms are kept in places of maximum light intensity it is advisable to use very far-detuned light fields to prevent heating through photon scattering.

In a first implementation of the dimple trap the vertical confinement is realized by a 160 GHz blue-detuned evanescent wave. The detuning is dynamically set by changing the laser diode temperature through an external control input of the laser diode temperature controller. It however turns out that the lifetime of the trap significantly decreases as detuning increases and at the same time a strong heating of the ensemble is observed. Possibly this is due to defects in the evanescent wave which begin to become important as the depth of the evanescent wave decreases. The heating might be due to a selective removal of cold atoms (anti-evaporation) as these atoms probe the evanescent wave surface more frequently due to their larger bounce rate. In all consecutive experiments the repulsive evanescent wave was generated by light from the 1.6 nm blue-detuned titanium:sapphire laser. This beam originates as first order beam from the AOM of the hollow beam setup and is directly brought into the vacuum chamber via four mirrors. Two lenses focus the evanescent wave beam down to 400 μm waist and a half-waveplate adjusts the polarization to be TM. At the 1.15 W of available power and an angle of incidence of 3.2 ° above the critical angle this amounts to a maximum potential (Van-der-Waals attraction included) of $U/k_B = 325\,\mu$K at the center of the evanescent wave spot. The AOM allows for fast switching within microseconds and provides means to modulate the intensity of the beam. All implementations of the dimple trap design used light at 1064 nm for the attractive light field. At the corresponding detuning of almost 200 nm heating by photon scattering can be utterly neglected compared to the effect of the evanescent wave.

A part of the dimple trap experiments was performed using a 400 mW single longitudinal mode Nd:YAG laser (CrystaLaser) until it was replaced by a 10 W Yb-Fiber laser (IPG-Laser, model PYL-10) with a clean transverse mode ($M^2 < 1.1$) but a spectral width of more than 1 nm. The optical setup is straightforward and is depicted in figure 4.7. After the beam emerges from the fiber laser collimation optics, its plane of polarization is rotated to vertical by a half-waveplate and it is then focussed onto the crystal of an AOM. This AOM splits the beam into a zeroth order beam that is used as the red evanescent wave and a first order beam that proceeds through two lenses and

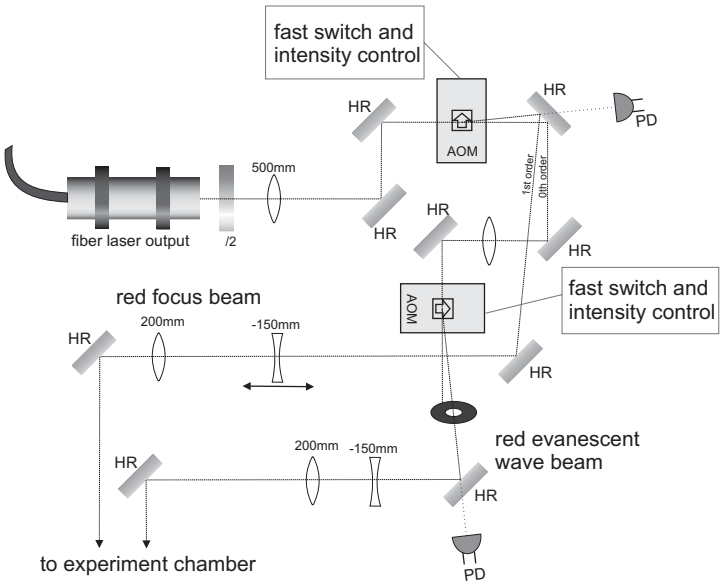

Figure 4.7: *Optical setup for the dimple laser and the red evanescent wave*

is reflected into the vacuum chamber by a mirror underneath the apparatus. The first lens is placed on a translation stage so that enlarging the focus size on the prism surface from 30 μm to 200 μm becomes possible by shifting the lens along the beam axis. As the Rayleigh range of the beam at a focus size of $w_0 = 30\,\mu$m is only 2.7 mm it is necessary to accurately position the optics so that prism surface and focus exactly coincide. Since with the 400 mW laser the potential depth and thus the atom transfer into the red focus strongly depends on the focal size, one obtains a clear signal as to how accurate the focus placement is. After atom transfer has been optimized using the position of the first lens the beam can be extracted after the second lens and its focus size be determined.

The AOM is used for three purposes. Firstly it is used to switch the beam. Secondly it is needed to accurately blank the beam for few milliseconds with microsecond resolution for horizontal trap frequency measurements described in Section 5.3. And finally it is used to implement an evaporation ramp by reducing the laser intensity in a controlled way. For this purpose a photodiode that is placed behind a dielectric mirror picks up the weak transmitted signal and feeds it back into a control unit adjusting the applied RF-power of the AOM. In experiments with the Nd:YAG laser about 330 mW of light at 1064 nm were available and focussed to 30 μm at the prism surface yielding an attractive potential of $U/k_B = 48\,\mu$K depth. The fiber laser beam provides up to 7.2 W but with a waist of $w = 160\,\mu$m is not as tightly focussed. The resulting potential in this case is $U/k_B = 45\,\mu$K.

4.2.4 The Double Evanescent Wave Trap

Since the light used for the red evanescent wave originates from the zeroth order beam of an AOM a good transverse beam profile can only be obtained when the AOM is turned off. This imposes the restriction that dimple laser and red evanescent wave cannot be used at the same time in a defined way. However since the red evanescent wave provides horizontal confinement of its own both beams can be used independently in consecutive trapping stages.

The red evanescent wave beam passes through a second AOM whose purpose is again to allow for independent switching and intensity control. In case of the DEW trap it is crucial to be able to switch off the light within less than a microsecond because in temperature measurements (see Section 6) slower switching would affect the obtained results. It is necessary to use special photodiodes (Hamamatsu 5832-01) to monitor fast intensity changes of the 1064 nm light because standard photodiodes show excessively long reaction times ($\approx 50\mu$s) due to the creation of electron-hole pairs deep within the bulk of the semiconductor material by the infrared light. Two lenses create the 160μm large focus of the beam at the prism surface. As the Rayleigh range in this case is 7.6 cm, measuring the length of the beam path is sufficiently accurate to place the focus on the prism surface. The red evanescent wave enters the vacuum chamber through the same viewport as the near resonant evanescent wave whereas the evanescent wave stemming from the titanium:sapphire laser enters from the opposite side. In order to have good optical access for the red evanescent wave the final dielectric mirror reflecting the near-resonant evanescent wave into the vacuum chamber is transparent for the 1064 nm light. Therefore the last mirror for the red evanescent wave can be placed behind it and sends the beam right through it. The angle of incidence is only 0.2 ° above the critical angle and thus leads to a very large $1/e$-decay length of the intensity of 2.0 μm. At a power of 1.2 W as used in all measurements the attractive dipole potential of the red evanescent wave is $U/k_B = 43\,\mu$K. The combination with attractive Van-der-Waals interaction and repulsive far off resonant evanescent wave gives rise to a $U/k_B = 13\,\mu$K deep potential well located 0.9 μm above the surface.

4.3 Measurement Procedures

4.3.1 Experiment Control

The many experimental parts of the GOST project have to be coordinated and synchronized sometimes with an accuracy of microseconds. Therefore each dynamical part is controlled by either a TTL input for switching or a control input for analogue adjustments such as the intensity ramps of various lasers. The control signals are generated by a separate timing board (Adwin-4LD with an Inmos T400 digital signal processor) after the desired control sequence has been entered through the LabView interface on a PC.

The timing processor is able to provide timing information through 48 digital channels and applies arbitrary time-dependent voltages between -10 and 10 Volts to two analogue ports. Although the temporal accuracy is better than $1\,\mu$s the minimum time step between consecutive switching processes is $50\,\mu$s which turned out to be a limitation for the accuracy of trap frequency measurements and temperature measurements in the DEW-trap.

Currently the two analogue ports are used to apply the intensity ramps of the dimple laser and the red evanescent wave but in the measurements discussed in Section 4.4.2 they were used to ramp the intensity of the hollow beam and the diode laser temperature of the near resonant evanescent wave.

4.3.2 Measurement Cycle

Loading relatively weakly confining and nearly conservative dipole traps with atoms that are initially at temperatures of several hundred degrees celsius is not a trivial task. Various intermediate cooling and trapping stages bridge the vast gap between initial atom velocities and capture velocities of the traps.

In the initial MOT stage about 3×10^8 atoms are collected in six seconds from a Zeeman-slowed atomic beam. Shortly before they are transferred into the GOST a polarization gradient cooling stage further reduces the temperature to few microkelvin and compresses the atomic cloud. This cooling stage is employed by a 50 ms linear increase of the MOT laser detuning from initially -8 MHz up to -60 MHz directly before the laser light is switched off. At the same time offset magnetic fields shift the zero point of the magnetic field and consequently the compressed atomic cloud close to (< 0.5 mm) the evanescent wave and inside the hollow beam perimeter. Due to the large size of the atomic cloud, only its central region can be placed inside the confining ring.

After their release the atoms drop onto the evanescent wave and gain approximately $U_{pot}/k_B = 80\,\mu$K of kinetic energy corresponding to their initial potential energy in the field of gravity ($z = 0.5$ mm). One second of Sisyphus cooling and plain evaporation through the hollow beam prepares up to 30 million trapped atoms at $20\,\mu$K in the GOST.

In case of forced evaporative cooling experiments in the GOST itself, the Sisyphus cooling is employed for four seconds until either one of the potentials is ramped down. When the GOST serves as a reservoir for the microtraps the hollow beam will be switched off five seconds after the initial transfer and the evanescent wave will be replaced by the far-detuned evanescent wave. At this time the focussed dimple laser has been on for 1.5 seconds which is ample time for the elastic collision loading to be completed (see Section 5.1). In more recent experiments its intensity was linearly increased during these 1.5 seconds to ensure adiabatic loading. After the reservoir is removed at $t = 5$ s plain evaporation relaxes the dimple trapped ensemble to its new equilibrium state until at $t = 6$ s the forced evaporative cooling in the dimple is initiated. An exponential

intensity ramp down to a few percent of the initial density drives the evaporation. This ramp is completed after somewhere between 400 ms and 4 s depending on the initial trapping conditions.

For DEW-trap measurements the dimple laser is only moderately attenuated within two seconds to 2 W total power. At this point about 1.8×10^6 atoms remain in the dimple at a temperature of 3.0 μK. Transfer into the DEW-trap is accomplished by a reduction of the dimple laser power in 50 ms to zero and a simultaneous increase of the red evanescent wave power to 1.2 W. It takes about 200 ms for atoms untrapped by the DEW-trap to laterally escape. After this time we observe at maximum 10^5 trapped atoms in the DEW-trap. Evaporative cooling is applied directly after the transfer by ramping down the power of the red laser beam.

The measurement cycle is closed by switching on the MOT-laser beams and the quadrupole magnetic field which drives the atoms back into the MOT. After the remaining atom number has been determined the atomic beam block is removed and a consecutive experiment cycle begins.

4.3.3 Diagnosis Tools

Obtaining information from only a few thousand atoms about their temperature, density or other experimentally accessible parameters can only be accomplished by using resonant light and forcing the few atoms to strongly interact with it and provide clear signals. This inherently means measuring in a way that destroys the ensemble state as it was before. Another consequence is the need for repetitive measurements in order to extract information on indirectly accessible quantities such as temperature. During any of the dipole trapping stages the lasers involved are detuned sufficiently far from resonance so that they don't disturb the delicate ensemble state significantly. This implicitly means that the atoms don't communicate information about their state during these phases. A standard practice for measuring a desired quantity is to recapture the atoms back into the MOT and determine their number as a function of various parameters. How this can yield information on temperature, trap frequencies etc. will be explained below.

The fluorescence of the atoms is measured by a CCD camera (Princeton Instruments RTE/CCD-768-K/1) in a 30 ms exposure of the atomic cloud in a -8 MHz detuned MOT. The CCD camera has been calibrated using an absolute atom number determination by absorption imaging which we estimate is good up to a factor of 1.5. The possible error affects atom number and depending quantities such as density or phase-space density whereas temperature or trap frequencies are deduced from relative atom numbers and thus not subject to this systematic error. The method of absorption imaging is extensively described in other references (e.g. [Ham99]) so that this paragraph will be limited to technical details relevant in this setup. The probe beam that illuminates the atom cloud is derived from the stable reference laser and shifted on resonance by

double-passing an AOM (85 MHz). It is then inserted into a single mode fiber to make the probe beam geometrically insensitive to mechanical vibrations. After emerging from the fiber the probe beam polarization is cleaned using a polarizing beam splitter cube and the beam is horizontally shone through the atom cloud and into a CCD camera. The camera lens images the absorption profile of the atom cloud onto the CCD chip. The intensity of the probe beam is chosen such that a 1 ms pulse optimally uses the dynamic range of the camera. This is far below saturation intensity and of the order of $1\,\mu\mathrm{W/cm^2}$. The final calibration factor turns out to be 13600 atoms per thousand fluorescence counts in a camera picture of 30 ms exposure at an aperture of 5.6.

4.3.4 Measuring Atom Number

Measuring the atom number of an ensemble is straightforward. The fact that retransfer from the GOST or the microtraps back into the MOT is very efficient, opens up the possibility of measuring the number of atoms by resonance fluorescence detection. Background light and CCD-dark currents are responsible for a detection noise that limits the minimum number of detected atoms to a few thousand which is good enough for all relevant purposes. Measurement results are ultimately limited in quality by shot-to-shot fluctuations of the atom number between consecutive cycles. In the current experiment we find them to be roughly 5 %. Since a measurement of the atom number under various experimental conditions is the basis of all other relevant quantities this statistical error also effects them. In spite of these small fluctuations the experiment has evolved to be considerably stable.

4.3.5 Thermometry

The measurement scheme which is applied in the GOST experiment is a release-and-recapture method: For a short time interval Δt one of the confining potentials is removed and the ensemble can ballistically expand. After restoring the confinement a certain fraction κ of the atoms remain in the trap. The size of this fraction depends on the release time Δt and also on the ensemble temperature T. Recording this fraction for various release times yields a dataset of the function $\kappa(\Delta t)$ that can now be used to extract T as a single fit parameter of a theoretical model.

This method is inherently very time consuming. For each value of $\kappa(\Delta t)$ at least two experiment cycles have to be completed (one cycle with a release pulse and one without pulse for normalization). The complete temperature determination usually requires at least about 20 cycles and takes roughly five minutes.

Vertical versus Horizontal Temperature

In most cases only the "vertical temperature" is measured by a release/recapture from the evanescent wave. If the ensemble is thermalized this kinematic "temperature" is equal to the thermodynamical temperature. The reason that in most cases a vertical measurement of T is performed lies in the growing difficulties and inaccuracies of the horizontal method at low T. At temperatures below about five microkelvin the vertical oscillation period in the trap is much smaller than the time it takes an atom to move laterally out of the hollow beam perimeter. Therefore it will experience many reflections from the evanescent wave before getting away. Since occasionally such a refection is not specular the overall motion of a slow atom resembles a diffusion rather than a ballistic trajectory. In addition to that, the horizontal escape time is also comparable to the elastic collision time $1/\gamma_{el}$ (hydrodynamic regime). Like a diffuse reflection from the evanescent wave, an elastic collision with another atom will alter the motion of an escaping atom in a way that is hard to take into account theoretically. The model we use does not include these complications and thus results of a horizontal measurement will become progressively inaccurate as T decreases.

Approximations

In some cases one can use approximations to simplify the theoretical model and reduce the numerical effort that is necessary to extract T. The GOST allows for such a simplified model which is derived below. Most cases however, require a more detailed discussion that adapts the general approach to the specific situation. The considerations necessary to extend the model to the focussed beam trap and to the DEW-trap are given in sections 5.2 and 6.2.

The approximations and assumptions that simplify the case for the GOST are the following: Firstly we approximate the evanescent wave potential by a hard wall and secondly we assume a thermalized ensemble. The first approximation is in general reasonably well justified if the ensemble temperature is higher than about one microkelvin. In this case the actual time an atoms spends inside the evanescent wave is small compared to that of the ballistic bouncing motion outside the light field. The density profile and the trajectories are therefore hard to distinguish from the case of an ideal hard wall potential. Usually also the second assumption is reasonable well satisfied if external modifications of the potentials (e.g. during evaporative cooling) take place slowly compared to the thermalization time of the ensemble.

Theoretical Model

The general approach to derive a fit function $\kappa(\Delta t)$ starts with the phase-space distribution function ρ. Using the assumptions given above the potential in which the atoms are trapped is the sum of gravity and an ideal hard wall potential. The problem is

completely one-dimensional:

$$\rho(z,v) = \frac{1}{\Omega} \cdot \exp\left(-\frac{z}{z_0}\right) \cdot \exp\left(-\frac{v^2}{v_0^2}\right) \cdot \Theta(z). \tag{4.1}$$

$\Theta(z)$ is the unit step function which equals one if $z > 0$ and zero elsewhere. It takes care of the fact, that atoms cannot be below the prism surface. Analogous to the considerations in Chapter 3, Ω is defined by $\Omega \equiv \int_{-\infty}^{\infty} dv \int_0^{\infty} dz \exp(-z/z_0) \cdot \exp(-mv^2/(2k_BT))$. z_0 and v_0 are given by $z_0 \equiv k_BT/(mg)$ and $v_0 = \sqrt{2k_BT/m}$. $\rho(z,v)$ is then normalized to one.

As soon as the evanescent wave is switched off, the ensemble ballistically expands. An atom that was initially ($t = 0$) at $z = z'$ and $v = v'$ can at a later time $t = \Delta t$ be found at $z = z' + v't - gt^2/2$ and $v = v' - gt$. This leads to the phase-space distribution function for a time $t = \Delta t$ [Man99]:

$$\rho(z,v,\Delta t) = \rho(z',v',0) = \rho(z - v\Delta t - g\Delta t^2/2, v + g\Delta t). \tag{4.2}$$

The fraction of remaining atoms $\kappa(\Delta t)$ for a time Δt can now be obtained by carrying out the integral

$$\kappa(\Delta t) = \int_{-\infty}^{\infty} dv \int_0^{\infty} dz\, \rho(z - v\Delta t - g\Delta t^2/2, v + g\Delta t). \tag{4.3}$$

The z-integration starts at $z = 0$ because atoms with a coordinate $z < 0$ have come in contact with the prism surface and are immediately lost. The integral solution can not be expressed in terms of analytical functions and therefore has to be evaluated numerically to extract the fit parameter T. Figure 4.8 shows a typical dataset along with the fit function for the temperature $T = 2.9\,\mu$K. In order to obtain a "horizontal" temperature, one uses a similar approach. A release-and-recapture method can be applied by switching the hollow beam instead of the evanescent wave. The theoretical model is derived along the same lines described above and a detailed discussion can be found in [Man99].

4.4 Preparation of the Reservoir

The cold and dense reservoir of atoms that is needed to load the microtraps and to exploit the advantages of the "dimple trick" is prepared in the GOST. The details of this reservoir preparation are provided in the following. Although similar measurements have been performed and documented earlier [Ryc00, Man99], it is useful to present some general results again because the experimental setup has been rebuild and modified since then. The subsection on storage and Sisyphus cooling will briefly summarize the behavior of the reservoir ensemble and characterize the starting conditions for subsequent transfer into the dimple trap or evaporative cooling. The section on evaporative cooling then presents results of forced evaporation through either one of the dipole potentials and discusses the limitations that finally motivate the introduction of the dimple trap.

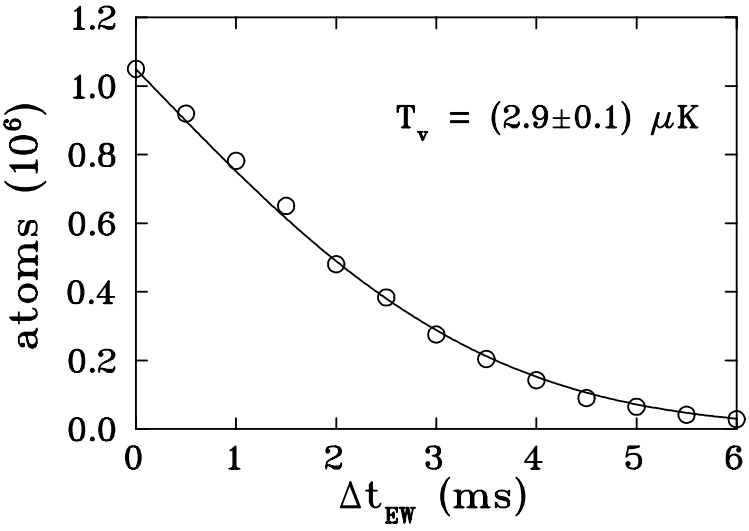

Figure 4.8: *Temperature measurement in the near resonant GOST. The open circles are experimental data points and the solid line is a fit based on the model described in the text with the single fit parameter T.*

4.4.1 Storage and Sisyphus-Cooling

Right after the atoms are transferred from the MOT into the GOST potential the ensemble is heavily disturbed in the sense that a vast amount of excess energy is deposited in the atoms. The Sisyphus cooling stage is an important intermediate step that removes this energy, builds up density and provides the necessary elastic scattering rates for evaporative cooling or collision loading of the microtraps. Figure 4.9 shows the evolution of atom number and temperature after the transfer has taken place.

The experimental parameters in this and all following measurements (unless otherwise specified) were as follows: The evanescent wave was detuned by 3 GHz to the blue side of the $F = 3 \rightarrow F'$ transition, had a total power of 45 mW and a circular spot size of 700 μm ($1/e^2$-radius). Its angle of incidence deviated by one degree from the critical angle at 43.6° and the light field was TM-polarized. The hollow beam was blue-detuned by 3 nm had a total power of roughly 300 mW and featured a diameter of 820 μm.

In the initial storage phase the atom number declines relatively fast on a timescale of ≈ 3.5 s. The observed losses are mainly due to two mechanisms: Firstly, atoms that rapidly transfer vertical excess energy into the horizontal motion will be able to penetrate the hollow beam and secondly, inelastic collisions mediated by the blue-detuned light field (see Section 3.5) will frequently occur due to the small evanescent wave detuning. Other measurements that have been performed at smaller hollow beam detunings and/or at higher intensities have shown that the lifetime can be increased up to ten seconds. Switching the evanescent wave detuning to 6 GHz at a later time ($\approx 1 - 2$ seconds

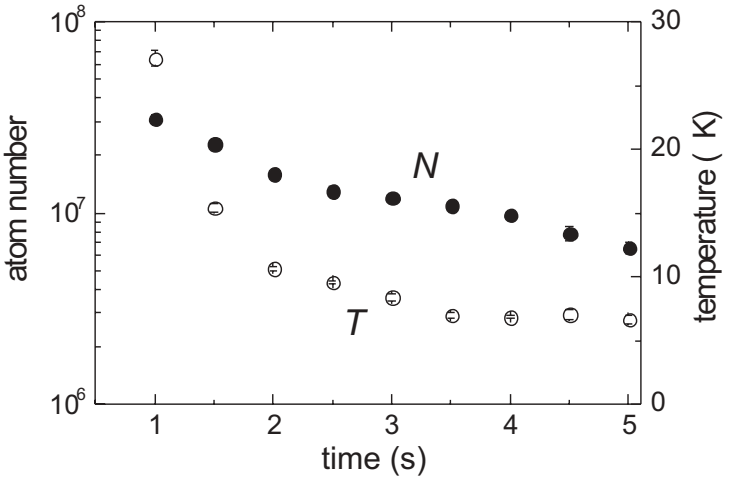

Figure 4.9: *Time evolution of N and T in the near-resonant GOST. Cooling is due to a Sisyphus process and plain evaporation through the hollow beam.*

after transfer) can also increase the lifetime as it reduces the collision losses. A detailed treatment of the collisional loss and further measurements can be found in reference [Ham99].

The ensemble temperature drops very rapidly from an initial value above $50\,\mu$K to an equilibrium of below $7\,\mu$K after five seconds. Up to one second after the transfer the obtained temperature must be considered an upper bound, because the thermalization between horizontal and vertical motion is not completed at this time. The temperature reduction is not exponential as expected from the Sisyphus process alone. This is not surprising considering the fact that plain evaporative cooling significantly contributes to the overall cooling effect. The significance of both mechanisms becomes evident as one increases the hollow beam potential or further detunes the evanescent wave. Both measures give rise to a higher equilibrium temperature and a smaller cooling rate. Since, however, they also increase the sample lifetime in the GOST, we're ultimately faced with a tradeoff between large atom number and low temperature. As a compromise, the experimental parameters specified above lead to a sample of approximately 10^7 atoms at a temperature of $7\,\mu$K after five seconds storage in the GOST. The peak density is $4.2 \times 10^{11}\,\mathrm{cm}^{-3}$, the phase-space density amounts to 1.1×10^{-5} and the atoms elastically collide at a rate of $12.6\,\mathrm{s}^{-1}$. At this point either forced evaporative cooling or transfer into the dimple trap is initiated.

4.4.2 Evaporative Cooling

Evaporative cooling in the GOST can be employed by reducing either one of the dipole potentials. Each method has its own merits and problems.

Forced evaporation through the evanescent wave is inherently one-dimensional (see Section 3.6.1) and therefore suffers from reduced efficiency. And because the temperature measurement is insensitive to whether the sample is thermalized or not, one cannot check if thermalization has been completed and in particular whether the horizontal temperature has been reduced. On the other hand this method of evaporative cooling allows for a fast removal of atoms whose vertical energy surpasses the limit defined by the potential. Within less than one oscillation ($T \approx 1\,\mathrm{ms}$) the atom will penetrate the evanescent wave and hardly get a chance to transfer excess energy onto a trapped collision partner.

Hollow beam evaporation exhibits somewhat contrary properties: Atoms are selected two-dimensionally and the combination of horizontal evaporation and vertical temperature measurement ensures that the temperature value is in the worst case an upper bound. For a properly optimized evaporation ramp both temperatures exactly match. The oscillation frequency in the wide hollow beam potential, however, is so small that a hot atom has ample time to transfer kinetic energy on to other trapped atoms by elastic collisions. That way it might stay in the trap although its kinetic energy was initially above the removal threshold. Both approaches have been tested and the results are documented below.

Forced evaporative cooling through the evanescent wave can in principle be implemented by either reducing the intensity or by increasing the detuning. Although the later technique is experimentally more challenging than the first (see [Ryc00]), it is the preferred one for two reasons: Both, photon scattering processes and the rate for light-assisted collisions are suppressed linearly with increasing detuning, whereas the reduction of the intensity would have no suppression effect. (A reduced intensity is compensated by the fact that atoms will penetrate deeper into the light field.)

The optimization procedure of the evaporation ramp went as follows. In steps of one second length the detuning was linearly increased by a variable value. At the end of each step the evaporation efficiency ϵ for this interval was determined and the ramp with the highest value of ϵ chosen.

The optimized evaporation ramp increased the evanescent wave detuning in three linear one-second steps from initially 3 GHz via 82 GHz and 160 GHz to finally 210 GHz. At the same time the intensity of the hollow beam was reduced to half of its initial value in order to further reduce heating. Figure 4.10 shows the resulting evolution of atom number N, temperature T, peak density n_0 and phase-space density D until one second after the end of the evaporation ramp at $t = 3\,\mathrm{s}$.

The first second of evaporation causes only a minor reduction of N and T which is due to the fact that it takes about one second until the potential is reduced far

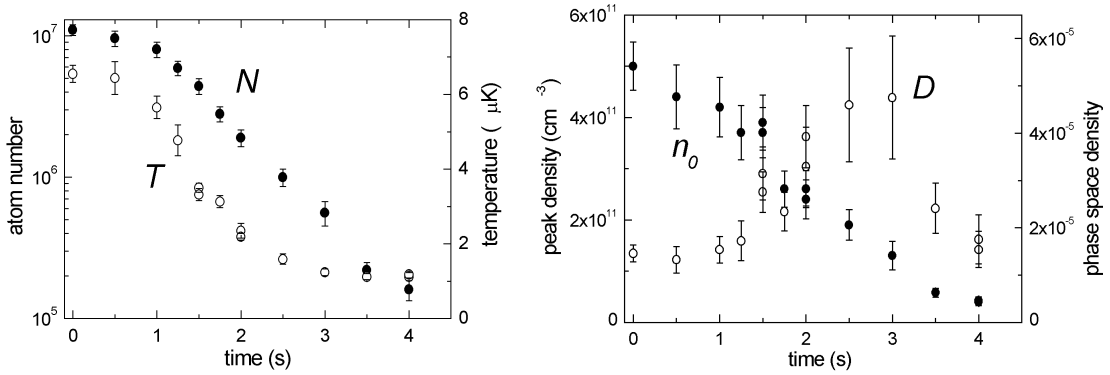

Figure 4.10: *Atom number, temperature, peak density and phase-space density during evaporation through the evanescent wave.*

enough to allow atoms to escape. The remaining two seconds of evaporation then bring about the drastic decrease of both N and T until at the end of the evaporation ramp the temperature stagnates at $T = 1\,\mu$K while the atom number further drops with an ensemble lifetime of roughly one second. During the whole evaporation process the peak density and therefore also the elastic collision rate have declined. The useful runaway regime could not be attained. In spite of this, phase-space density increased by a factor of five and reached a value of $D = 5 \times 10^{-5}$. The evaporation efficiency of $\epsilon < 0.5$ turns out to be relatively poor. Because of the initially too small elastic collision rate and the progressively decreasing lifetime of the sample during forced evaporation it is hard to gain in phase-space density and seems impossible to build up elastic collision rate. Furthermore it is not evident that the sample was thermalized during the whole process so that the results might even be less favorable. The crucial problem one is faced with here, is the short lifetime of the sample. The faster thermalization takes place in comparison to losses the more efficient can forced evaporation cool and increase the phase-space density.

We find a similar situation in case of evaporative cooling through the hollow beam. In this case the forced evaporation is implemented by abruptly reducing the intensity of the hollow beam to about 50 % and then ramping it exponentially further down to 5 % of its maximum value. Optimization is performed by varying the length of the evaporation ramp. During the whole process the evanescent wave is detuned to about 30 GHz to reduce heating and light-assisted collisions. Figure 4.11 shows the results of an optimized three seconds long evaporation ramp.

Again one finds that the atom number declines progressively fast during evaporation and continues to do so even after the intensity is no longer reduced at $t = 3\,$s. The temperature simultaneously decreases but cannot be reduced below $1.5\,\mu$K. In this case

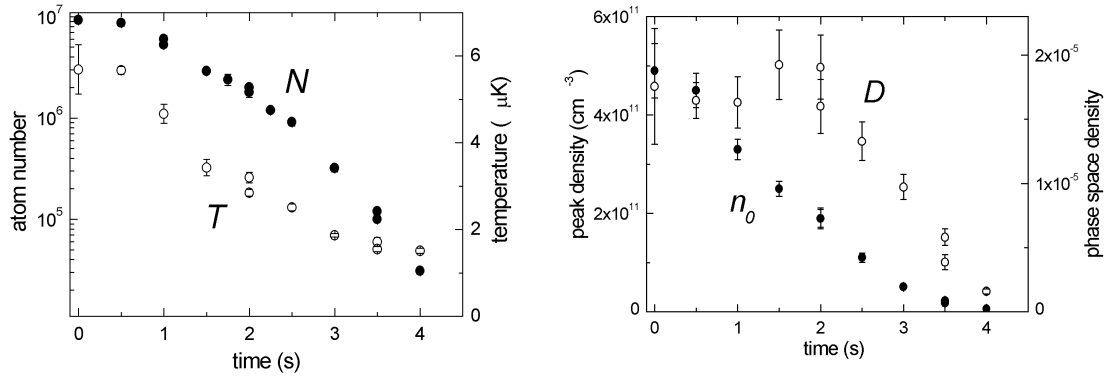

Figure 4.11: *Atom number,temperature, peak density and phase-space density during evaporation through the hollow beam.*

however, this value is an upper bound for the true temperature since the measurement takes place vertically whereas the energy selection is horizontal. The temperature stagnation near the end of the ramp can therefore either result from a breakdown of the evaporation process or from an incomplete thermalization between the degrees of freedom (strictly speaking, these two options are basically the same thing). Concerning the peak density and phase-space density, it is therefore not surprising to find the first decline during the whole evaporation ramp while the later initially increases a little before rapidly dropping.

Again we find that the initial elastic collision rate is too small compared to the losses from the trap in order for the evaporation process to be sufficiently efficient. At first sight the evaporation through the hollow beam seems even less efficient than forced evaporation through the evanescent wave. But considering the effect of the inaccurate temperature measurement and the tendency to assess the evanescent wave evaporation too optimistic might already even out this difference.

In summary, evaporation through the evanescent wave seems little promising because at small potential barriers defects in the evanescent wave light field cause the lifetime and therefore inevitably the evaporation efficiency to drop. The approach through the hollow beam suffers from the arguments given above and so it seems promising to alter the horizontal potential in a way that avoids these limitations. The result of this considerations is the introduction of the dimple laser.

Chapter 5

Focussed Beam Surface Trap

The focussed beam surface trap has proven to be a very powerful tool to implement efficient evaporative cooling in this experiment. Due to the dimple trick it is possible to create very dense ensembles and achieve very large the elastic collision rates and thus increase the efficiency of the evaporation.

The results that are presented hereafter have been obtained from two different configurations of the dimple trap. In a first set of experiments a relatively weak (330 mW) Nd:YAG-laser was focussed to only 30 μm beam waist. In this case the approximation of a large reservoir with a small perturbation is well justified. It was used to investigate general properties such as the loading mechanism and compare them to the theoretical expectations. The second configuration was realized with a strong (7.2 W) ytterbium-fiber laser focussed to a much wider spot of 160 μm waist. More than six million atoms could be trapped in this focus. Although the approximation of a small perturbation to a large reservoir breaks down in this case, this approach proves useful for subsequent evaporative cooling.

The following three sections address general properties of the dimple trap (5.1), introduce some new aspects of the temperature measurement scheme (5.2) and discuss the experimental conditions that are created (5.3). Section 5.4 is dedicated to the issue of evaporative cooling and what progress has been made in both configurations. Current limitations are finally discussed in Section 5.5.

5.1 Transfer and Storage

This section discusses measurements concerning the details of the microtrap's loading process. The theoretical expectations of the loading efficiency are confirmed and the time-dependence of the loading is investigated and modelled using a simple model based on rate equations. All investigations concerning the loading process were done with the tightly focussed Nd:YAG laser. The results of this investigation have also been published

in reference [Ham02b].

Loading Measurements

The experimental scheme that was used to obtain the data presented here slightly differs from the experiment cycle described in Section 4.3.2. Four seconds after the atomic sample has been transferred into the GOST the evanescent wave is detuned from initially 3 GHz to 128 GHz by fast temperature tuning of the laser diode. The linear detuning ramp of two seconds length prepared a sample of 3.5×10^6 atoms at a temperature of $T \approx 4\,\mu$K in a nearly conservative trap. The ensemble lifetime in this far-detuned stage is only 1.4 seconds but still sufficient for this purpose. After the detuning ramp is completed the dimple is suddenly switched on at $t = 6$ s and collision loading begins. A variable time Δt later the reservoir is removed by switching off the hollow beam and letting any atom untrapped by the dimple escape. 200 ms later all reservoir atoms have left and one can determine the number of dimple trapped atoms by recapture into the MOT. Naturally also some atoms that were initially trapped in the dimple can escape due to plain evaporation and inelastic collisions. Figure 5.1 shows the evolution of the number of dimple trapped atoms N (•) and the number of reservoir atoms N_{res} (○).

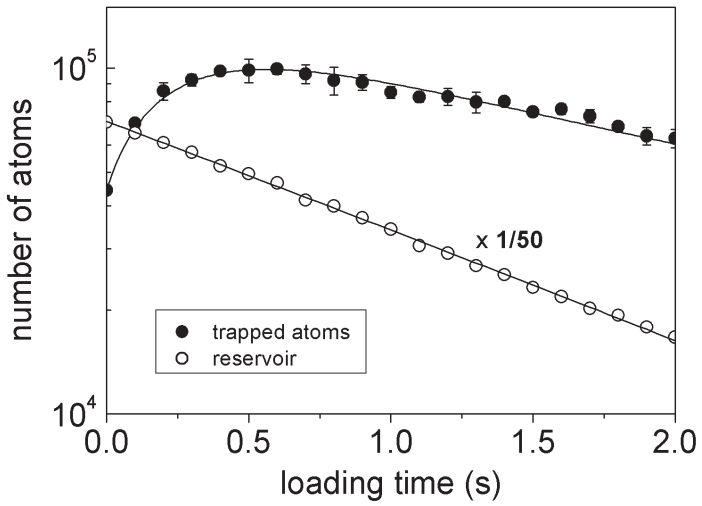

Figure 5.1: *Collision loading of atoms into the dimple. The solid lines are fits obtained from the model decribed in the text.*

The solid lines are fits of a simple exponential decay in case of N_{res} and a model derived from the following differential equation in case of N

$$\dot{N} = -\kappa N_{res}(N - aN_{res}) - bN^2. \tag{5.1}$$

This model assumes that the dimple does not significantly affect the reservoir and in particular does not alter its temperature. κN_{res} is the loading rate that explicitly contains the number of reservoir atoms in order to take into account that loading depends on elastic collisions in the reservoir. Loading measurements at smaller reservoir sizes indeed confirmed the dependence on N_{res}. The term $(N - aN_{res})$ represents the difference between the momentary number of trapped atoms and the equilibrium number aN_{res}. The last term $(-bN^2)$ is due to binary inelastic collisions which are assumed to be the major loss contribution. N_{res} can be substituted by the independently measured exponential decay $N_{res} = N_{res,0} \exp(-t/\tau_{res})$ with $N_{res,0} = 3.5 \times 10^6$ and $\tau_{res} = 1.4\,\mathrm{s}$. An additional decay measurement in the dimple (see figure 5.2) provides the parameter $b = 7.2 \times 10^{-6}\,\mathrm{s}^{-1}$. A fit with the two remaining parameters κ and a finally yields $\kappa = 3.3 \times 10^{-7}\,\mathrm{s}$ and $a = 0.08$.

While initially only 4×10^4 atoms ($\approx 1\,\%$) are trapped inside the dimple, collision loading increases the fraction by almost an order of magnitude to 8 % of the reservoir atom number within 0.5 seconds. The thermalization rate $\kappa N_{res,0} \approx 1\,\mathrm{s}^{-1}$ perfectly agrees with the thermalization time calculated from an elastic collision rate of $\gamma_{el} \approx 10\,\mathrm{s}^{-1}$. The maximum number of 10^5 trapped atoms is reached after about 0.5 seconds before the fast reservoir decay prevents further loading. The lifetime of the dimple trapped atoms surpasses that of the reservoir atoms because of a higher evanescent wave potential in the center of the evanescent wave spot where the dimple is created. The number of trapped atoms can be increased by switching the dimple on at the beginning of the evanescent wave detuning ramp. In this case a maximum of 2×10^5 atoms is observed after 200 ms storage in the dimple.

The wide focus created by the 7.2 W fiber laser in combination with the 3 nm detuned 1.15 W evanescent wave derived from the titanium:sapphire laser is able to load up to 40 % (6.4×10^6) of all atoms on a similar timescale ($\approx 1.5\,\mathrm{s}$). In this case the time dependence of the loading process is much more complicated and has not been investigated in detail.

Decay Measurements

Once the atoms are trapped inside the focus one can remove the reservoir and investigate the decay. Candidates for relevant loss mechanisms are light-assisted collisions, three-body collisions and right after the removal of the reservoir also losses due to plain evaporative cooling. In case of a reservoir temperature that satisfies $T_{res} \leq 1/10 \cdot U_{dimple}/k_B$ this last mechanism can be neglected.

Although we obtained excellent decay data for both configurations (Figure 5.2) it is not possible to entirely separate the loss contributions from two-body and three-body processes.

In order to extract the relevant rate coefficients β and L_3 from the data, we use the method explained in Section 3.5.2. Equation 3.77 is used to fit the data with the two

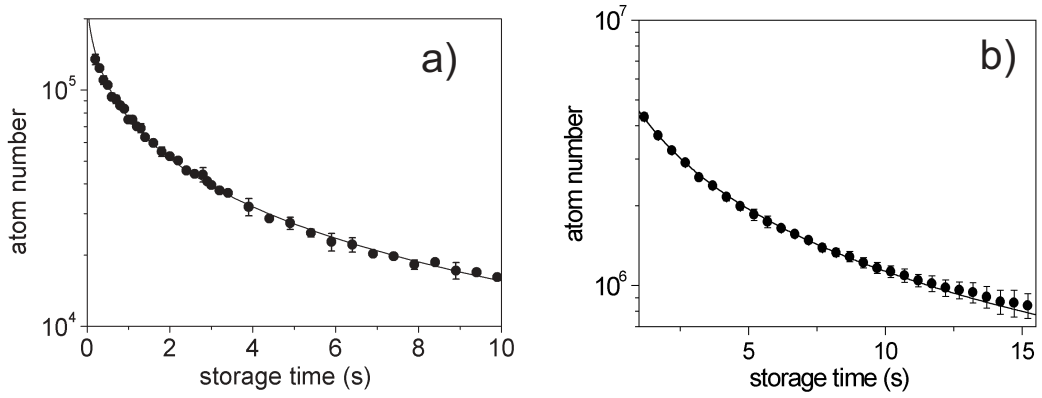

Figure 5.2: *Decay of atoms from the tight dimple (a) and the wide dimple (b).*

fit parameters β and L_3 and a fixed value α. The fit shows reasonable agreement with the experimental data for a range of values for α between zero and about $0.1\,\mathrm{s}^{-1}$. Due to this ambiguity we can only specify estimates and upper limits for β and L_3. The mean density $\langle n \rangle$ and mean quadratic density $\langle n^2 \rangle$ are substituted by the expressions 3.46 and 3.47. Because the temperature enters in both, it is important to know its value and guarantee that it does not change during the decay.

In the first configuration we are confronted with a tightly confined ensemble at a temperature of $2.9\,\mu\mathrm{K}$. The peak density at $t = 200\,\mathrm{ms}$ can be calculated to $7.8 \times 10^{13}\,\mathrm{cm}^{-3}$ by inserting the expected and experimentally confirmed (see Section 5.3) horizontal trap frequency of $\omega_0/2\pi = 555\,\mathrm{Hz}$ into expression 3.45. The fit to the data (solid line in figure 5.2 a)) then yields the values $\beta = 4.6 \times 10^{-14}\,\mathrm{cm}^3/\mathrm{s}$ and $L_3 = 5.9 \times 10^{-28}\,\mathrm{cm}^6/\mathrm{s}$ for a fixed $\alpha = 0$. Varying the value for α and repeating this fit procedure provides an estimate of $\beta = 5 \times 10^{-14}\,\mathrm{cm}^3/\mathrm{s}$ and an upper bound of $L_3 = 3 \times 10^{-27}\,\mathrm{cm}^6/\mathrm{s}$.

In agreement with previous results [Ham99], the β coefficient can be attributed to collisions mediated by the 128 GHz detuned evanescent wave. The bound for L_3 is in reasonable agreement with the estimates of other experiments [Ker01, Web02].

In case of the wide dimple trap with a trap frequency of approximately 110 Hz we initially trap more than six million atoms. Due to the high reservoir temperature in this case ($\approx 8.6\,\mu\mathrm{K}$) plain evaporative cooling reduces this value to $T = 5.1\,\mu\mathrm{K}$ after 1.2 s when an equilibrium is reached. At this time 4.3×10^6 atoms remain in the trap. This corresponds to a peak density of $3.2 \times 10^{13}\,\mathrm{cm}^{-3}$. The evaluation of the decay has to exclude data from within this plain evaporation phase because the changing temperature renders the dynamics at that time prohibitively complicated. The evanescent wave is now at a much larger detuning of 660 GHz ($\Delta\lambda = 1.5\,\mathrm{nm}$) but with its 1.1 W of total power and the smaller spot size of $400\,\mu\mathrm{m}$ still gives rise to a larger potential barrier. A

decay measurement shown in figure 5.2 b) evaluated by the same method used for the tight dimple yields a coefficient $\beta = 3.5 \times 10^{-14}\,\mathrm{cm}^3/\mathrm{s}$ and an upper bound for L_3 of $10^{-27}\,\mathrm{cm}^6/\mathrm{s}$.

The large initial number of atoms along with the large density and the long lifetime in the trap are useful properties to implement efficient evaporative cooling.

5.2 Temperature Measurements

Using evaporative cooling in the dimple trap, one can get to temperatures significantly below $1\,\mu$K. At this point the theoretical model discussed in Section 4.3.5 has to be refined as the details of the evanescent wave potential have to be taken into account now. Figure 5.3 b shows, that at low enough temperatures the density distributions for the cases of a hard wall potential and of an exponentially decaying evanescent wave potential are clearly distinct. At three microkelvin (Figure a) the approximation is very reasonable and the details of the potential don't enter significantly into a temperature measurement. However at $T = 0.5\,\mu$K the density distribution and thus also $\kappa(\Delta t)$ considerably differs from the ideal hard-wall case.

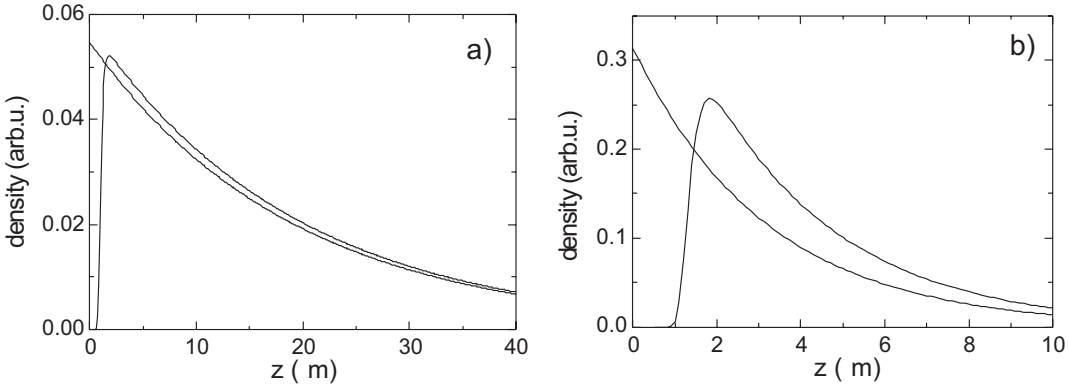

Figure 5.3: *Atomic densities for the ideal hard wall case and the more realistic, exponentially decaying potential of the evanescent wave. Figure a) corresponds to a temperature of $T = 3\,\mu K$ and figure b) to $T = 0.5\,\mu K$*

At $T = 0.5\,\mu$K the peak density is about 15 % smaller with its density peak about $2\,\mu$m above the prism surface. Especially this last point leads to a significantly altered behavior in the context of vertical temperature measurements. One can roughly estimate the temperature at which these effects come into play; most certainly the atoms will "feel" the detailed shape of the evanescent wave when the vertical extension $k_B T/mg$

is comparable to or smaller than the decay length Λ of the evanescent wave. The experimental value for Λ ($0.71\,\mu$m) leads to a temperature of $T = 111\,$nK although already at around $T = 1\,\mu$K we find slight modifications to the idealized model. Note that a refined model depends on the experimental details of the evanescent wave and in particular on its angle of incidence.

The fit function for this low temperature case can be derived using exactly the same arguments that have been used for the ideal hard wall evanescent wave. The only modification is the replacement of the idealized potential with the realistic one. The additional parameters that determine the detailed shape of the potential can be obtained from an independent measurement. Therefore T is still the only fit parameter in this refined model.

In the previous calculation the lower limit of integration was z=0, as all atoms that fall below this height hit the surface and are lost. In a calculation that takes into account the detailed shape of the potential, this limit has to be replaced by the position $z_{max} \approx 0.1\,\mu$m of the maximum of the potential as atoms falling below z_{max} cannot be retrieved. Performing a virtually identical numerical calculation as in Section 4.3.5 with the new potential shape and the changed lower limit of integration leads to a numerical fit function. A subsequent fitting procedure finally yields the result for T. Figure 5.4 shows the experimental data together with the theoretical model for an ensemble at $T = (410 \pm 20)\,$nK.

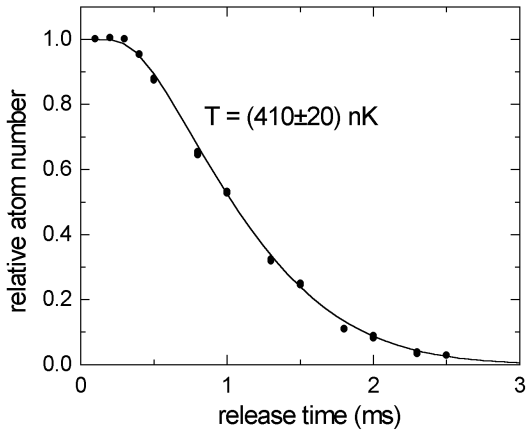

Figure 5.4: *Experimental data and theoretical temperature curve for* $0.41\,\mu K$*. A refined model that includes the details of the evanescent wave potential markedly differs from the ideal hard-wall approximation.*

Characteristic for these low temperatures is the plateau at short release times. Due to the distance between the atom cloud and the recapture boundary few atoms will

be lost for release times Δt shorter than the time t_0 that an atom needs to cover this distance in free fall. This refined model is in excellent agreement with the data obtained from the experiment. Note that T is still the only fit parameter entering here.

One important simplification that still enters into these considerations is the assumption of a classical ensemble in the sense that any vertical motion takes place classically and the discrete nature of the motional states in the vertical potential can be neglected. The gravito-optical potential leads to a splitting between the ground-state and first excited state of the vertical motion of about 95 nK and therefore justifies this simplification.

5.3 Trap Parameters

The important figures of merit, peak density n_0 and phase-space density D, depend directly on the three quantities atom number N, temperature T and the trap frequency ω_0. The trap frequency summarizes the conditions that are created by the individual shape and strength of the nearly harmonical confinement. It is accessible by different types of measurements of which two are explained in the next sections.

Measurement of Collective Oscillations

In the dimple trap this parameter is determined by exciting a collective oscillation of the ensemble and subsequently probing its phase as a function of time. A focussed laser beam with a gaussian intensity profile gives rise to a potential that is harmonic to a good approximation for energetically low-lying states. However, the closer the energy of a certain bound state is to the escape energy, the lower will be its oscillation frequency. Therefore it is imperative to reduce the ensemble temperature significantly below the value of the trap depth ($T \ll U/k_B$) in order to avoid the population of these "anharmonic" states. Atoms populating anharmonic states tend to dephase and damp the collective oscillation and will ultimately limit the measurement precision. Another unwanted effect concerning this measurement is the collision of atoms during the oscillation. Since the technique described in the following depends on the collective ballistic motion of the ensemble, any atom that is removed from this collective state of motion by a collision will lead to reduced contrast and damping. In some cases it is therefore advantageous to work with an ensemble of few atoms for this purpose. As a general rule, one has to ensure that the oscillation frequency ω_0 is much larger than the elastic collision rate γ_{el}, ($\omega_0 \gg 2\pi\gamma_{el}$). This explains why it is considerably hard to directly measure small trap frequencies using this method.

The technique we use is based on two short (1−2 ms) switch-off pulses of the confining light field separated by a variable time delay Δt. While the first pulse excites a collective oscillation the second pulse probes its phase. Varying the time separation between the

two pulses then allows for the recording of the entire oscillation. The experimental data obtained from such a measurement is shown in figure 5.5.

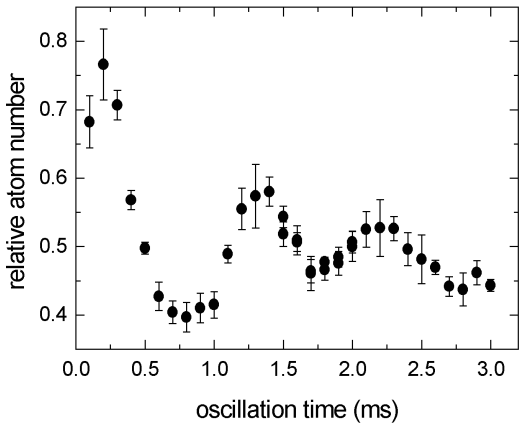

Figure 5.5: *Measurement of the collective oscillation of an ensemble to determine the trap frequency in the tight dimple.*

Phase-Space Representation

In order to understand the details of this process, it is useful to consider a phase-space representation of the ensemble in one dimension. The equilibrium ensemble occupies a circular region in phase-space (after appropriate scaling of x- and p-axis) as is shown in figure 5.6a.

The dotted circle bounds the region in phase-space that corresponds to trapped particles. Any particle outside this perimeter will leave the trap. Individual particles inside the trap move on circular phase-space trajectories as long as they don't collide with other atoms.

In order to excite a collective oscillation the confinement is removed and atoms move along straight lines parallel to the x-axis (p is unchanged in the absence of forces). This leads to a shearing of the phase-space distribution according to figure 5.6b. The angle φ between the long axis of the distribution and the x-axis gets smaller the longer the sample expands. After some 1.5 ms the confinement is restored and atoms that crossed the phase-space boundary of the trap are lost. The remaining fraction N_0 now resumes the circular motion and the collective oscillation is expressed by the fact that the distribution's long axis now rotates around the origin. Elastic collisions will slowly relax the elongated ensemble back to its circular equilibrium shape and eventually destroy the collective motion.

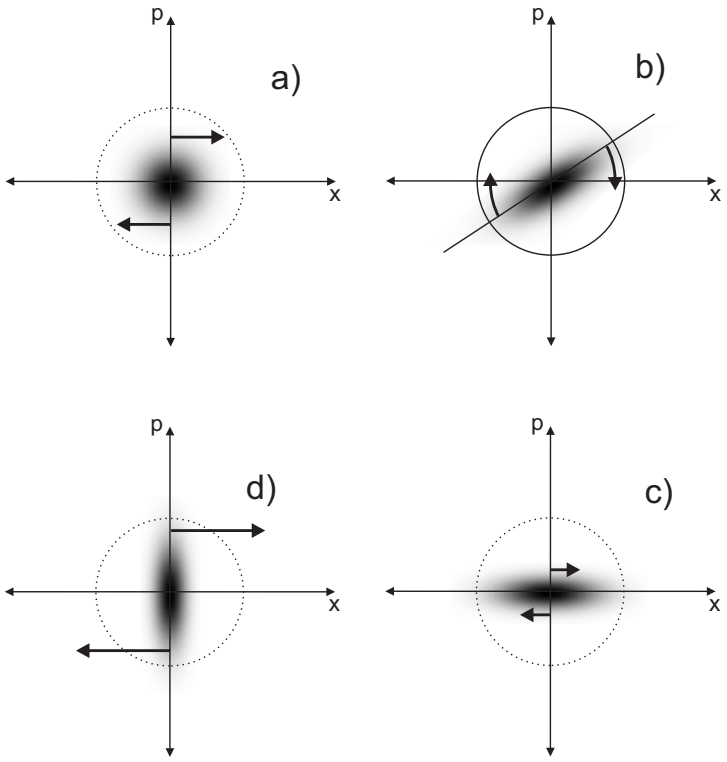

Figure 5.6: *Phase-space distribution of a one-dimensional harmonic oscillator in equilibrium (a), after a short release pulse (b), in a state of minimum (c) and maximum (d) momentum width.*

The rotating phase $\varphi(t)$ can be monitored by applying a second release pulse and measuring the remaining fraction of atoms N/N_0. This fraction will be at a local maximum if the phase-space ellipse is oriented horizontally along the x-axis ($\varphi = 0, \pi$). In this case the shearing motion is small because the the initial momentum of the atoms is small and few atoms can cross the trap boundary (figure 5.6c). The opposite case of a recapture minimum is given when the phase-space distribution is aligned with the p-axis and thus results in a particulary large momentum spread ($\varphi = \pi/2, 3/2\pi$). The initially large momentum quickly removes atoms during the release pulse (shearing phase) and the remaining fraction is small (figure 5.6d). The starting phase $\varphi(0)$ of the rotation is determined by the length of the excitation pulse and lies between $\pi/2$ (pulse length zero) and zero (infinitely long pulse).

The trap frequency can now be obtained by measuring the time between consecutive maxima or minima (corresponds to $T/2$) or between a maximum and a minimum ($T/4$). The visible increase of the trap frequency ω_0 in the course of the oscillation (figure 5.5) is due to the fact that the initial ellipse reaches into the outer region of the trapping

zone where the anharmonicity of the trap leads to a reduced trap frequency. As the oscillation progresses and elastic collisions slowly contract the ellipse towards its circular equilibrium state these outer trajectories are depopulated and the average oscillation frequency rises. We therefore disregard the first cycle in our evaluation.

Numerical Values

We find a trap frequency of $\omega_0/2\pi = (555 \pm 30)\,\mathrm{Hz}$ for the tight focus configuration. This agrees nicely with the expected value of 540 Hz for the parameters given above. The trap frequency scales as $\omega_0 \propto \sqrt{P}/w^2$ with the laser power P and the focus waist w. For the wide dimple ($P = 7.2\,\mathrm{Watt}$, $w = 160\,\mu\mathrm{m}$) we therefore expect a trap frequency $\omega_0/2\pi = 110\,\mathrm{Hz}$. A measurement similar to the one discussed above yielded a much larger trap frequency than this expected value. We believe that some error in the measurement caused this inconsistency. Elastic collision rates extracted from thermalization measurements as well as the experimentally accessible value for the trap depth of $U/k_B \approx 50\,\mu\mathrm{K}$ along with the reliable beam waist of $w = 160\,\mu\mathrm{m}$ consistently suggest a trap frequency of about 110 Hz. A significantly larger value would lead to an unreasonably small three-body loss coefficient and an unrealistically large peak density. In the following we will therefore use a value of $\omega_0/2\pi = 110\,\mathrm{Hz}$.

These numbers can now be used in combination with the expressions 3.45 and 3.49 to find the values for the peak density and the phase-space density. During an evaporative cooling ramp the trap frequency and all depending quantities are affected by the decreased intensity and in general have to be rescaled ($n_0, D \propto I/I_0$). The tight configuration with initially 1.2×10^5 atoms at $T = 2.7\,\mu\mathrm{K}$ thus yields an impressive $8 \times 10^{13}\,\mathrm{cm}^{-3}$ peak density with a corresponding phase-space density for a completely unpolarized sample of $D = 8 \times 10^{-3}$. Note that these numbers are about 300 times larger than what one finds in the reservoir alone. The elastic collision rate also drastically increases to above 2 kHz and thus allows forced evaporative cooling to take place on a sub-one-second time scale.

The $\omega_0/2\pi = 110\,\mathrm{Hz}$ trap frequency of the wide configuration along with the initially 4.3×10^6 atoms at $T = 5.1\,\mu\mathrm{K}$ give rise to a peak density of $n_0 = 3 \times 10^{13}\,\mathrm{cm}^{-3}$ and a phase-space density of $D = 0.001$.

5.4 Evaporative Cooling

The dimple loading itself has greatly increased density and phase-space density. Now the excellent starting conditions for forced evaporative cooling can be used to take the next step towards quantum degeneracy. In the tightly focussed configuration we cool the ensemble by exponentially reducing the laser power within 400 ms to 10 % of its maximum value. The evanescent wave detuning was at 160 GHz during the evaporation.

Figure 5.7 documents the evolution of atom number, temperature, peak density and phase-space density during the course of the ramp.

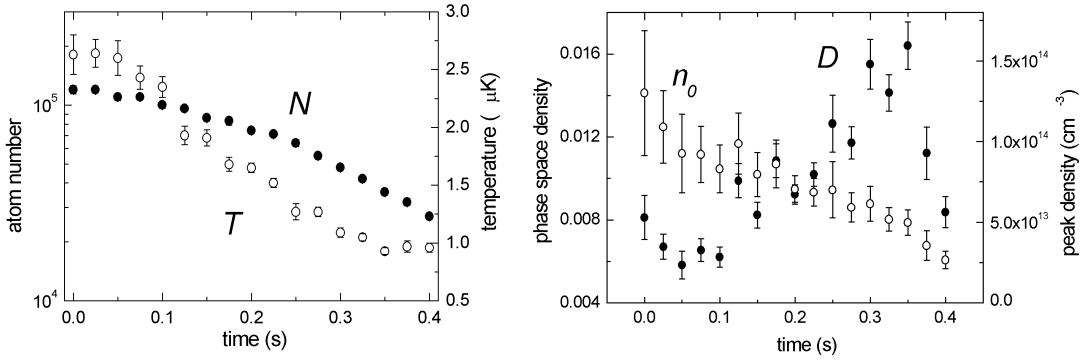

Figure 5.7: *Atom number, temperature, peak density and phase-space density during evaporation from the tight dimple. The detuning of the evanescent wave was* $160\,GHz$.

The ensemble starts with 1.2×10^5 atoms at a temperature of $2.7\,\mu$K. This corresponds to a peak density of $n_0 \approx 10^{14}\,\mathrm{cm}^{-3}$ and a phase-space density of $D = 0.008$ in case of equal distribution over all m_F-substates. In the beginning a steady cooling down to $0.9\,\mu$K in 300 ms accompanied by a loss of 80 % of the atoms is observed. At this point however, losses strongly increase while the temperature levels off. The abrupt termination of the evaporative cooling process indicates the onset of a strong inelastic collision loss. Possible mechanisms have been investigated and are discussed in Section 5.5 but a conclusive and thorough investigation will only be possible with a polarized ensemble in a future series of experiments.

Up to the termination point of the evaporative cooling the phase-space density was increased to slightly below 0.01 before it rapidly dropped in the last 100 ms of the ramp. The peak density n_0 only moderately declined but stayed at all times above $10^{13}\,\mathrm{cm}^{-3}$. Evidently the introduction of the dimple and the forced evaporation applied here already constitute a major improvement compared to the standard GOST configuration.

In the wide focus configuration the ensemble starts with 3.2×10^6 atoms at a temperature of $5.8\,\mu$K (figure 5.8). Due to the fact that no GOST evaporation phase has preceded and that the dimple is not small compared to the reservoir the starting temperature is significantly higher now. The optimized evaporation ramp is four seconds long and reduces the potential to 10 % of its original value. The first part of the evaporation cools the ensemble within three seconds to below $0.5\,\mu$K and maintains a constant peak density of about $2 \times 10^{13}\,\mathrm{cm}^{-3}$. In the section between one and three seconds the atom number is reduced by a factor of less than five while the phase-space density increases by more than a factor of 20. This corresponds to a very large evaporation

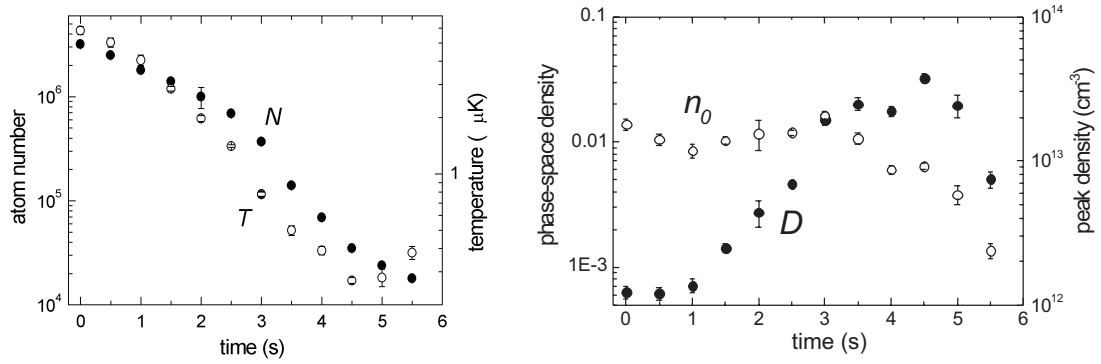

Figure 5.8: *Atom number, temperature, phase-space density and peak density during evaporation from the wide dimple. The evanescent wave was detuned by* 3 *nm.*

efficiency of $\epsilon \approx 2$. The constant density along with the strongly reduced temperature indicate that the elastic collision rate significantly increased during these two seconds. After 3.5 s of forced evaporative cooling the phase-space density has drastically increased from initially 6.5×10^{-4} to 0.02.

At $t = 3$ s the loss of atoms rapidly increases and eventually leads to a deteriorating evaporation efficiency and a fast destruction of the ensemble. Both peak density and phase-space density drop rapidly shortly before the evaporation stops.

The fact that both configurations show very similar behavior in spite of their different configurations and evanescent wave light fields indicates a common loss process that sets in below $T = 1\,\mu$K. Possible explanations and ways to solve this problem are discussed in the following section.

5.5 Limitations

Influence of the Dipole Potential

In order to understand the limitations arising from the encountered losses and to find a remedy, we have investigated the nature of the loss process. A first set of measurements recorded the decay of the sample in the wide dimple configuration after the evaporation was finished. At an evanescent wave detuning of 3 nm the dimple laser power was adiabatically ramped to different levels between maximum power corresponding to a potential depth of $U/k_B = 45\,\mu$K and the 10 % level of the evaporation ramp. Figure 5.9 nicely demonstrates how the very small lifetime of a weak trap (3-4 s) continuously increases to a much larger value (≈ 17 s) for full laser power. No significant difference between full power and half power exists which indicates some saturation behavior.

As the decay is obviously non-exponential the losses seem to be caused by a collision mechanism.

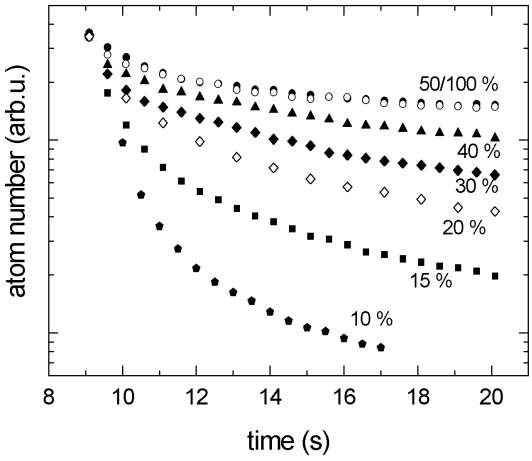

Figure 5.9: *Decay measurement of an evaporatively cooled and then adiabatically compressed ensemble at various laser powers. At low laser power of* 10 % *the lifetime is strongly reduced compared to the stronger confining cases.*

Surprisingly this measurement suggests a lifetime increase with increasing density. One would expect collisional losses to get more severe as density and consequently the collision rate is increased. A possible explanation is the simultaneous increase of the temperature during this adiabatic transformation. If the collision cross section strongly depends on T the adiabatic heating could affect the collision rate and thus could compensate for the increased density. In view of the fact that the decay is clearly non-exponential collisional losses seem the most probable mechanism.

We considered two mechanisms: One is the loss through three-body collisions and the other a binary collision process that changes the magnetic substate of an atom and, if residual magnetic fields are present, releases Zeeman energy.

As for the three-body collisions, this process strongly depends on the density of the sample. Therefore also the effect of the ensemble temperature on the collision cross section has to be extremely large to be able to compensate the density dependence. With our current knowledge of three-body collisions this cannot be ruled out but seems unlikely. A currently performed series of investigations of this subject by T. Weber *et al.* [Web] will be able to shed some new light on this problem in the near future.

Influence of the Magnetic Field

The alternative of m_F-state changing collisions seems the most probable explanation at the current state of investigations. The relation between sample lifetime and laser power can be explained by the fact, that at a certain laser power the resulting potential depth is larger than the Zeeman energy released in one such collision and therefore the colliding atoms are retained. No sharp threshold behavior is expected, because even in a potential whose depth is below the release energy, an atom undergoing such a process can remain trapped if its excess energy is predominantly deposited in the vertical degree of freedom. The observed saturation of the lifetime sets in as the potential depth becomes larger than the release energy.

We investigated heating of the sample at different laser power levels but found no significant difference between them. If the event rates are equal for exothermal (Zeeman energy is released and transformed into kinetic energy) and endothermal (the opposite process) inelastic collisions the net heating effect is zero and the observation can be explained. The amount of energy stored in the Zeeman splitting can be obtained from the expression

$$\Delta E = -\mu_B \cdot g_F \cdot \Delta m_F \cdot B. \tag{5.2}$$

With the Bohr magneton $\mu_B = 5.789 \times 10^{-9}\,\mathrm{eV/Gauss}$, the g-factor for cesium ($F = 3$) of $g_F = -1/4$ and an assumed value of $\Delta m_F = 1$ we find that a residual B-field of 0.27 Gauss is sufficient to remove atoms from the $4.5\,\mu$K deep potential well at the end of the ramp. Still this value is above of what we expect to be present in this experiment. All external magnetic fields except those that are carefully applied to compensate for earth' magnetic field have been switched off at that time. The possible compensation error is certainly below 10^{-3} Gauss and therefore way below the value that could explain the loss. Since also circularly polarized light can give rise to a lifted degeneracy of the Zeeman sublevels we carefully checked and confirmed the linear polarization of the focussed beam and tested whether changing the evanescent wave polarization from TM to TE made any difference. It did not. (Strictly speaking these tests are only conclusive if some vertical external B-field defines the quantization axis of the atomic system and therefore the polarization of the light with respect to it.) In order to investigate the explicit dependence between B-field and ensemble lifetime we went the opposite way and applied a vertical magnetic field of variable strength. In a relatively crude measurement with an uncalibrated field we recorded the remaining atom number N after some storage time $t = 6\,\mathrm{s}$ as a function of the applied magnetic field for two different laser powers ($P = P_{max}, P_{max}/2$) The data shown in figure 5.10 demonstrates that above a certain field strength B the lifetime in the reduced potential suddenly becomes smaller than the one in the full strength potential.

It continuously drops until at a still stronger field also the lifetime in the full-strength potential drops. The clear threshold behavior further supports the hypothesis of m_F-state changing collisions as predominant loss mechanism.

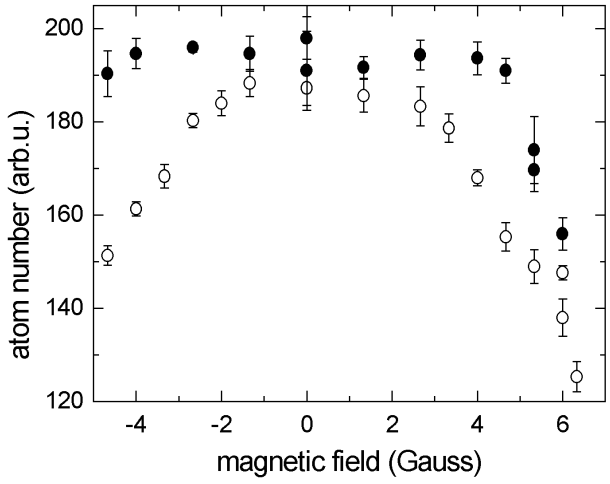

Figure 5.10: *Atom number after six seconds at various magnetic field levels. Open circles correspond to* 3.6 *W and filled circles to* 7.2 *W laser power.*

In spite of these indications there might still be other mechanisms that contribute to the loss. A much better suited and more convincing way to investigate the role of this process will be the utilization of a polarized sample of atoms in the $|F = 3, m_F = 3\rangle$ state. A magnetic field along the vertical direction will push the $|3, 3\rangle$ state energetically so far below neighboring m_F-states that m_F-state changing collisions are excluded both energetically and because of angular momentum conservation.

The question on what process limits the evaporation progress will conclusively be answered only with polarized atoms. If the indications about the mechanism prove to be right, polarizing the atoms would conveniently provide an easy remedy for this problem.

Chapter 6

Double Evanescent Wave Trap

Experiments in the DEW-trap are aimed at investigating two-dimensional behavior. Its efficient evaporative cooling leads to the attainment of equally high phase-space density as what could be achieved in the dimple so far and reaches the crossover to two-dimensionality. Before sections 6.4 and 6.5 provide detailed results on these subjects, we will discuss loading and storage properties (Section 6.1), thermometry in the DEW-trap (Section 6.2) and explain the measurement of the trap frequency (Section 6.3). The results discussed here will also be published in reference [Ham02a].

6.1 Transfer and Storage

The trapping potential that was created and used for all experiments reported on hereafter originates from the 1.15 Watt blue-detuned laser at 850.5 nm (1.6 nm blue detuning) and the 1.2 Watt red-detuned laser at 1064 nm (≈ 212 nm red detuning). With a waist of $w_b = 400\,\mu$m and a deviation of $\Theta_b = 3.2°$ from the critical angle of total internal reflection the blue-detuned light field creates an evanescent wave with a repulsive dipole potential of $U_b/k_B = 325\,\mu$K and a decay length of $\Lambda_b = 395$ nm. The red-detuned beam is focussed to only $w_r = 160\,\mu$m and its deviation from the critical angle $\Delta\Theta_r$ of 0.2° is much smaller. The resulting attractive evanescent wave features a potential of $U_r/k_B = 43\,\mu$K and a decay length of $\Lambda_r = 2\,\mu$m. According to Equation 3.50 the combination of both counteracting dipole potentials together with gravity and Van-der-Waals attraction give rise to an attractive potential pocket $0.9\,\mu$m above the material surface and with a total depth of $U/k_B = 13\,\mu$K. Its potential as a function of z at the common center of both evanescent wave spots can be seen in figure 6.1. The different lines illustrate how the potential changes during forced evaporative cooling when the red-detuned laser's power is reduced. At $P_r = 0$ the gravito-optical potential is restored (dashed line).

In spite of its dimple-like structure and the positive experiences made with the

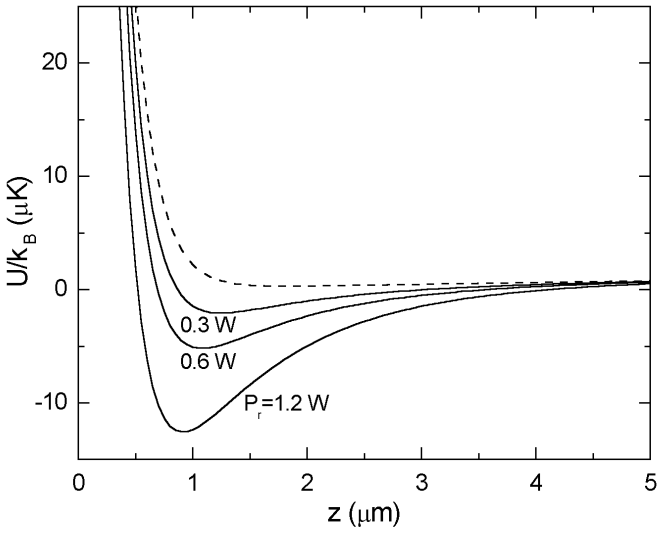

Figure 6.1: *Potential of the DEW-trap for different laser powers P_r as a function of distance z from the prism.*

loading of the focussed red beam, experiments show that collision induced loading from a reservoir (in this case a trapped ensemble in the dimple) does not significantly enhance the loading efficiency. This is due to the fact that in contrast to the case of the dimple trap where the lifetime inside the dimple was larger than that of the reservoir we find the lifetime of 1.4 s inside the DEW-trap to be much shorter.

The loading scheme that finally yields the best results therefore provides temporal overlap between reservoir and DEW for only 50 ms. During this limited time interval the dimple laser intensity is linearly ramped from initially 2 Watts to zero while at the same time the red evanescent wave's laser power is increased to 1.2 Watt. Transfer into the DEW-trap is mainly optimized by matching the phase-space region occupied by the ensemble with the region that leads to trapping. In detail this means slow reduction of the dimple intensity from 7.2 Watt down to 2 Watt which results in cooling with a simultaneous decompression. This combined evaporative and adiabatic cooling stage of 2 seconds prepares a sample of 1.8×10^6 atoms at 3.0 μK in the dimple. The corresponding peak number density amounts to $10^{13}\,\mathrm{cm}^{-3}$ and the phase-space density is about 10^{-3} if the sample is fully unpolarized. About 5 % of this ensemble and a total of 10^5 atoms can be observed 150 ms after transfer into the DEW-trap when untrapped atoms have laterally escaped.

The ensemble decay then strongly depends on the details of the confinement. We measured decay curves at different laser powers of the red-detuned beam (figure 6.2) by

using the transfer scheme described above and then ramping the laser power from the initial value of $P = 1.2\,\mathrm{W}$ to the desired value in 50 ms. We found that a slightly more powerful laser at 2.2 Watt will yield a significantly shorter lifetime (0.33 s) whereas the weaker confinement shows comparable lifetimes as the standard power of 1.2 W.

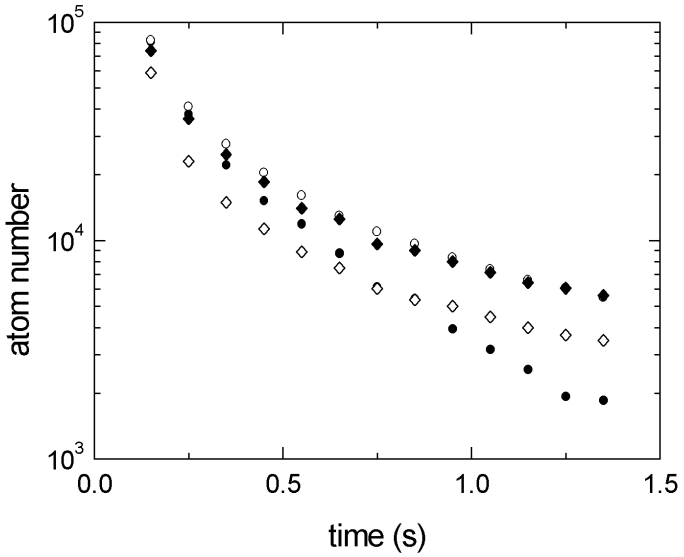

Figure 6.2: *Decay measurements for different laser powers P_r of the red-detuned evanescent wave laser ($P_r = 2.2\ W\,(\bullet)$, $P_r = 0.22\ W\,(\diamondsuit)$, $P_r = 0.88\ W\,(\circ)$, $P_r = 0.44\ W$)*

In a less intense light field at around $P_r = 1\,\mathrm{W}$ the decay behavior markedly differs and exhibits a comparatively slow and clearly non-exponential loss. The shallow potential does not affect the transfer but due to the longer lifetime one observes significantly more atoms at later times. At only 200 mW of red laser light the transfer efficiency is affected and although trapped atoms are kept equally long the total number is considerably lower. This indicates that the limiting factor for the transfer efficiency is the small spatial overlap between dimple and DEW-trap rather than the depth of the potential. The strong nearly exponential loss at large laser intensity suggests a dominant single particle effect and probably can be attributed to the fact that atoms stored in the deep potential close to the surface will start to feel the defects of the repulsive evanescent wave.

The non-exponential decay in a shallower potential most likely arises from the same collision mechanisms that were discussed in the context of the dimple trap. In particular light-assisted collisions most certainly play a crucial role since atoms are pulled into the intense region of the excitation light by the attractive evanescent wave. A thorough

investigation of this issue is postponed until a polarized ensemble can be utilized to clearly separate collisional and single particle losses via the Feshbach resonance and to separate light-assisted collisions from m_F-state changing collisions.

6.2 Temperature Measurements

The temperature measurement in the DEW-trap is in principle similar to the case of the GOST and the dimple trap. The ensemble is released for a variable time Δt by simultaneously removing both the repulsive and the attractive evanescent wave. Then the repulsive evanescent wave is restored and atoms are recaptured into the MOT where the remaining atom number is determined. Experimentally it is important to extinguish the evanescent waves simultaneously within one microsecond because an unbalanced potential of only one light field can drastically increase an atom's vertical energy within less than one oscillation period ($\approx 100\,\mu$s) and thus influence the temperature result. The complete dataset can then be compared to the theoretical model. The fit function is derived by replacing the gravito-optical potential in the considerations above with the combined potential of attractive and repulsive evanescent wave (gravitation and Van-der-Waals attraction can be neglected in this case), and proceeding along the same lines as before. This, again leads to a numerical expression for the fit function.

When the ensemble temperature is significantly smaller than the potential well of the DEW-trap the atoms are confined to a very thin layer at a distance d from the prism surface. In this case one can obtain a conveniently simple approximated fit function by starting from a δ-function as initial density distribution:

$$\rho(z,v) = \frac{1}{\Omega} \cdot \delta(z-d) \cdot \exp\left(-\frac{mv^2}{2k_BT}\right). \tag{6.1}$$

Ω denotes the normalization constant. Ballistic expansion and integration over the region of phase-space that leads to recapture finally yields an expression for the fraction of recaptured atoms as a function of the release time

$$\kappa(t) = \frac{1}{2}\left(1 - \mathrm{erf}\left(\sqrt{\frac{m}{2k_BT}}\left(\frac{gt}{2} - \frac{d}{t}\right)\right)\right). \tag{6.2}$$

The error function $\mathrm{erf}(x)$ is defined by $\mathrm{erf}(x) \equiv 2/\sqrt{\pi}\int_0^x e^{-t^2}dt$. This approximation yields excellent results for temperatures somewhat below $3\,\mu$K. In order to fit the data it is much easier to start from this analytical expression instead from a purely numerical one. As the temperature results of both approaches below $3\,\mu$K are identical within the statistical error, we use the analytical expression for all following evaluations.

Like for the dimple trap, temperature measurements in the DEW-trap depend on the specific details of the potential. In this approximation all experimental parameters

are summarized in the minimum position d that can be obtained from the evanescent waves' angles of incidence and their intensities. In addition to the temperature T this method introduces d as a second fit parameter. This becomes necessary as during evaporative cooling the attractive potential and thus also d is changed and separately calculating d for each situation would be unpractical. However, T and d are only very weakly correlated in the fit and no ambiguous results arise from this evaluation. We have compared the calculated values of d for several different experimental situations with the ones obtained from a fit and found excellent agreement between them. Figure 6.3 demonstrates the good agreement between experiment and theory for two different temperature measurements using this procedure.

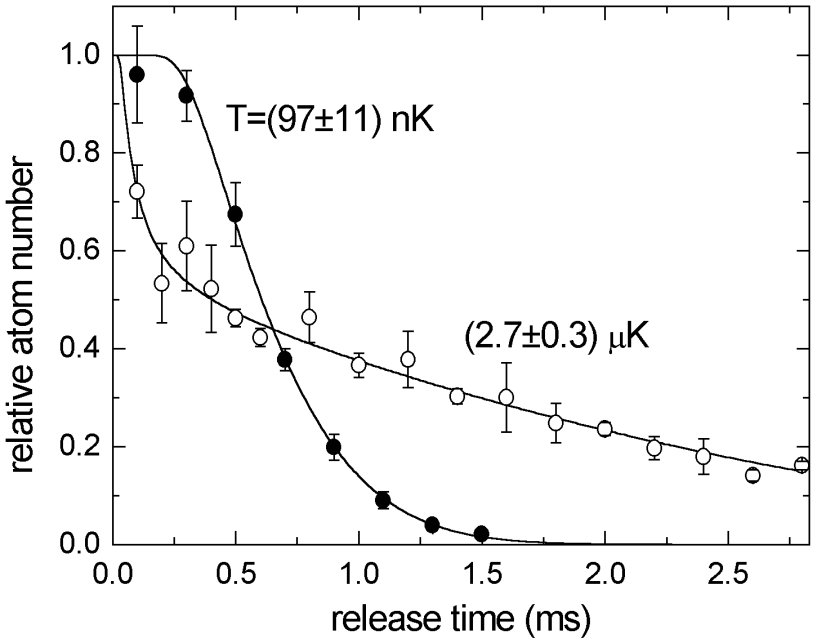

Figure 6.3: *Two temperature measurements in the DEW-trap for ensembles at* $2.7\,\mu K$ *and* $97\,nK$ *using the low temperature approximation explained in the text.*

In case of the "hot" ($2.7\,\mu$K) ensemble, half of the atoms are lost almost immediately while the remaining part is slowly declining. This behavior reflects the fact, that half of the atoms have an initial velocity component directed towards the prism which removes them almost instantaneously while the other half initially moves away from the prism. The timescale on which they return to the surface, is determined by the ensemble temperature.

A "cold" $(97 \pm 11)\,$nK ensemble exhibits a clearly distinct behavior. At very short

release times of up to 300 μs no significant loss of atoms occurs and the curve features a plateau as in the low temperature case of the GOST. Its origin is again the fact, that the atoms need approximately 300 μs to reach the recapture boundary during their fall. At longer times the fraction of remaining atoms steeply declines with a slope increasing with falling temperature.

While classically one would expect a step function at zero temperature, quantum mechanically the zero-point oscillation prevents this situation and maintains a finite width of the curve. As the temperature information is mainly extracted from the slope, this fact already indicates that this measurement technique is bound to become inaccurate at temperatures where $k_B T \approx \hbar\omega_0$. The next paragraph will discuss this issue in a more quantitative way.

Quantum Effects

At temperatures around $T = \hbar\omega_0/k_B$ when quantum mechanical behavior can no longer be neglected, mainly two effects come into play: Firstly the atomic motion contains a zero-point energy contribution that is comparable to the thermal energy of the atoms and secondly the motion itself does not follow the laws of classic ballistic expansion but rather obeys quantum mechanics rules. In some sense fortunate is the fact that the measurement technique that is used here is very insensitive to the details of the atomic motion. Figure 6.4 shows a comparison of theoretical temperature curves for two very different ensemble states in the GOST and the DEW-trap. One is the result from an

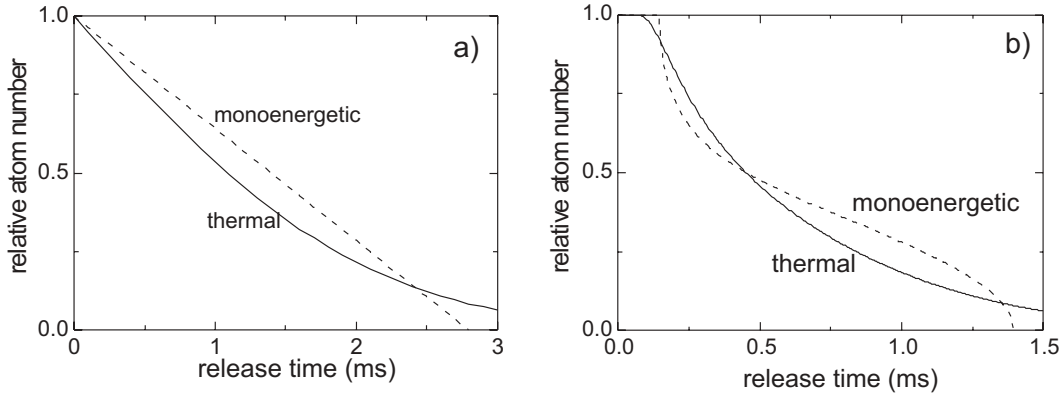

Figure 6.4: *Theoretical temperature measurement curve $\kappa(\Delta t)$ for a monoenergetic and a thermal ensemble in the GOST (a) and the DEW-trap (b).*

ensemble in thermal equilibrium while the other represents the extreme (hypothetic) case of a sample of monoenergetic atoms with randomly distributed phases of their

oscillation. Even these extreme cases can only be distinguished by the details of a measurement curve and therefore it is justified to say that this technique determines the mean kinetic energy of an ensemble rather than its temperature.

The modifications of the detailed motion of the atomic ensemble due to quantum mechanical corrections are likewise hardly resolved by this scheme and therefore we only have to concern ourselves with the modification of the mean kinetic energy due to the zero-point oscillation. The problem can therefore be restated as follows: How can we derive a thermodynamical temperature T from a quantum mechanical system whose mean kinetic energy $\bar{E}$ is known? The potential is assumed to be purely harmonic with an oscillation frequency ω_0 since we are only interested in the case where $k_B T \approx \hbar\omega_0$ and thus the anharmonicity of the trap is negligible. According to statistical physics the probability for an atom to be found in a state corresponding to the energy $E_n = \hbar\omega_0(n + 1/2)$ is given by

$$p(n) = \frac{1}{\Omega} \cdot \exp\left(\frac{\hbar\omega_0}{k_B T}(n + 1/2)\right), \tag{6.3}$$

with the partition function

$$\Omega \equiv \sum_{n=0}^{\infty} \exp\left(\frac{\hbar\omega_0}{k_B T}(n + 1/2)\right) = \frac{1}{2} \cdot \sinh^{-1}\left(\frac{\hbar\omega_0}{2k_B T}\right). \tag{6.4}$$

The mean energy for a given T can be calculated from the well known formula

$$\bar{E} = -\frac{\partial}{\partial\beta}(\ln \Omega). \tag{6.5}$$

β denotes the inverse temperature $\beta \equiv 1/k_B T$. One finds

$$\bar{E} = \frac{\hbar\omega_0}{2} \cdot \frac{\cosh\left(\frac{\hbar\omega_0}{2k_B T}\right)}{\sinh\left(\frac{\hbar\omega_0}{2k_B T}\right)}, \tag{6.6}$$

and solving for T we finally get the correction formula that relates the mean kinetic energy obtained experimentally to the true thermodynamic temperature:

$$T = \frac{\hbar\omega_0}{2k_B} \cdot \operatorname{arccoth}^{-1}\left(\frac{2\bar{E}}{\hbar\omega_0}\right). \tag{6.7}$$

Figure 6.5 demonstrates how our measurement technique is rendered inaccurate at $2\bar{E}/\hbar\omega_0 \approx 1$ due to the diverging slope of the function at this point.

Reduced kinetic energy means the ratio between $\bar{E}$ and the vibrational energy quantum $\hbar\omega_0$. Reduced temperature stands for the expression $k_B T/\hbar\omega_0$ that relates the thermal energy to the vibrational energy. At around $\bar{E} = \hbar\omega_0$ the resulting corrections are moderate and of the order of 10 % whereas this method becomes useless as $\bar{E}$ approaches $\hbar\omega_0/2$.

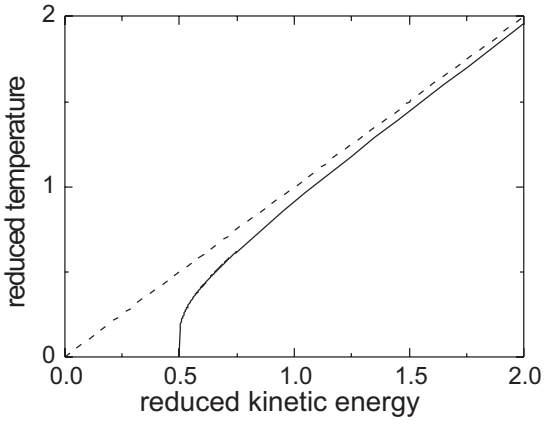

Figure 6.5: *Correction function for low temperatures in the DEW-trap that translates the experimentally measured mean kinetic energy into a thermodynamic temperature. The dashed line represents the classical expectation.*

6.3 Trap Parameters

In order to specify the ensemble properties inside the DEW-trap we have to know the trap frequencies in addition to the number of trapped atoms and the temperature. A method that enables us to measure expected trap frequency of around 10 kHz was first used by S. Friebel *et al.* [Fri98] in Munich. It is based on the parametric heating of atoms by a sinusoidal modulation of the trapping potential with a frequency $\omega_{mod} = 2\omega_0/n$ (n being an integer). ω_0 denotes the vertical oscillation frequency. Figure 6.6 shows the raw data of a measurement performed with $P_r = 0.9\,\mathrm{W}$.

After the DEW-trap has been loaded, the power P_r of the red-detuned laser beam is ramped to a variable value within 50 ms. Then the repulsive evanescent wave is intensity-modulated with a modulation depth of 10 % and a variable frequency for a duration of 150 ms. Another 100 ms later when all released atoms have escaped, the remaining fraction is measured.

If the modulation frequency equals ω_0 or $2\omega_0$ the remaining fraction of atoms exhibits clear minima that arise from the efficient heating at these frequencies. Due to the lateral spread of the atoms inside the trap the width of these minima is considerably large. In outer regions of the evanescent wave spots the vertical potential is less deep and features a smaller trap frequency than in the center. Additionally the anharmonicity of the vertical potential itself contributes to this spectrum of oscillation frequencies. As both effects introduce only smaller frequencies, the average trap frequency obtained by this method lies slightly below the calculated value for a harmonic approximation in the trap center. The solid line in figure 6.7 shows such a calculation as a function of the red

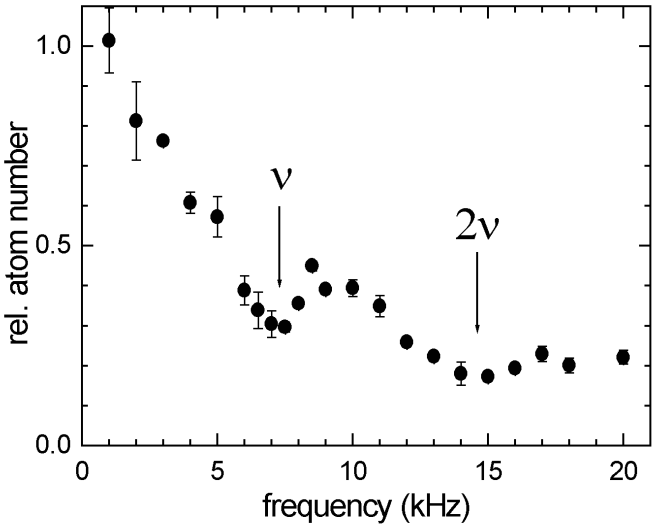

Figure 6.6: *Measurement of the fraction of atoms remaining in the DEW-trap (P_r = 0.9 W) after 150 ms of trap modulation. The measurement shows broad minima at the trap frequency ν and its second harmonic 2ν.*

laser power P_r.

Each value of the function has been obtained by numerically locating the potential minimum of the vertical potential and extracting the trap frequency from a harmonic approximation to this minimum. The experimental data points have been obtained from various measurements similar to the one shown in figure 6.6. The systematic deviation of the experimental data can be explained by the considerations given above. Notably the trap frequency does not become zero at vanishing laser power P_r. The offset value of $\omega_0/2\pi = 1.1\,\mathrm{kHz}$ is the oscillation frequency in the gravito-optical potential that is always present in addition to the DEW potential.

The oscillation frequency in the horizontal confinement is expected to be around 50 Hz. In this case one has to rely on a calculated value as the frequency is too low to be accessible by a measurement using parametric heating. Exciting and probing a collective oscillation of an ensemble similar to the method presented in Section 5.3 is also excluded because the release pulse would leave the atoms in an unbalanced vertical potential and eject them from the trap. At $P_r = 1.2\,\mathrm{W}$ we calculate a vertical trap frequency of $\omega_0/2\pi = 10.2\,\mathrm{kHz}$ and horizontally we find values of 59 Hz and 42 Hz. The elongated shape of the red evanescent wave spot gives rise to a factor $\cos\Theta_i$ between the two perpendicular horizontal axes. Θ_i is the angle of incidence of the red laser beam. The aspect ratio of around 200 newly expresses the fact that this very anisotropic trap is well suited to address two-dimensionality related topics. With the knowledge of all

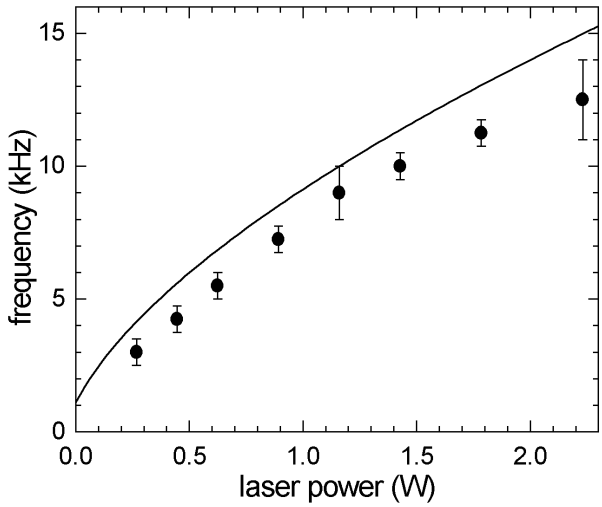

Figure 6.7: *Calculated and measured values for the vertical trap frequency for different laser powers P_r.*

required trap frequencies one can now turn to the issues of evaporative cooling and two-dimensionality.

6.4 Evaporative Cooling

In order to increase phase-space density and to cool the atomic ensemble into a single vertical vibrational state, forced evaporative cooling is applied. This is done by exponentially ramping down the laser power P_r of the red-detuned evanescent wave from initially 1.2 W down to 42 mW (3.5 %) in 400 ms.

This evaporation method is in principle three-dimensional because the light field that is ramped down provides the confinement for all three dimensions. Since however, in addition to the tightly confining potential also the standard gravito-optical potential retains atoms vertically, released atoms are bound to leave the trap laterally. Atoms leaving the tight confinement vertically have only reduced spatial overlap with the trapped ensemble, but it is not entirely clear to what extend these untrapped atoms can still transfer kinetic energy to trapped ones. The efficiency of this scheme lies between that of the two- and the three-dimensional case.

The evaporation ramp starts immediately after loading (at $t = 0$) but the 150 ms needed to have initially untrapped atoms escape, prevents reliable measurements of the particle number N and temperature T in the beginning. The time evolution of all relevant quantities can be seen in figures 6.8 and 6.9.

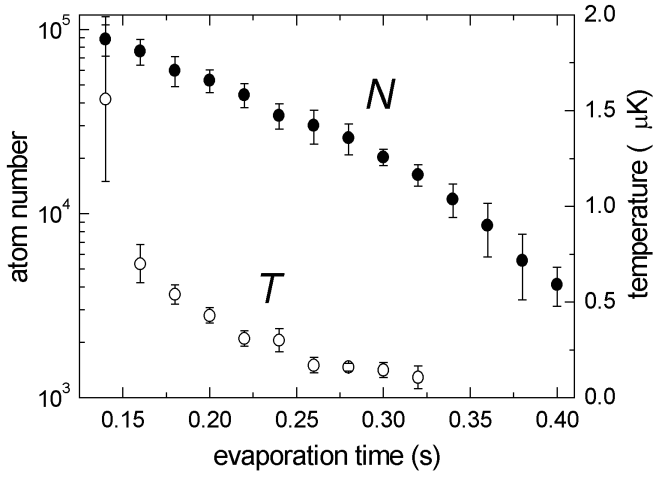

Figure 6.8: *Atom number* (○) *and temperature* (●) *during evaporation from the DEW-trap.*

The results look very promising between the first dataset at $t = 150\,\mathrm{ms}$ ($P_r = 28\,\%$) and $t = 270\,\mathrm{ms}$ ($P_r = 8\,\%$). During this time we observe an exponential decline of the atom number accompanied by a drastic reduction of the temperature from $1\,\mu\mathrm{K}$ down to $\approx 100\,\mathrm{nK}$. The cooling is a combined effect of evaporative cooling and of adiabatic expansion. At $8\,\%$ of the initial laser power the vertical trap frequency has dropped to about $2.5\,\mathrm{kHz}$ with evident consequences for the density. The strong contribution of evaporative cooling can be seen in figure 6.9. Between $t = 150\,\mathrm{ms}$ and $t = 270\,\mathrm{ms}$ the phase-space density increases by two orders of magnitude and almost reaches 0.1 (still assuming equal distribution among all seven magnetic substates of the ground-state). Together with the moderate decrease of N by only a factor of three this makes the evaporation process highly efficient. The maximum value of $D \approx 0.1$ is comparable to the highest phase-space densities obtained with cesium ensembles so far [Han01a].

After $t = 270\,\mathrm{ms}$ the temperature is not reduced any further and the particle loss progresses at an increased rate. After $t = 320\,\mathrm{ms}$ atom numbers and statistics are insufficient to obtain reliable temperature data. It seems that one is again faced with an inelastic loss process that prevents further progress towards the BEC-threshold. We believe that also in this case will the transition to a polarized sample be helpful for both the evaporation itself and for the investigation of the limitations observed here.

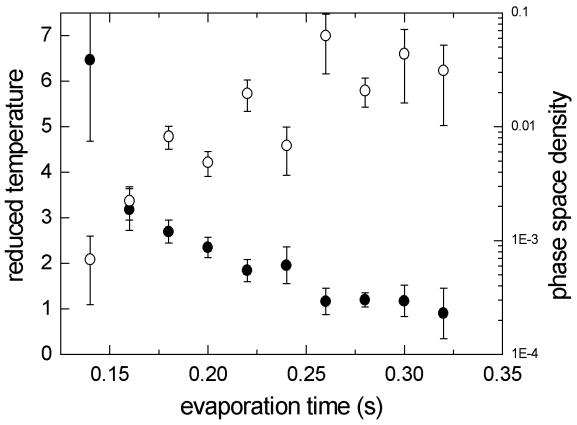

Figure 6.9: *phase-space density and peak density during evaporation from the DEW trap*

6.5 Two-Dimensionality

In order to analyze these results in the context of two-dimensionality it is useful to introduce a reduced temperature $\tau \equiv k_B T/\hbar\omega_0$. It relates the thermodynamic temperature T to the vibrational energy splitting between ground-state and first excited state. The filled circles (•) in figure 6.9 indicate how this reduced temperature drops in the course of evaporative cooling and finally approaches one at $t = 270\,\mathrm{ms}$. The vibration frequency ω_0 changes during evaporation and is taken from the calculation shown in figure 6.7. The final value of $\tau = 1$ corresponds to a mean vibrational number of only $\bar{n} = 0.58$ and to a ground-state population of 63 %. This situation can be regarded as the crossover regime to a quasi two-dimensional system.

Notably the evaporation stops right at $\tau = 1$ and recalling the statements of reference [Pet01] this is not surprising. At $\tau = 1$ the thermalization between strongly confined and nearly free degrees of freedom is expected to break down due to the reasons given in Section 3.6.3. Even if the evaporative cooling continues to cool the horizontal motion, it would not show in our measurement because the technique we use is insensitive to the horizontal temperature and the decoupling inhibits the communication between horizontal and vertical degree of freedom. We therefore believe to see first effects of two-dimensionality in this measurement.

This concludes the report on what has been achieved with unpolarized atoms and what insights have been obtained with respect to limitations and future improvements.

Chapter 7

Summary and Outlook

This last chapter is intended to summarize what has been achieved with the surface microtraps so far, and it will outline the future directions of the experiment.

7.1 Summary

We have successfully implemented two different types of surface microtraps and investigated their behavior in terms of loading, trapping conditions, thermometry and evaporative cooling towards BEC and two-dimensionality.

The Focussed Beam Surface trap

The implementation of the focussed beam surface trap has been a major experimental breakthrough to overcome efficiency problems of evaporative cooling encountered in earlier experiments with the GOST. Its strong local compression and the efficient collision loading mechanism that selects predominantly low-energetic atoms from the reservoir create ensembles of a peak-density of $7 \times 10^{13}\,\mathrm{cm}^{-3}$, a phase-space density of 3×10^{-3} and a dramatically increased elastic collision rate of $\sim 2\,\mathrm{kHz}$. The enhanced thermalization speed then allows for very efficient evaporative cooling that leads to a phase-space density of 0.01.

Experimentally we have worked with two distinct configurations of the dimple. A tightly focussed ($w = 30\,\mu\mathrm{m}$) 330 mW Nd:YAG beam gave rise to an approximately $50\,\mu\mathrm{K}$ deep potential well, that hosted up to 1.8×10^5 atoms. At $2.9\,\mu\mathrm{K}$ and with an experimentally determined trap frequency of 555 Hz it provided conditions well suited for a detailed study of the collisional loading process and for consecutive evaporative cooling. A much stronger (7.2 W) but also wider ($w = 160\,\mu\mathrm{m}$) laser focus in combination with a much further detuned ($> 660\,\mathrm{GHz}$) evanescent wave created a potential of similar depth but due to the favorable spatial overlap with the reservoir trapped up to 6.5×10^6 atoms. At a trap frequency of 110 Hz comparable peak density and phase-space density have

been achieved but the much larger ensemble and the extended lifetime further improve the prospects of evaporation.

The Double Evanescent Wave Trap

A second surface microtrap scheme called the DEW-trap was, more than ten years after its first proposal by Y.B. Ovchinnikov *et al.*, experimentally implemented. This highly anisotropic and strongly confining potential is particularly suitable for studies on two-dimensionality. The trap frequencies of around 10 kHz vertically and 50 Hz horizontally lead to an aspect ratio of 200 and separate states of the vertical motion by a temperature equivalent of several hundred nanokelvin. A multi-stage loading process including an intermediate dimple phase transfers up to 10^5 atoms into the trap where they can be stored for few seconds.

The fact that a single laser is involved in the confinement of all three dimensions makes the consecutive forced evaporative cooling stage highly efficient. At a cost of less than 90 % of the atoms phase-space density is increased by two orders of magnitude up to almost 0.1. The combination of evaporative and adiabatic cooling manages to push the temperature down to below 100 nK and even though the vertical trap frequency is simultaneously reduced, a situation is created where the vibrational energy is equal to the thermal energy. At this point 63 % of the atoms populate the motional ground-state and the mean vibrational number is only 0.58. Further increase of phase-space density is prevented by the breakdown of thermalization between horizontal and vertical freedom at the crossover to the two-dimensional regime.

7.2 Future Goals

After these surface microtraps have been implemented and characterized, their useful properties now open up new interesting prospects for the future.

Quantum Degeneracy

A first step will be the attainment of Bose-Einstein condensation in the focussed beam trap. In order to achieve this goal, we will polarize the atoms to the absolute ground-state $|F = 3, m_F = 3\rangle$. An immediate consequence of polarizing the ensemble is the increase of the phase-space density by the degeneracy factor 7 and the doubling of the elastic collision rate due to the symmetrization factor of identical bosons. In addition to that, it will avoid the binary collisions that so far prevented further progress of evaporative cooling. At a field strength of several Gauss the energetic splitting between neighboring m_F-states is sufficiently large to exclude any m_F-state changing collisions that have have most likely been responsible for the losses so far. Without the loss from these collisions, evaporation is expected to proceed to the condensation point. With a

polarized sample systematic investigations of decay processes become possible and will provide reliable values for the rate coefficients of the different collision processes.

Tuning Scattering Properties

In the $|F = 3, m_F = 3\rangle$ state the scattering length of the particle and thus its entire scattering behavior becomes a tunable parameter and the whole range of scattering lengths can be accessed with moderately strong magnetic fields of between zero and 50 Gauss. Depending on the specific application it can be favorable to switch to either negative, positive or zero scattering length.

Increasing a to large positive values can for instance compensate for the slowing thermalization and decreased density in the microtraps during evaporation. A rising a will strongly increase the elastic collision rate until the unitary limit is reached. Also three-body collisions which depend on a as $L_3 \propto a^4$ will be an important factor to consider for the choice of a. Close to the Feshbach resonance, where the value of a jumps from $+\infty$ to $-\infty$ the last molecular bound state (see Section 3.5) is close to the dissociation threshold and in turn will render the release energy of such a collision very small. In certain cases it might therefore be advisable to choose a to lie in a region around 49 Gauss and minimize the thermal energy input into the system.

A negative scattering length even completely eliminates this thermal energy and would otherwise be of interest for studies of the dynamics of a BEC-collapse. Creating the condensate at positive scattering length and then switching to a negative value will probably be the easiest way to achieve this.

Quantum Degeneracy in 2D

As soon as a BEC becomes available in the focussed beam trap it will be interesting to transfer it into the DEW-trap and study coherence properties and other aspects related to 2D. A condensate would immediately make also the far two-dimensional regime available and enable us to test theories on scattering in this regime. Of main interest will be the connection between tunability of the condensate and the reduced dimensionality. Section 3.6.3 already discussed how the transition into this regime could conveniently be investigated by tuning the mean field interaction of the condensate via a Feshbach resonance.

Improved Diagnostics

A future topic of more practical nature will be the improvement of diagnostics of the experiment. Polarized atoms offer the possibility of applying a magnetic levitation field. At a vertical gradient of 31.3 Gauss/cm the force acting on the magnetic dipole moment exactly compensates gravity and at a field gradient above this value even lifts the atoms up. This can be used to implement a new temperature measuring technique that would

enable us to accurately measure very low temperatures and detect a later BEC. For this approach the ensemble would be levitated in a magnetic gradient field so that after some release time the expanded atom cloud can be imaged. This time-of-flight method has in principle been used in many experiments and accurately measures to very small temperatures.

Aside from the issue of thermometry a levitation field can enhance the evaporation from the DEW-trap by removing vertically unbound atoms that are retained in the gravito-optical potential. The evaporation process would then be truly three-dimensional. Slow increase of the levitation field might even lead to an adiabatic cooling effect once the intensity of the red-detuned evanescent wave has been significantly ramped down.

Bibliography

[And95] M.H. Anderson, J.R. Ensher, M.R. Matthews, C.E. Wieman, and E.A. Cornell. Observation of Bose-Einstein Condensation in a Dilute Atomic Vapor. *Science*, 269(0):198, July 1995.

[Arn97] M. Arndt, M. Ben Dahan, D. Guéry-Odelin, M.W. Reynolds, and J. Dalibard. Observation of a Zero-Energy Resonance in Cs-Cs Collisions. *Phys. Rev. Lett.*, 79(4):625, July 1997.

[Ask62] G.A. Askar'yan. *Sov. Phys. JETP*, 15, 1962.

[Bag91] V Bagnato and D. Kleppner. Bose-Einstein condensation in low-dimensional traps. *Phys. Rev. A.*, 44:3, April 1991.

[Bal94] S. Bali, D. Hoffman, and T.Walker. *Europhys. Lett.*, 27, 1994.

[Bar01] M.D. Barrett, J.A. Sauer, and M.S. Chapman. All-Optical Formation of an Atomic Bose-Einstein Condensate. *Phys. Rev. Lett.*, 87(1):010404, July 2001.

[Blo00] I. Bloch, T.W. Hänsch, and T. Esslinger. Measurement of the spatial coherence of a trapped Bose gas at the phase transition. *Nature*, 403(6766):166, January 2000.

[Bor91] M. Born and E. Wolf. *Principles of Optics*. Pergamon Press, 1991.

[Bou94] P. Bouyer. *Confinement par Laser D'Atomes froids dans une cavité Gravitionnelle et dans un piège à pompage optique*. PhD thesis, Ecole Normale Superior, Paris, 1994.

[Bou02] I. Bouchoule, M. Morinaga, C. Salomon, and D.S. Petrov. Cesium gas strongly confined in one dimension: Sideband cooling and collisional properties. *Phys. Rev. A.*, 65:033402–1, February 2002.

[Cas48] H. B. G. Casimir and D. Polder. The Influence of Retardation on the London-van der Waals Forces. *Phys. Rev.*, 73:360, February 1948.

[Chi00] Cheng Chin, Vladan Vuletic, Andrew J. Kerman, and Steven Chu. High Resolution Feshbach Spectroscopy of Cesium. *Phys. Rev. Lett.*, 85(13):2717, April 2000.

[Coo79] R.J. Cook. Coherent dynamics of N-level atoms and molecules. III. An analytically soluble periodic case. *Phys. Rev. A*, 20:539544, 1979.

[Cou96] J.-Y. Courtois, J.-M. Courty, and J. Mertz. Internal dynamics of multilevel atoms near a vacuum-dielectric interface. *Phys. Rev. A*, 53:1862, 1996.

[Dal85] J. Dalibard and C. Cohen-Tannoudji. Dressed-atom approach to atomic motion in laser light: the diploe force revisited. 2:1707, 1985.

[Dal99] J. Dalibard. Collisional Dynamics of ultra-cold atomic gases. *Proceedings of the international school of physics "Enrico Fermi"*, page 321, 1999.

[Dav95] Kendall B. Davis, Marc-Oliver Mewes, Michael A. Joffe, Michael R. Andrews, and Wolfgang Ketterle. Evaporative Cooling of Sodium Atoms. *Phys. Rev. Lett.*, 74(26):5202, June 1995.

[Den99] Johannes Denschlag, Donatella Cassettari, and Jörg Schmiedmayer. Guiding Neutral Atoms with a Wire. *Phys. Rev. Lett.*, 82(10):2014, March 1999.

[Det01] S. Dettmer, D. Hellweg, P. Ryytty, J.J. Arlt, W. Ertmer, K. Sengstock, D.S. Petrov, G.V. Shlyapnikov, H. Kreutzmann, L. Santos, and M. Lewenstein. Observation of Phase Fluctuations in Elongated Bose-Einstein Condensates. *Phys. Rev. Lett.*, 87(16):4, October 2001.

[Dow96] J.P. Dowling and J. Gea-Banacloche. Evanescent Light-Wave Atom Mirrors, Resonators, Waveguides, and Traps. *Adv. At. Mol. Opt. Phys.*, 37, 1996.

[Fes62] H. Feshbach. *Ann. Phys (NY)*, 19:287, 1962.

[Fol00] Ron Folman, Peter Krüger, Donatella Cassettari, Björn Hessmo, Thomas Maier, and Jörg Schmiedmayer. Controlling Cold Atoms using Nanofabricated Surfaces: Atom Chips. *Phys. Rev. Lett.*, 84(20):4749–4752, May 2000.

[Fol02] R. Folman, P. Krüger, J. Schmiedmayer, J. Denschlag, and Carsten Henkel. Microscopic Atom Optics: From wires to an atom chip. *Adv. At. Mol. Opt. Phys.*, 48:263, 2002.

[For02] J. Fortagh, H. Ott, S. Kraft, A. Günther, and C. Zimmermann. Surface effects in magnetic microtraps. *Phys. Rev. A*, 66:041604, October 2002.

[Fri98] S. Friebel, C. D'Andrea, J. Walz, M. Weitz, and T.W. Hänsch. CO_2-laser optical lattice with cold rubidium atoms. *Phys. Rev. A, Rapid Comm.*, 57(1):4, January 1998.

[Gau98] H. Gauck, M. Hartl, D. Schneble, H. Schnitzler, T. Pfau, and J. Mlynek. Quasi-2D Gas of Laser Cooled Atoms in a Planar Matter Waveguide. *Phys. Rev. Lett.*, 81(24):5298, December 1998.

[Gor80] J.P. Gordon and A. Ashkin. Motion of atoms in a radition trap. *Phys. Rev. A*, 21, 1980.

[Gör01] A. Görlitz, J.M. Vogels, A.E. Leanhardt, C. Raman, T.L. Gustavson, J.R. Abo-Shaeer, A.P. Chikkatur, S. Gupta, S. Inouye, T. Rosenband, and W. Ketterle. Realization of Bose-Einstein Condensates in Lower Dimensions. *Phys. Rev. Lett.*, 87(13):4, September 2001.

[Gri00] R. Grimm, M. Weidemüller, and Y. Ovchinnikov. Optical dipole traps for neutral atoms. *Adv. At. Mol. Opt. Phys.*, 42, 2000.

[Ham99] M. Hammes. Untersuchungen zur Speicherung und Kühlung dichter Atomensembles in der Gravito-optischen Oberflächenfalle. Master's thesis, Universität Heidelberg und Max-Planck-Institut für Kernphysik, 1999.

[Ham01] M. Hammes, D. Rychtarik, and R. Grimm. Evaporative cooling of cesium atoms in the gravito-optical surface trap. *C.R. Acad. Sci. Paris IV*, 2:625, March 2001.

[Ham02a] M. Hammes, D. Rychtarik, B. Engeser, H.-C. Nägerl, and R. Grimm. Evanescent-wave trapping and evaporative cooling of an atomic gas near two-dimensionality. *submitted for publication*, August 2002.

[Ham02b] M. Hammes, D. Rychtarik, H.-C. Nägerl, and R. Grimm. Cold atom gas at very high densities in an optical surface microtrap. *Phys. Rev. A*, April 2002.

[Han01a] D. J. Han, Marshall T. DePue, and David S. Weiss. Loading and compressing Cs atoms in a very far-off-resonant light trap. *Phys. Rev. A*, 63:9, January 2001.

[Hän01b] W. Hänsel, P. Hommelhoff, T. W. Hänsch, and J. Reichel. Bose-Einstein condensation on a microelectronic chip. *Nature*, 413:498, October 2001.

[Hän01c] W. Hänsel, J. Reichel, P. Hommelhoff, and T. W. Hänsch. Magnetic Conveyor Belt for Transporting and Merging Trapped Atom Clouds. *Phys. Rev. Lett.*, 86(4):608–611, January 2001.

[Har91] S. Haroche. Fundamental Systems in Quantum Optics. *Proceedings of the Les Houches Summer School*, 1991.

[Hes86] Harald F. Hess. Evaporative cooling of magnetically trapped and compressed spin-polarized hydrogen. *Phys. Rev. B*, 34(5):3476, September 1986.

[Jea82] Sir James Jeans. *An introduction to the kinetic theory of gases*. Cambridge University Press, 1982.

[Jr.02] James P. Burke Jr., Sai-Tak Chu, Garnett W. Bryant, C. J. Williams, and P. S. Julienne. Designing neutral-atom nanotraps with integrated optical waveguides. *Phys. Rev. A*, 65(043411), April 2002.

[Kag87] Yu. Kagan, B.V. Svistunov, and G.V. Shlyapnikov. *Sov. Phys. JETP*, 66:480, 1987.

[Kaz73] A.P. Kazantsev. *Sov. Phys. JETP*, 36, 1973.

[Ker01] A.J. Kerman, C. Chin, V. Vuletic, S. Chu, P. Leo, C.J. Williams, and P.S. Julienne. Determination of Cs-Cs interaction parameters using Feshbach spectroscopy. *C.R. Acad. Sci. Paris IV*, 2:633, March 2001.

[Ket96] Wolfgang Ketterle and N.J. van Druten. Evaporative Cooling of Trapped Atoms. *Adv. At. Mol. Opt. Phys.*, 37(0):181, 1996.

[Ket99a] W. Ketterle, D.S. Durfee, and D.M. Stamper-Kurn. Making, probing and understanding Bose-Einstein condensates. In M. Inguscio, S. Stringari, and C.E. Wieman, editors, *Proceedings of the International School of Physics - Enrico Fermi*, page 67. IOS Press, 1999.

[Ket99b] W. Ketterle, D.S. Durfee, and D.M. Stamper-Kurn. Making, probing and understanding Bose-Einstein condensates. *Proceedings of the International School of Physics "Enrico Fermi",IOS Press, Amsterdam, 1999*, page 67, 1999.

[Leo00] Paul J. Leo, Carl J. Williams, and Paul S. Julienne. Collision Properties of Ultracold ^{133}Cs Atoms. *Phys. Rev. Lett.*, 85(13):2721, April 2000.

[Mab94] H. Mabuchi and H. J. Kimble. Atom Galleries for Whispering Atoms: Binding Atoms in Stable Orbits Around an Optical Resonator. *Opt. Lett.*, 19:749–751, 1994.

[Man99] Inka Manek. *Gravito-optical Surface Trap for Cesium Atoms*. PhD thesis, Ruprecht-Karls Universität, Heidelberg, April 1999.

[Mar97] M. Marinescu, A. Dalgarno, and J. F. Babb. Retarded long-range potentials for the alkali-metal atoms and a perfectly conducting wall. *Phys. Rev. A*, 55(2):1530, February 1997.

[Mer68] N.D. Mermin. Crystalline Order in Two Dimensions. *Phys.Rev.*, 176:4, July 1968.

[Met99] H.J. Metcalf and P. van der Straten. *Laser Cooling and Trapping*. Springer-Verlag, 1999.

[Mie96] F.H. Mies, C.J. Williams, P.S. Julienne, and M. Krauss. *J.Res.Natl.Inst.Stand.Technol.*, 101:521, 1996.

[Min87] V.G. Minogin and V.S. Letokhov. *Laser light pressure on atoms*. Gordon and Breach, New York, 1987.

[Mos99] U. Moslener. Weiterentwicklung der gravitooptischen Oberflächenfalle (GOST). Master's thesis, Universität Heidelberg und Max-Planck-Institut für Kernphysik, 1999.

[Ott01] H. Ott, J. Fortagh, G. Schlotterbeck, A. Grossmann, and C. Zimmermann. Bose-Einstein Condensation in a Surface Microtrap. *Phys. Rev. Lett.*, 87(230401), November 2001.

[Pet95] Wolfgang Petrich, Michael H. Anderson, Jason R. Ensher, and Eric A. Cornell. Stable, Tightly Confining Magnetic Trap for Evaporative Cooling of Neutral Atoms. *Phys. Rev. Lett.*, 74(17):3352, April 1995.

[Pet00] D.S. Petrov, M. Holzmann, and G.V. Shlyapnikov. Bose-Einstein Condensation in Quasi-2D Trapped Gases. *Phys. Rev. Lett.*, 84(12):2551, March 2000.

[Pet01] D.S. Petrov and G.V. Shlyapnikov. Interatomic collisions in a tightly confined Bose gas. *Phys. Rev. A*, 64:012706–1, 2001.

[Pin97] P. W. H. Pinkse, A. Mosk, M. Weidemüller, M.W. Reynolds, T.W. Hijmans, and J. T. M. Walraven. Adiabatically Changing the Phase-Space Density of a Trapped Bose Gas. *Phys. Rev. Lett.*, 78(6):990, February 1997.

[Raj80] R.K. Raj, D. Bloch, J.J. Snyder, G. Camy, and M Ducloy. High-Frequency Optically Heterodyned Saturation Spectroscopy Via Resonant Degenerate Four-Wave Mixing. *Phys. Rev. Lett.*, 44(19):1251, December 1980.

[Ryc00] David Rychtarik. Evaporative Kühlung in der Gravito-optischen Oberflächenfalle. diploma thesis, Ruprecht-Karls Universität, Heidelberg, 2000.

[Saf98] A.I. Safonov, S.A. Vasilyev, I.S. Yasnikov, I.I. Lukashevich, and S. Jaakkola. Observation of Quasicondensate in Two-Dimensional Atomic Hydrogen. *Phys. Rev. Lett.*, 81(21):4545, November 1998.

[Sak94] J. J. Sakurai. *Modern Quantum Mechanics*. Addison-Wesley, 1994.

[Sch99] U. Schünemann, H. Engler, R. Grimm, M. Weidemüller, and M. Zielonkowski. Simple scheme for tunable frequency offset-locking of two lasers. *Rev. Sci. Instrum.*, 70:242, 1999.

[Shi82] J.H. Shirley. Modulation transfer processes in optical heterodyne saturation. *Optics Letters*, 7(11):537, July 1982.

[SK98] D.M. Stamper-Kurn, H.-J. Miesner, A.P. Chikkatur, S. Inouye, J. Stenger, and W. Ketterle. Reversible Formation of a Bose-Einstein Condensate. *Phys. Rev. Lett.*, 81(11):2194, September 1998.

[Söd95] J. Söding, R. Grimm, and Yu. B. Ovchinnikov. Gravitational laser trap for atoms with evanescent-wave cooling. 119:652, 1995.

[Söd98] J. Söding, D. Guéry-Odelin, P. Desbiolles, G. Ferrari, and J. Dalibard. Giant Spin Relaxation of an Ultracold Cesium Gas. *Phys. Rev. Lett.*, 80(9):1869, March 1998.

[Tie92] E. Tiesinga, A. J. Moerdijk, B. J. Verhaar, and H. T. C. Stoof. Conditions for Bose-Einstein condensation in magnetically trapped atomic cesium. *Phys.Rev.A*, 46:1167, August 1992.

[Vul99] Vladan Vuletić, Andrew J. Kerman, Cheng Chin, and Steven Chu. Observation of Low-Field Feshbach Resonances in Collisions of Cesium Atoms. *Phys. Rev. Lett.*, 82(7):1406, February 1999.

[Wal92] H. Wallis, J. Dalibard, and C. Cohen-Tanoudji. Trapping Atoms in a Gravitational Cavity. *Appl. Phys. B*, 54:407, 1992.

[Wal94] T. Walker and P. Feng. Measurements of collisions between laser-cooled atoms. *Adv. At. Mol. Opt. Phys.*, 34:46, 1994.

[Web] Tino Weber. Private Communication.

[Web02] T. Weber, J. Herbig, M. Mark, Hanns-Christoph Nägerl, and Rudolf Grimm. Tunable Bose-Einstein Condensate of Cesium. *submitted for publication*, October 2002.

[Wei99] J. Weiner, V.S. Bagnato, S. Zilio, and P.S. Julienne. Experiments and theory in cold and ultracold collisions. *Rev. Mod. Phys.*, 71, 1999.

[Wen00] Markus Wenin. Adiabatische Phasenraumdichteänderung in einem zeitabhängigen Potential. Diploma thesis, Universität Innsbruck, Fall 2000.

[Wyl84] J. M. Wylie and J. E. Sipe. Quantum electrodynamics near an interface. *Phys. Rev. A*, 30:1185, September 1984.

[Y.B91] Y.B.Ovchinnikov, S. Shul'ga, and V. Balykin. An atomic trap based on evanescent light waves. *J. Phys. B: At. Mol. Opt. Phys.*, 24:3173–3178, March 1991.

Danksagung

Zuletzt möchte ich mich bei all denen bedanken, deren moralische oder tatkräftige Unterstützung zum Abschluss des Projekts “Doktorarbeit” beigetragen hat:

Danke an,
Rudi, für die vier angenehmen, interessanten und lehrreichen Jahre in Heidelberg und Innsbruck und die hervorragende Betreuung während dieser Zeit.

meine Eltern, deren Unterstützung über einen Zeitraum von mehr als 28 Jahren alle Bereiche abdeckte, in denen sie möglich oder nötig war.

David, der – wohl oder übel im selben Boot sitzend – drei Jahre lang die Launen der hessischen “Pappnase” aushalten musste und trotzdem noch noch die Nerven hatte zur Pflicht noch die Kür in den Bergen Tirols durch zu stehen.

die Jungs von nebenan, Tino, Jens, Christoph, Michael, Bastian, Selim, Markus (Senior), Gerhard, Johannes, Matthias, Gregor und Klaus. Für ein äusserst unterhaltsames und anregendes Arbeitsumfeld und alles was darüber hinaus ging.

Christine, Andreas, Toni und Stefan, für jegliche Art von logistischer Unterstützung.

meine Brüder, die mich mit einem erfrischenden Desinteresse an meiner Arbeit immer wieder auf die Idee gebracht haben stattdessen ein ausgedehntes Bergsportprogramm abzuhalten.